



**Solar energy-driven liquid-based direct air capture with
CO₂ utilisation to produce sustainable aviation fuel:
modelling, simulation and performance assessment**

Yide Han

Supervisor: Prof Meihong Wang

A thesis submitted in partial fulfilment of
the requirements for the degree of
Doctor of Philosophy

The University of Sheffield
Faculty of Engineering
School of Chemical, Materials and Biological Engineering

September 2024

The world needs science that inspires.

----- Cell Press 50th Anniversary

I believe that scientists should be focusing on science, because if they're worrying about all the other things, science comes essentially last.

-----Nature Brief Quote of the day

Pour ce qui est de l'avenir, il ne s'agit pas de le prévoir, mais de le rendre possible.

----- De Antoine de Saint-Exupéry

Abstract

Climate change and global warming pose significant threats to our environment due to the increasing concentration of CO₂ in the atmosphere. To address these challenges, renewable energy-powered direct air capture (DAC) combined with CO₂ utilisation offers a sustainable pathway for decarbonisation within a circular economy. Despite its potential, current liquid-based DAC (L-DAC) technology relies on natural gas combustion to provide the high-temperature heat needed for calcination, which limits its overall sustainability and carbon reduction potential.

This work proposes a novel solar-driven L-DAC process design combined with CO₂ utilisation to produce carbon-neutral jet fuel. Specifically, the design features a 1 Mt CO₂ per year solar-driven L-DAC system using a hydrogen-fluidised solar calciner. The solar-driven L-DAC system utilises the captured CO₂ and fluidised hydrogen for onsite conversion into sustainable aviation fuel (SAF) via a one-step direct CO₂-Fischer-Tropsch synthesis (FTS) approach.

This thesis employs a combination of methodologies, including process modelling, simulation, comparison/validation, and scale-up to develop a large-scale L-DAC with CO₂ utilisation process model. A comprehensive performance assessment highlighting key findings and practical implications of the process is also presented.

This study reveals several important research findings: (a) Implementing a solar calciner in L-DAC harnesses thermal energy directly from sunlight, resulting in a 63% reduction in electricity consumption and a 59% reduction in onsite CO₂ emissions compared to the DAC process proposed by Carbon Engineering; (b) The minimum selling price (MSP) of SAF

made from solar-driven L-DAC with direct CO₂-FTS is estimated at US\$4.4 kg⁻¹ which is cost-effective compared with the previous stepwise process; (c) Sensitivity analysis based on geographical locations indicates that the favourable deployment locations are in low-risk countries with high solar irradiance and low hydrogen cost; (d) A detailed roadmap from first-of-a-kind (FOAK) plants to Nth-of-a-kind (NOAK) plants, demonstrates the potential for commercialisation of the technology to policymakers and industry investors.

This research provides valuable insights into the commercial development and operation of next-generation large-scale L-DAC systems with CO₂ utilisation powered entirely by renewable energy. The findings highlight the potential for solar-driven L-DAC to significantly advance the commercial viability of SAF, supporting global decarbonisation efforts and the transition to a circular economy.

Keywords: Direct air capture; CO₂ utilisation; sustainable aviation fuel; solar energy; Fischer-Tropsch synthesis; process design; process modelling\simulation; scale-up; techno-economic assessment

Acknowledgement

I would like to express my deepest gratitude to my supervisor, Prof Meihong Wang, for his unwavering guidance, support, and encouragement throughout my PhD research, as well as during my MSc studies. His inspiration, expertise, and dedication have been a constant source of motivation for me to pursue and excel in this field of research. Prof Wang's mentorship has been invaluable, and he deserves far more than a few words of thanks.

I am also deeply grateful to Dr Olajide Otitoju, an expert in CO₂ capture, for his continuous guidance and teaching since my MSc research project and throughout my PhD journey. My heartfelt thanks go to Dr Ariane D. Kamkeng, an expert in CO₂ utilization, for teaching me the technology of CO₂ utilisation. Without their contributions and support, this work would not have been possible.

I would like to thank my colleagues for their academic support, including Dr Yue Chai, Dr Yuxing Ding, Dr Yurong Liu, Dr Hui Yan, and Dr Toluleke E. Akinola. I also wish to extend my gratitude to the other members in our group for their mental and emotional support, including but not limited to Dr Hui Meng, Mr Yao Zhang, Mr Shengyuan Huang and Mr Jin Ma.

I am immensely grateful to my parents for their financial support, which provided me with the opportunity to study in the UK. I also appreciate the financial support from the EU RISE project OPTIMAL, led by Prof Wang, which enabled me to visit East China University of Science and Technology (ECUST) for 5-month in 2023 and Xi'an Jiaotong University (XJTU) for 4-month in 2024 during my PhD studies. I am thankful to Prof Feng Qian and Prof Wenli Du at ECUST, and Prof Junjie Yan and Prof Daotong Chong at XJTU for their host during my visits.

Finally, I would like to express my deepest appreciation to my wife, Yu, and my family for their unwavering support, patience, and understanding throughout my studies. Their encouragement, especially during times of hardship and frustration, has been invaluable, and I could not have accomplished this without them.

Peer-reviewed Publications and Conference Presentations

Peer-reviewed journal publications:

Part of this thesis has been submitted for publication:

- **Han, Y.**, Kamkeng, A., Otitoju, O., Ding, Y., Wang, M., 2024. Techno-economic assessment of modified Fischer-Tropsch synthesis process for direct CO₂ conversion into jet fuel. *Fuel*. (submitted in 05/2024, under review, minor modification in 8/2024)
 - ✓ This paper covers the content in Chapter 5 of this PhD thesis.
- **Han, Y.**, Otitoju, O., Kamkeng, A., Wang, M., Yan, H., Millard, F., Ding, Y., Du, W., Qian, F., 2024. A large-scale solar-driven direct air capture and utilisation process to produce sustainable aviation fuel. *Nature Chemical Engineering*. (submitted in 09/2024, under review)
 - ✓ This paper covers the contents in Chapters 3, 4, 5, 6 and 7 of this PhD thesis.

International conference presentations:

- Han, Y., et al., 2024. Renewable energy-driven solvent-based direct air capture and CO₂ utilisation to produce sustainable aviation fuel: modelling, simulation and performance assessment. 17th International Conference on Greenhouse Gas Control Technologies (GHGT-17). 20–24 October 2024, Calgary Canada.
 - ✓ Presented as poster.
- Han, Y., et al., 2024. Solvent-based direct air capture and CO₂ utilisation to produce sustainable aviation fuel: techno-economic assessment. 2024 Process Development Symposium Europe (PDS Europe), Nancy, France, 26–28 June 2024.
 - ✓ Presented as poster.
- Han, Y., et al., 2023. Technical performance prediction of modified Fischer-Tropsch synthesis process for direct CO₂ conversion into jet fuel through modelling and simulation. European Conference on Fuel and Energy Research and its Applications (2nd FERIA Conference), Sheffield, UK, 4-6 September 2023.
 - ✓ Delivered as oral presentation.

Table of Contents

Abstract.....	I
Acknowledgement.....	III
Peer-reviewed Publications and Conference Presentations.....	IV
Table of Contents	V
List of Tables	XI
List of Figures.....	XIII
Nomenclatures.....	XVII
Abbreviations	XX
Chapter 1. Introduction.....	1
1.1 Background	1
1.1.1 Energy demand, CO ₂ emissions and climate change.....	1
1.1.2 Carbon capture, utilisation and storage.....	2
1.1.3 DAC technology overview.....	4
1.1.4 CO ₂ utilisation technology overview	6
1.2 Motivation for this study.....	8
1.2.1 DAC as a key CO ₂ removal technology.....	8
1.2.2 L-DAC is promising but is energy-intensive and cost-intensive.....	9
1.2.3 Transition of energy source from natural gas to solar energy.....	9
1.2.4 Demonstrating L-DAC at a large scale as a priority	10

1.2.5	<i>DAC for decarbonisation in net zero aviation</i>	11
1.2.6	<i>DACCU avoids CO₂ transport and storage</i>	11
1.2.7	<i>DACCU for a circular economy</i>	12
1.3	Aim and objectives of this PhD study	12
1.4	Novel contributions of this study	13
1.5	Scope of this study	15
1.6	Research methodology	15
1.7	Software tools to be used for this study	16
1.7.1	<i>Aspen Plus®</i>	16
1.7.2	<i>Aspen Custom Modeller®</i>	17
1.7.3	<i>System Advisor Model</i>	17
1.8	Outline of the thesis	18
Chapter 2.	Literature review	20
2.1	Overview	20
2.2	Different plants, lab rigs and liquid sorbents for L-DAC	20
2.2.1	<i>Worldwide commercial L-DAC plants</i>	20
2.2.2	<i>Pilot plants and experimental data</i>	22
2.2.3	<i>Lab rigs and experimental data</i>	26
2.2.4	<i>Aqueous sorbents used for L-DAC</i>	27
2.3	Review of model-based studies for L-DAC process	28

2.3.1	<i>Model development for L-DAC</i>	28
2.3.2	<i>Modelling and simulation studies of L-DAC</i>	35
2.3.3	<i>Studies of the L-DAC process based on different energy sources</i>	35
2.3.4	<i>Technical, economic and environmental evaluation studies of L-DAC</i>	36
2.4	Review of CO ₂ -FTS technology	41
2.4.1	<i>Experimental work</i>	41
2.4.2	<i>Model-based studies</i>	41
2.5	Summary	45
Chapter 3.	Model development, simulation and comparison of liquid-based DAC process	47
3.1	Overview	47
3.2	Model development of L-DAC at commercial scale	47
3.2.1	<i>Thermodynamic model and chemical reactions</i>	48
3.2.2	<i>Process model development</i>	50
3.3	Model comparison of L-DAC at commercial scale	56
3.4	Conclusion	59
Chapter 4.	Model development, simulation, validation and scale-up of solar calciner	61
4.1	Overview	61
4.2	Pilot solar calciner and newly-proposed solar calciner	61
4.2.1	<i>Pilot air-fluidised solar calciner</i>	61
4.2.2	<i>Newly-proposed hydrogen-fluidised solar calciner</i>	64

4.3 Model development of solar calciner at pilot scale.....	66
4.3.1 Assumptions	66
4.3.2 Model implementation	66
4.4 Validation of solar calciner at pilot scale.....	69
4.5 Scale-up of solar calciner from pilot scale to commercial scale.....	71
4.6 Conclusion	77
Chapter 5. Model development, simulation and validation of direct CO₂-FTS process	78
5.1 Overview	78
5.2 Model development of CO ₂ -FTS process at lab scale	78
5.2.1 Assumptions	78
5.2.2 Modelling of hydrocarbon distribution.....	79
5.2.3 Model implementation of CO ₂ -FTS process using Aspen Plus® and Aspen Customer Modeller®.....	81
5.3 Model validation at lab scale.....	83
5.4 Simulation of the modified CO ₂ -FTS process for jet fuel production at commercial scale	87
5.4.1 Assumptions	87
5.4.2 CO ₂ -FTS process for jet fuel production	87
5.4.3 Ex-situ water removal through gas recycling.....	88
5.5 Conclusion	89
Chapter 6. Process design, model development and simulation of solar-driven DACCU process for SAF production	90
6.1 Overview	90

6.2 Process design	90
6.2.1 Innovations.....	90
6.2.2 Process description.....	92
6.3 Model development of solar-driven DACCU at commercial scale	98
6.3.1 Model development of solar-driven DAC process at commercial scale.....	98
6.3.2 Model development of solar calcination at commercial scale.....	98
6.3.3 Model development of CO ₂ -to-SAF at commercial scale	99
6.4 Simulation of solar-driven DACCU at commercial scale.....	99
6.5 Conclusion	99
Chapter 7. Evaluation of solar-driven DACCU process for SAF production: techno-economic assessment, sensitivity analysis, geographical analysis and roadmap analysis	103
7.1 Overview	103
7.2 TEA framework and methodology.....	103
7.2.1 Capital expenditure.....	107
7.2.2 Operational expenditure	108
7.2.3 Levelized cost and minimum selling price	109
7.2.4 Sensitivity analysis	110
7.2.5 Preliminary LCA.....	110
7.2.6 Location screening.....	111
7.2.7 Calculation of land use	112
7.3 TEA.....	113

7.3.1	<i>Baseline TEA.....</i>	<i>113</i>
7.3.2	<i>Comparison with DAC proposed by Carbon Engineering</i>	<i>118</i>
7.3.3	<i>Comparison with previous DACCS</i>	<i>120</i>
7.3.4	<i>Comparison with previous DACCU.....</i>	<i>121</i>
7.4	Sensitivity analysis under optimistic and pessimistic scenarios	122
7.5	Geographical analysis	131
7.6	Roadmap analysis	136
7.7	Conclusion	138
Chapter 8.	Conclusions and recommendations.....	140
8.1	Conclusions of the thesis.....	140
8.2	Recommendations for future work.....	143
References	146

List of Tables

Table 2.1 Review of mass transfer studies of structured packing for air contactor	29
Table 2.2 Summary of literature review on modelling and simulation of L-DAC	34
Table 2.3 Reported technical specifications of L-DAC	39
Table 2.4 Reported economic evaluation of L-DAC	40
Table 2.5 Summary of studies performed for CO ₂ -FTS process to jet fuel at lab-scale	43
Table 2.6 Previous studies on modelling and simulation of CO ₂ -FTS process to liquid fuels	44
Table 3.1 Chemistry settings of equilibrium reactions for rate-based air contactor model	49
Table 3.2 Chemistry settings of kinetic reactions for rate-based air contactor model	50
Table 3.3 Modified Sulzer 250Y PVC packing setting in Aspen Plus®	53
Table 3.4 Specifications of unit operations for L-DAC process	55
Table 3.5 The simulated L-DAC components in Aspen Plus®	56
Table 3.6 Stream inputs into the 1MtCO ₂ /year L-DAC process model	57
Table 3.7 Model stream results and comparison with stream results from CE's DAC process	58
Table 3.8 Comparison of simulated unit performance with CE's design	59
Table 4.1 Specification of fluidised bed setup in Aspen Plus®	67
Table 4.2 Equations for enthalpy correlation and thermal efficiency calculation.....	68
Table 4.3 Process specifications of solar calcination process at pilot scale.....	69
Table 4.4 Validation of two representative experimental data of solar calcination.....	70

Table 4.5 Design and operating parameters of large-scale hydrogen-based solar calciner through scaling approach.....	76
Table 5.1 Products and chemical reactions implemented for the CO ₂ -FTS model.....	82
Table 5.2 Input parameters used for model validation.....	84
Table 5.3 Model validation results of selectivity for different product categories	86
Table 6.1 Design specification of major units of 1 MtCO ₂ /year solar-driven DACCU plant	97
Table 7.1 Technical parameters for the solar-driven DACCU plant for the base case, optimistic and pessimistic scenarios.....	105
Table 7.2 Five selected CSP project locations used for geographical analysis.....	112
Table 7.3 Equipment installed cost breakdown by section at base case	116
Table 7.4 CAPEX summary of 1 MtCO ₂ /yr solar-driven DACCU plant by section at base case	117
Table 7.5 Sensitivity analysis summary of MSP, related to Figure 7.12	128
Table 7.6 Sensitivity analysis summary of LCOD, related to Figure 7.13	129
Table 7.7 Regional hydrogen cost, PV cost and WACC	132

List of Figures

Figure 1.1 Schematic of carbon capture, utilisation and storage (IEA, 2020a)	3
Figure 1.2 Schematic illustration of the L-DAC process (Fasihi et al., 2019).....	5
Figure 1.3 Schematic illustration of Climeworks S-DAC process (Beuttler et al., 2019)	6
Figure 1.4 Schematic description of the indirect and direct Fischer-Tropsch synthesis-based CO ₂ utilisation pathways (Panzone et al., 2020)	7
Figure 1.5 Overview of the methodology used in this thesis	16
Figure 2.1 Envisioned large-scale L-DAC plant (1PointFive, 2024).....	21
Figure 2.2 CO ₂ capture contactor (1. Fan; 2. Fluid Basin; 3. Fluid Pump; 4. Packing; 5. Fluid Distributor; 6. Air Outlet with Demister.) (Mahmoudkhani et al., 2009)	23
Figure 2.3 Schematic of CE's outdoor prototype air contactor (Holmes et al., 2013).....	24
Figure 2.4 CE's pilot DAC plant (Carbon Engineering, 2023).....	25
Figure 2.5 Process design of a CE's commercial DAC plant (Keith et al., 2018).....	33
Figure 3.1 Block flow diagram of L-DAC process	51
Figure 3.2 Model development for one air contactor module.....	52
Figure 3.3 Model development for commercial-scale air contactor	52
Figure 4.1 Photograph of the 1-MW Odeillo's solar furnace	62
Figure 4.2 Schematic diagram of the pilot-scale solar reactor and the dimension of 1 st stage fluidised bed	63
Figure 4.3 Schematic of the solar calciner—a hydrogen-based four-stage horizontal fluidised bed.....	65
Figure 4.4 Schematic of the solar calcination, encompassing the heliostat field, parabolic mirror and solar calciner.....	65

Figure 4.5 Four-stage horizontal solar calciner in Aspen Plus® flowsheet.....	67
Figure 4.6 Hydrodynamics in the solar calciner. (a) Solids volume fraction along height. (b) CO ₂ mass fraction along height (FB: fluidised bed).....	71
Figure 4.7 Scale-up principle of solar calciner for achieving the same reaction conversion.....	74
Figure 4.8 Bed height and solid voidage as a function of bubble volume fraction at large-scale.....	75
Figure 5.1 Flowsheet diagram of CO ₂ -FTS process implemented in Aspen Plus® using Fortran® Routines	83
Figure 5.2 Model prediction of ASF plot compared with experimental data	85
Figure 5.3 Model prediction and experimental values of CO ₂ -FTS product selectivity	86
Figure 5.4 Commercial CO ₂ -FTS process for jet fuel production	88
Figure 5.5 Commercial CO ₂ -FTS with gas recycling for jet fuel production	89
Figure 6.1 Process chemistry of solar-driven DACCU process.....	93
Figure 6.2 Simplified process flow diagram of the solar -driven DACCU process, incorporating the solar-driven DAC and CO ₂ -to-SAF sections.	94
Figure 6.3 Process flow diagram and stream results of solar-driven DAC section excludes solar calcination.....	100
Figure 6.4 Process flow diagram and stream results of solar calcination subsection in solar-driven DAC section	101
Figure 6.5 Process flow diagram and stream results of CO ₂ -to-SAF section	102
Figure 7.1 Schematic overview of techno-economic input and output parameters	104
Figure 7.2 Global map of current high-temperature CSP plants with bubble size representing plant scale	111
Figure 7.3 Principle of SAM analysis for land use calculation.....	113

Figure 7.4 The base case results for (a) minimum selling price of SAF and (b) levelized cost of proposed solar-driven DACCU process	114
Figure 7.5 Detailed CAPEX breakdown of solar-driven DACCU in the base case	115
Figure 7.6 Annual operational cost of solar-driven DACCU in the base case disaggregated by process step	118
Figure 7.7 Comparison between natural gas combustion-based DAC (NG-DAC) and the proposed solar-driven DAC (CSP-DAC) for (a) electricity demand, (b) life cycle CO ₂ emissions, and (c) levelized cost	120
Figure 7.8 Comparison of proposed DACCU with previous DACCS and DACCU studies in terms of (a) levelized cost and (b) MSP.	121
Figure 7.9 Map of DAC plant CO ₂ capture productivity as a function of CO ₂ concentration, V _{air} and ATD.	123
Figure 7.10 The impact of scaling factor on the number of solar calciners and total hydrogen flow rate..	124
Figure 7.11 Process improvement on CO ₂ conversion and SAF yield under gas recovery rate from 0-99%	125
Figure 7.12 Single variable sensitivity analysis of baseline cost for MSP of SAF	126
Figure 7.13 Single variable sensitivity analysis of baseline cost for LCOD.....	127
Figure 7.14 World map of land use for solar-driven DACCU plant.....	131
Figure 7.15 MSP of SAF with low-carbon hydrogen sourced at country-specific prices at (a) local WACC and (b) global averaged WACC of 4.2%.	134
Figure 7.16 Levelized cost of DACCU with low-carbon hydrogen sourced at country-specific prices at (a) local WACC and (b) global averaged WACC of 4.2%.....	135
Figure 7.17 Roadmap to reducing base case cost of MSP by successive changes to cost-relevant parameters from FOAK to NOAK	137

Figure 7.18 Roadmap to reducing base case cost of LCOD by successive changes to cost-relevant parameters from FOAK to NOAK	138
--	-----

Nomenclatures

A, B, C, D	Equilibrium constant
A_{module}	Cross-section area of each air contactor module (m ²)
a_{ij}	Reaction order of component i in reaction j
b	Carbon number at break point
C_i	Concentration of species
c	Olefin desorption rate constant
D_T	Bed diameter (m)
d_b	Mean bubble diameter (m)
d_p	Particle diameter (μm)
E	Activation energy (kJ/kmol)
f	Sorbent flow rate (m ² /s)
f_1 and f_2	Fractions of hydrocarbons
F_G	Flow rate of gas (kg/h)
F_s	Flow rate of solids (kg/h)
h	Height of a module (m)
h_{air}	Enthalpy of air (J)
h_{CaCO_3}	Enthalpy of CaCO ₃ (J)
K_a	Interchange coefficient (1/s)
K_{eq}	Temperature-dependent equilibrium constants
k_1, k_5 and $k_{6,0}$	Kinetic constants
L	Bed dimension (m)
\bar{M}	Average molecular weight (g/mol)
M_{CaCO_3}	Molecular weight of CaCO ₃
M_n	Molecular weight of hydrocarbon n
n	Scaling factor
N_{HC}	Total molar flowrate of produced hydrocarbons (kmol/hr)
n_{HC_n}	Molar flowrate of hydrocarbon n (kmol/hr)
N_m	Mass transfer numbers
$N_{modules}$	Number of air contactor modules

N_r	Reaction numbers
P_i	Partial pressure (MPa)
P_n	Distributor orifice diameter (m)
Q_l	Average liquid flow rate (L/m ² s)
R	Universal gas constant
Re	Reynolds number
r	Reaction rates (m ³ /kmol·s)
S_n	Selectivity of hydrocarbon n
T	Temperature (K)
t_{op}	Operating time (s)
u	Fluid velocity (m/s)
u_b	Bubble velocity (m/s)
U_G	Gas superficial velocity (m/s)
U_{mf}	Minimum fluidisation velocity (mm/s)
v	Particle velocity (m/s)
W_n	Weight fraction of hydrocarbon n
X_i	Conversion of reactant i (mol%)
x_{CaCO_3}	Mass fraction of CaCO ₃
x_n	Mole fraction of hydrocarbon n
$Y_{jet\ fuel}$	Yield of jet fuel (mol%)

Greek letters

α	Chain growth probabilities
α_{out}	CaCO ₃ conversion
β	Coefficient of drag force
λ	Fitting parameter
ε	Bed voidage
ε_b	Volume fraction of bubble
ε_s	Solid bed voidage
μ	Fluid viscosity (Pa·s)
ϕ	Particle sphericity

ρ_f	Fluid density (kg/m ³)
ρ_s	Particle density (kg/m ³)
$\rho_{Sorbent}$	Density of the sorbent (kg/L)
η_{fan}	Fan efficiency
η_{th}	Thermochemical efficiency
η_{thch}	Thermal efficiency
ΔH	Enthalpy of reaction
ΔP	Pressure drop (Pa)

Abbreviations

ACM	Aspen Custom Modeller®
AE	Alkaline electrolyser
APS	American Physical Society
ASF	Anderson-Schulz-Flory
ASU	Air separation unit
ATD	Air travel distance
BECCS	Bioenergy with carbon capture and storage
BFD	Block flow diagram
CAPEX	Capital expenditure
CCS	Carbon capture and storage
CCUS	Carbon capture, utilisation and storage
CDR	Carbon dioxide removal
CE	Carbon Engineering
CF	Capture fraction
CFB	Circulating fluidised bed
CHP	Combined heat and power
CI	Carbon intensity
CRF	Capital recovery factor
CSP	Concentrated solar power
DAC	Direct air capture
DACCS	Direct air capture and CO ₂ storage
DACCU	Direct air capture and CO ₂ utilisation
DNI	Direct normal irradiation
EOR	Enhanced oil recovery
FB	Fluidised bed
FOAK	First-of-a-kind
FTS	Fischer-Tropsch synthesis
GHG	Greenhouse gas
HRSG	Heat recovery steam generator
HT	High temperature
IEA	International Energy Agency

IFC	Indirect field costs
IPCC	Intergovernmental Panel on Climate Change
LCA	Life cycle assessment
LCOD	Levelized cost of solar-driven DACCU
MSP	Minimum selling price
NG	Natural gas
NOAK	N th -of-a-kind
NREL	National Renewable Energy Laboratory
NSRD	National Solar Radiation Database
OPEX	Operational expenditure
PB	Packed bed
PCC	Post-combustion carbon capture
PEM	Proton exchange membrane
PV	Photovoltaics
RE-SNG	Renewable synthetic natural gas
RWGS	Reverse water gas shift
SAF	Sustainable aviation fuel
SAM	System Advisor Model
SM	Solar multiple
SMR	Steam methane reforming
SNG	Synthetic natural gas
SOEC	Solid oxide electrolysis cell
SSA	Specific surface area
TDFC	Total direct field costs
TEA	Techno-economic assessment
TFC	Total field costs
TNFC	Total non-field costs
TPC	Total project costs
WACC	Weighted average cost of capital

Chapter 1. Introduction

This chapter establishes the foundation of the thesis and guiding through the context and structure of the research. Section 1.1 provides an overview of the study's background. The motivation driving this study is detailed in Section 1.2, followed by the aim and objectives presented in Section 1.3. Section 1.4 highlights the novel contributions of this PhD thesis, emphasising the unique aspects of the work. The scope of the study is defined in Section 1.5, delineating the boundaries and focus areas of the research. Section 1.6 describes the research methodology, outlining the approach taken to achieve the study objectives. The software tools used in the research are presented in Section 1.7. Finally, Section 1.8 provides an outline of the thesis, summarising the content in the remaining chapters of this PhD thesis.

1.1 Background

1.1.1 Energy demand, CO₂ emissions and climate change

Global energy demand has been steadily increasing due to population growth, industrialisation, and technological advancements. According to the International Energy Agency (IEA), global energy consumption has risen by approximately 50% over the past three decades, driven primarily by fossil fuels such as coal, oil, and natural gas. Despite significant progress in renewable energy technologies, fossil fuels still comprise about 80% of the global energy mix, posing significant challenges to achieving global climate goals.

The combustion of fossil fuels is the largest source of anthropogenic CO₂ emissions, which contribute substantially to global warming and climate change. According to the Intergovernmental Panel on Climate Change (IPCC), atmospheric CO₂ concentrations have risen from approximately 310 ppm in pre-industrial times to over 420 ppm today. This

increase in CO₂ level is closely linked to observed extreme weather patterns and climate disruptions, signalling that human-induced climate change has already caused widespread adverse impacts and irreversible damage to natural ecosystems and human societies (IPCC, 2023).

To mitigate these impacts, drastic reductions in CO₂ emissions are essential to limit global temperature rise to below 2°C above pre-industrial levels, as outlined in the Paris Agreement. Failing to meet these targets could lead to severe environmental, economic, and social consequences, including more frequent extreme weather events, rising sea levels, and loss of biodiversity. Addressing these emissions is therefore critical not only for mitigating climate change but also for ensuring sustainable development and safeguarding the environment for future generations.

1.1.2 Carbon capture, utilisation and storage

Carbon capture, utilisation and storage (CCUS) technologies have emerged as essential tools for reducing CO₂ emissions from industrial and energy sectors. As shown in Figure 1.1, CCUS involves capturing CO₂ from point sources (such as power plants and industrial facilities) or directly from the air, and then either storing it underground or utilising it in various applications (such as enhanced oil recovery and producing CO₂-derived fuels).

However, traditional CCUS technologies (such as post-combustion carbon capture) have limitations when it comes to addressing CO₂ emissions from dispersed and diffuse sources, such as those from transportation, agriculture, and smaller-scale industrial processes. This is where direct air capture (DAC), a subset of CCUS, plays a crucial role. DAC captures CO₂

directly from the ambient air, making it uniquely capable of addressing emissions that are not tied to specific point sources.

By removing CO₂ from the atmosphere, DAC not only complements conventional CCUS approaches but also provides a pathway to negative emissions, which are vital for achieving net-zero and negative carbon targets. As such, DAC represents an innovative extension of CCUS technologies, enhancing their overall potential to mitigate climate change by targeting CO₂ that is history accumulated in the atmosphere.

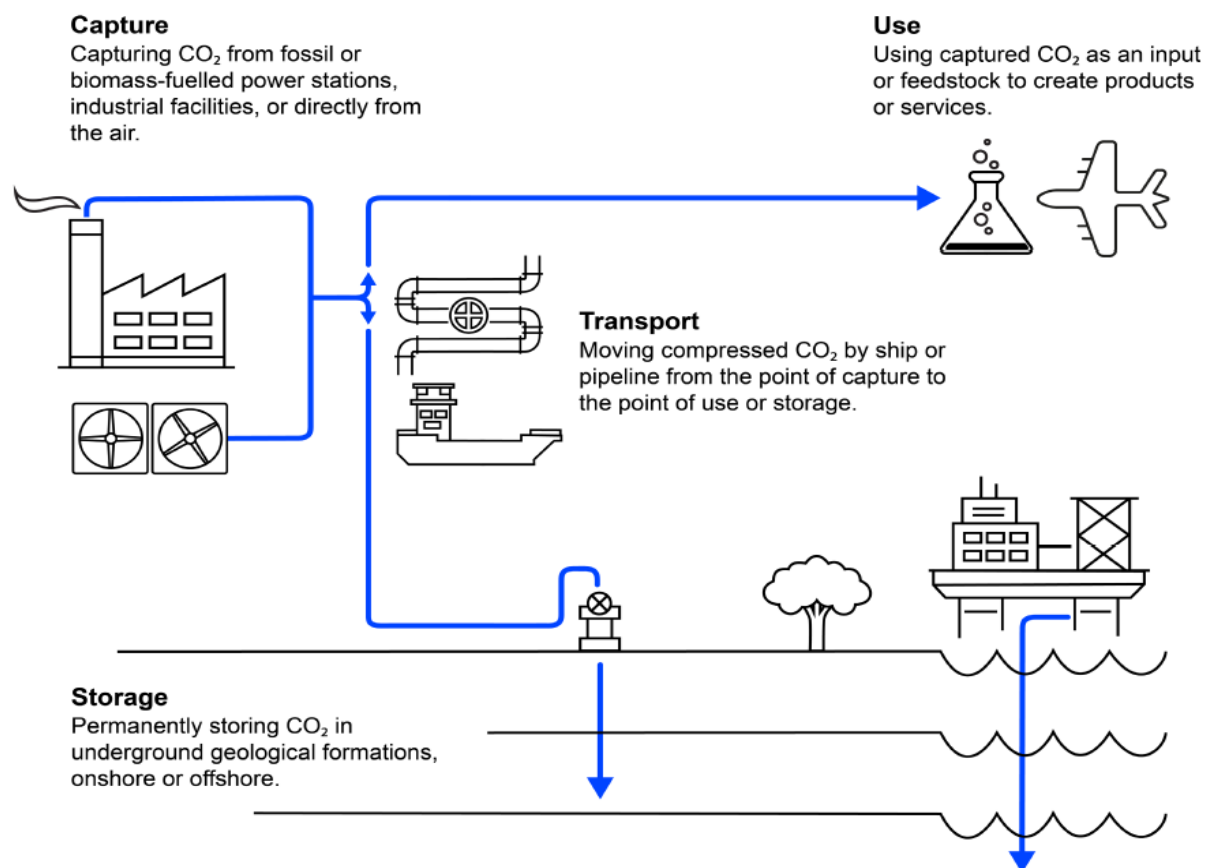


Figure 1.1 Schematic of carbon capture, utilisation and storage (IEA, 2020a)

1.1.3 DAC technology overview

DAC is an emerging technology for removing CO₂ directly from the atmosphere. Currently, there are two major DAC technologies: liquid-based DAC (L-DAC) and solid-based DAC (S-DAC). L-DAC uses chemical solutions to absorb CO₂, followed by desorption through calcium looping. S-DAC employs solid sorbent filters to adsorb CO₂, which is then collected through various regeneration methods. Additionally, other emerging approaches, such as electrochemical DAC and hybrid DAC, are under development.

1.1.3.1 L-DAC

L-DAC typically comprises two chemical loops, as illustrated in Figure 1.2, a commercial process developed by Canadian company Carbon Engineering Ltd (CE). The first chemical loop involves CO₂ absorption, where ambient air driven by fans contacts with the sprayed aqueous alkaline solution like sodium hydroxide (NaOH) or potassium hydroxide (KOH) in the air contactor. CO₂ reacts with the alkaline solution to form a carbonate solution. To regenerate the alkaline solution for reuse in the absorption process, the carbonate solution is mixed with calcium hydroxide (Ca(OH)₂) to form solid calcium carbonate (CaCO₃) and regenerate the alkaline solution in the pellet reactor. The CaCO₃ is heated in calciner at nearly 900°C to release CO₂ which is also the most energy-intensive step. With the addition of water in the slaker, Ca(OH)₂ is regenerated with the CaO produced from calciner (Fasihi et al., 2019).

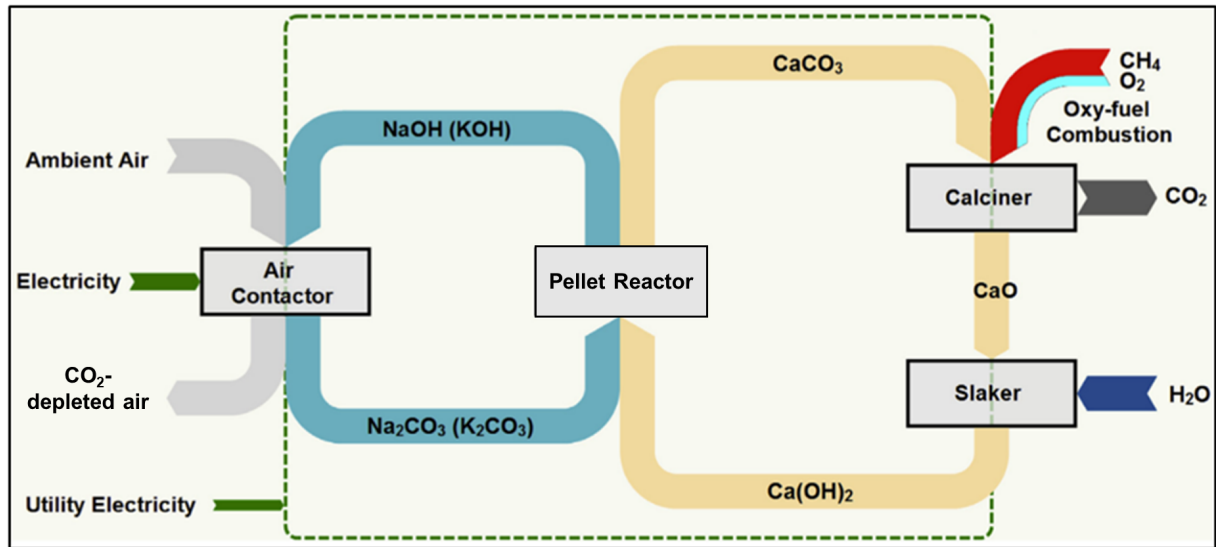


Figure 1.2 Schematic illustration of the L-DAC process (Fasihi et al., 2019)

1.1.3.2 S-DAC

S-DAC uses solid sorbent in a single unit where adsorption and desorption occur one after another (see Figure 1.3). During the adsorption phase, ambient air enters the system naturally or is blown by fans. At ambient temperature, CO_2 chemically binds to the filter, and CO_2 -free air leaves the system. Once the sorbent becomes saturated with CO_2 , the system transitions to the desorption phase, where the CO_2 is released. This is achieved either by creating a vacuum or introducing steam into the system to lower pressure or increase temperature. The released CO_2 is then collected for purification, compression or utilisation. The remaining air is swept out through a pressure drop by vacuuming or inserting steam into the system. Based on specific sorbent properties, desorption happens by heating the system at a particular temperature. To begin a new cycle, the system is cooled back to ambient conditions (Fasihi et al., 2019).

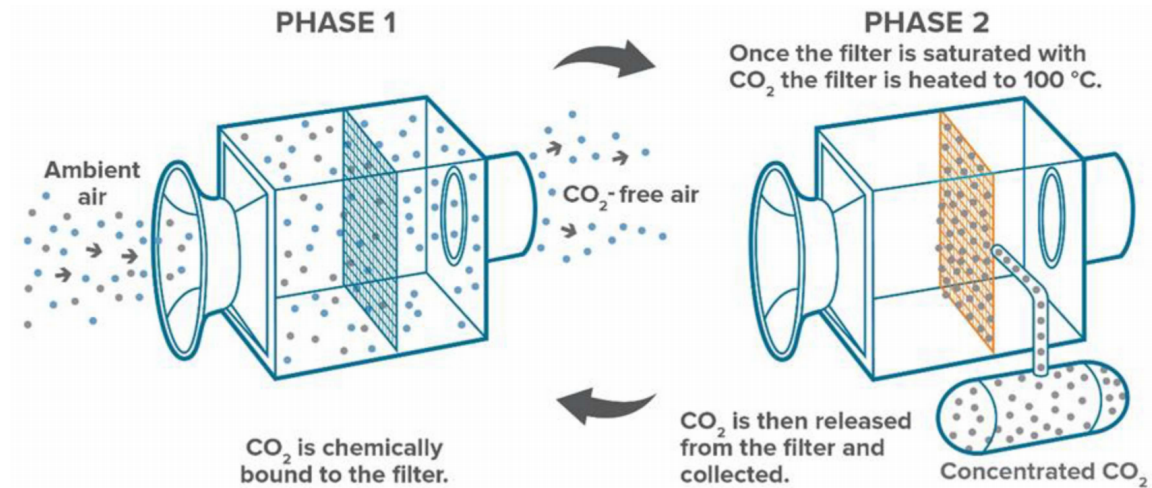


Figure 1.3 Schematic illustration of Climeworks S-DAC process (Beuttler et al., 2019)

1.1.3.3 DACCS and DACCU

Direct air capture and CO_2 storage (DACCS) and direct air capture and CO_2 utilisation (DACCU) are two ultimate fates of DAC. For the storage pathway, CO_2 is permanently sequestered in subsurface geologic formations where it remains trapped or reacts with present minerals to become carbonate rock and is, therefore, a true carbon-negative mitigation strategy. In terms of the DACCU pathway, air-captured CO_2 is used as a commodity feedstock to produce value-added carbon-neutral products like chemicals and fuels.

1.1.4 CO_2 utilisation technology overview

CO_2 conversion can be regarded as a promising approach to produce carbon-neutral products and create a circular economy (IEA, 2019). A broad range of CO_2 -derived products, including synthetic fuels (e.g. gasoline and jet fuel) (Ishaq and Crawford, 2023, Zang et al., 2021b, van der Giesen et al., 2014), chemical materials (e.g. plastics and fibres) (Zhou et al., 2022, Dutta et al., 2017), and building materials (e.g. cement and construction aggregates) (Li

et al., 2022, Desport and Selosse, 2022) have been introduced in the literature. CO₂-derived fuels can serve as alternatives for hard-to-electrify transportation sectors, including heavy-duty trucks, shipping, and aviation. As these modes of transportation continue to rely partially on liquid fuels, the necessity for new pathways to produce low-carbon synthetic liquid fuels will persist (Bushuyev et al., 2018).

CO₂ utilisation via the Fischer-Tropsch synthesis (FTS) process provides the pathway to generate synthetic jet fuel. The FTS process refers to a polymerisation process which uses syngas (CO and H₂) as the source for the synthesis of hydrocarbon (HC) chains. FTS reactions could produce alkanes, olefins and alcohol products. In the indirect method (see Figure 1.4), firstly is syngas production from CO₂ through solid oxide electrolysis cell (SOEC), reforming and reverse water gas shift (RWGS) followed by the FTS process in two or more reactors (Kamkeng and Wang, 2023). The one-step method, also known as the modified CO₂-FTS process has recently gained more attention as it allows the RWGS reaction and FTS reactions to be in a single reactor (Ye et al., 2019).

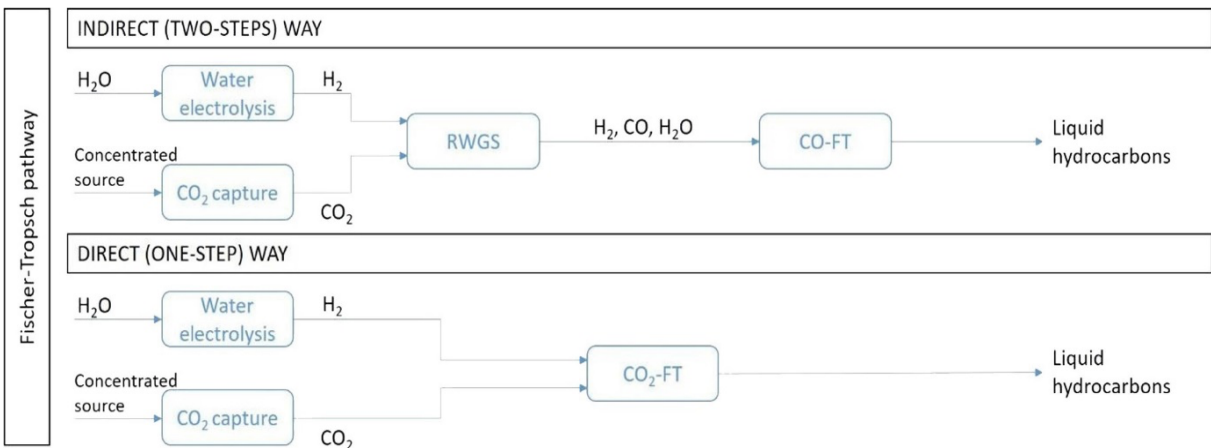


Figure 1.4 Schematic description of the indirect and direct Fischer-Tropsch synthesis-based CO₂ utilisation pathways (Panzone et al., 2020)

1.2 Motivation for this study

The section outlines the key motivations for this research, highlighting the critical challenges of large-scale L-DAC and the unique opportunities presented by integrating solar energy into DACCU systems for SAF production.

1.2.1 DAC as a key CO₂ removal technology

Global energy-related CO₂ emissions reached a new record of 37.4 Gt in 2023, while current CCUS technologies capture less than 0.5% of these emissions. A comprehensive CO₂ reduction portfolio must be deployed quickly and efficiently to achieve the net-zero target. In the net-zero scenario, CCUS is expected to contribute nearly 15% (6.7 Gt/year) of the CO₂ reduction potential. This will require CO₂ capture across various sectors, including existing power plants and factories, emerging hydrogen and bioethanol production, and hard-to-abate sectors such as the atmosphere and transportation (IEA, 2020b, IEA, 2024a).

Within the CCUS toolbox, DAC is emerging as a crucial carbon dioxide removal (CDR) technology. Unlike point-source CO₂ capture technologies that targets emissions from industrial facilities, DAC can directly remove CO₂ from ambient air, making it an essential tool for tackling emissions that are historically accumulated or otherwise unavoidable, such as those from heavy-duty and long-haul transportation. Compared to other CDR approaches such as afforestation and reforestation, and bioenergy with carbon capture and storage (BECCS), DAC offers scalability without the need for extensive land use or ecological trade-offs. As global CO₂ levels continue to rise, DAC's role is expected to expand, with projections estimating the capture of over 85 Mt of CO₂ by 2030 and up to 980 Mt by 2050

(IEA, 2024b). This study explores the potential of integrating renewable energy, particularly solar energy to enhance DAC's scalability and sustainability.

1.2.2 L-DAC is promising but is energy-intensive and cost-intensive

The L-DAC process developed by CE stands out for its relatively low energy consumption of 5.25-8.81 GJ/t_{CO2} (Keith et al., 2018), outperforming other amine-based (15.74 GJ/t_{CO2}) (Kiani et al., 2020) and solid-based DAC approaches (7.2-9.5 GJ/t_{CO2}) (Lebling et al., 2021, IEA, 2024b). Furthermore, CE's DAC technology is adapted from existing commercial units and is at the demonstration stage (technology readiness level [TRL] 7-8), which has the great opportunity to be commercially successful (Bisotti et al., 2024).

However, the energy demand for L-DAC is higher when compared with conventional point sources-based carbon capture technologies such as post-combustion carbon capture using solvents (2.76-5.34 GJ/t_{CO2}) (Otitoju et al., 2021). This is mainly because the low concentration of CO₂ in the atmosphere (approximately 420 ppm) necessitates processing large volumes of air, leading to substantial energy consumption. The cost of L-DAC is also very high estimated at US\$200-700/t_{CO2} (IEAGHG, 2021). Reducing the high energy and cost barriers is critical for making DAC a viable carbon removal solution, and this research seeks to address these challenges by leveraging solar energy to power DAC systems.

1.2.3 Transition of energy source from natural gas to solar energy

Current L-DAC systems primarily rely on natural gas combustion to provide the electricity and heat demands. It should be noted that the high-temperature (~900°C) thermal energy demand accounts for over 75% of the total energy demand (Keith et al., 2018, Sabatino et al., 2021). From a life cycle point of view, to capture and store 1 t of atmospheric CO₂, 0.58

t (+0.2/-0.03 t) CO₂-equivalent emissions would be released, which partially offsets the captured CO₂ (Madhu et al., 2021). Transitioning to renewable energy sources, can significantly reduce these emissions and maximise the carbon removal potential of DAC (IEAGHG, 2021, Madhu et al., 2021, Liu et al., 2020). Solar energy is a clean, abundant, and renewable resource. More importantly, it can provide the high-temperature heat via concentrated solar energy for L-DAC, thereby reducing the reliance on fossil fuels, and lowering the overall carbon footprint. This study focuses on integrating solar energy to enhance the sustainability and environmental friendliness of DACCU systems.

1.2.4 Demonstrating L-DAC at a large scale as a priority

Currently, there are no fully operational large-scale DAC plants (e.g., 1 MtCO₂/year) globally, with most existing systems being small pilot projects or at demonstration stages (IEA, 2024b). Scaling up DAC is crucial to meeting global carbon removal targets and significantly impacts atmospheric CO₂ levels. Developing large-scale DAC plants is essential for achieving the necessary economies of scale, reducing costs, and improving the technology's overall efficiency. However, scaling up poses significant challenges in terms of energy supply, infrastructure, and integration with existing energy grids. This research focuses on addressing these challenges by exploring solar-driven DACCU systems as a sustainable and scalable solution, ultimately contributing to the development of large-scale DAC plants capable of capturing millions of tonnes of CO₂ annually.

However, reaching the level of DAC deployment target by 2050 in the net-zero scenario, IEA suggested that it will require “on average eight large-scale (1 MtCO₂/year) DAC plants to be built each year during the current decade, 50 plants to be built each year during 2030-2040 and almost 40 plants a year to be built between 2040 and 2050.” In total, around

thousands of large-scale DAC plants could create an environmental impact at global scale (IEA, 2024b).

1.2.5 DAC for decarbonisation in net zero aviation

The aviation industry is one of the most challenging sectors to decarbonise, responsible for 10% of transportation emissions and 2.5% of global emissions (1.03 Gt CO₂ in 2019) (Quéré et al., 2018). With the continued rise in air travel, CO₂ emissions from aviation are projected to reach 1.9 Gt by 2050 (Bergero et al., 2023). However, replacing conventional aviation fuel with alternative renewable energy options such as batteries or hydrogen is not feasible in the short term because aircraft rely on energy-dense liquid fuel (Cui et al., 2024). SAF, produced from non-petroleum feedstocks, has emerged as a promising solution due to its high energy density and drop-in compatibility with existing aircraft engines (Cui et al., 2024). This study investigates the application of DAC as low-carbon feedstock for large-scale SAF production, providing a pathway to decarbonisation aviation (Vardon et al., 2022, Sacchi et al., 2023).

1.2.6 DACCU avoids CO₂ transport and storage

DACCU presents a compelling alternative to traditional CO₂ storage by enabling the immediate conversion of captured CO₂ into valuable products, such as fuels, chemicals, or building materials. This approach not only adds economic value but also reduces the need for extensive CO₂ transport networks and underground storage facilities, overcoming significant logistical and economic barriers. By integrating DAC with CO₂ utilisation, this study not only addresses the challenge of atmospheric carbon removal but also adds economic value, enhancing the overall viability of DAC technology.

1.2.7 DACCU for a circular economy

The circular economy is a sustainable model that focuses on reducing waste, reusing resources, and recycling materials to minimise environmental impact. DACCU supports this model by capturing CO₂ from the air and turning it into valuable products like chemicals and synthetic fuels (Erans et al., 2022, Hepburn et al., 2019). This would enable the recycling of valuable materials instead of storing them in deep reservoirs (Langie et al., 2022, Bushuyev et al., 2018, IEA, 2019). This study investigates a solar-driven DACCU system, creating a closed-loop where captured CO₂ is recycled into SAF.

1.3 Aim and objectives of this PhD study

This PhD research aims to provide a sustainable decarbonisation strategy for a circular economy through the process design of a large-scale solar-energy powered liquid-solvent based DAC process with one-step CO₂-FTS to produce value-added fuel (i.e., aviation fuel) via modelling\simulation, and technical, economic and environmental performance analyses. The research objectives include the following:

- A comprehensive literature review of L-DAC and CO₂-FTS process.
- Model development, simulation and model comparison of the L-DAC process in Aspen Plus®.
- Model development, simulation, model validation and scale-up of the solar calciner in Aspen Plus® and Aspen Custom Modeller® (ACM).
- Model development, simulation, model validation and scale-up of the CO₂-FTS in Aspen Plus® and ACM.

- Integration of the L-DAC, solar calciner and CO₂-FTS models to form the solar-driven DACCU process in Aspen Plus® with linkage to ACM.
- Technical and economic performance assessment of solar-driven DACCU process under the baseline scenario and comparison with previous DAC studies (including DAC, DACCS and DACCU).
- Further performance assessment through sensitivity analysis under optimistic and pessimistic scenarios, geographical analysis at five selected locations, and roadmap analysis for future cost projection.

1.4 Novel contributions of this study

This work proposes a large-scale route to produce SAF from the air using solar-driven L-DAC and direct CO₂- FTS processes. The key novelties of this work include:

- I. **Design of a large-scale solar-driven L-DAC with solar calciner:** The proposed L-DAC process uses a specially designed solar calciner with hydrogen as the fluidisation medium. This is different from the CE's design, which uses a natural gas-based calciner with oxygen as the fluidisation medium (Keith et al., 2018). Compared with CE's L-DAC, the new design eliminates some units (i.e. the air separation unit (ASU) and CO₂ absorber) and reduces the reliance on fossil fuels for high-temperature CaCO₃-mediated desorption. This helps reduce electricity demand, capital costs for minor units and the carbon footprint of the DAC process.
- II. **Large-scale DACCU with one-step FTS:** The DACCU process involves a tailored one-step CO₂-FTS process using Fe-Mn-K catalyst to produce jet fuel range hydrocarbons (C₈-C₁₆). The application of the newly designed H₂-fluidised solar

calciner in the DAC process also allows for the use of H_2 as feedstock for CO_2 hydrogenation. Compared to the previous stepwise DACCU process applying conventional indirect route of FTS-based CO_2 hydrogenation, the proposed process using direct CO_2 -FTS is well-suited for industry applications. It eliminates steps such as syngas production, H_2 preparation and CO_2 purification, making it easier to operate and more cost-effective. Additionally, an ex-situ water removal strategy and gas recycling are adopted to maximize process efficiency and economic viability.

- III. **Techno-economic assessment (TEA) based on different geographical locations:** A comprehensive TEA has been conducted for the large-scale DACCU based on five geographical locations worldwide. The sensitivity analysis considered optimistic and pessimistic scenarios to highlight the cost of hydrogen and gas recycle ratio as key variables for process improvements and optimisations. The feasibility of the proposed DACCU plant is further investigated in the USA, Chile, Spain, South Africa and China. Favourable deployment locations are those regions with high solar irradiance, low land costs and low local weighted average costs of capital (WACC). As is currently known, no study has been conducted on the TEA of siting the DACCU plant in these locations.
- IV. **A roadmap predicting DACCU cost reduction potential:** A roadmap for achieving future cost reduction is provided from first-of-a-kind (FOAK) plants to N^{th} -of-a-kind (NOAK) plants, demonstrating the potential for commercialisation of the technology to policymakers and industry investors. The proposed DACCU process could be economically viable compared to the current SAF market, particularly with deployment in low-risk countries, improvements in process efficiencies and cost reduction in H_2 production, CAPEX of CSP, and renewable electricity.

According to the current literature, no study has been carried out on DACCU from the perspective of the stated novelties.

1.5 Scope of this study

The scope of this work is highlighted as follows:

- This work only studied the L-DAC technology based on commercially available CE's DAC process.
- The hydrocarbon distributions obtained from the CO₂-FTS process are identical under the design conditions (i.e. using Fe-Mn-K catalyst at specific operating conditions).
- Modelling for the other aspects of the DACCU such as hydrogen production plants, CSP plants, and hydrocracking plants are not covered in this work.
- All models developed in this work are at steady-state.
- The geographical impacts of the proposed DACCU plant are investigated only at selected five locations (i.e., USA, Chile, Spain, South Africa, and China).
- The preliminary life cycle assessment (LCA) is only carried out for solar-driven L-DAC processes based on publicly available sources. A full cradle-to-grave LCA is not performed.

1.6 Research methodology

The research methodology used in this thesis is illustrated in Figure 1.5. It includes stages of process design, process model development (for L-DAC, solar calciner, CO₂-FTS and solar-driven DACCU) and plant performance assessment.

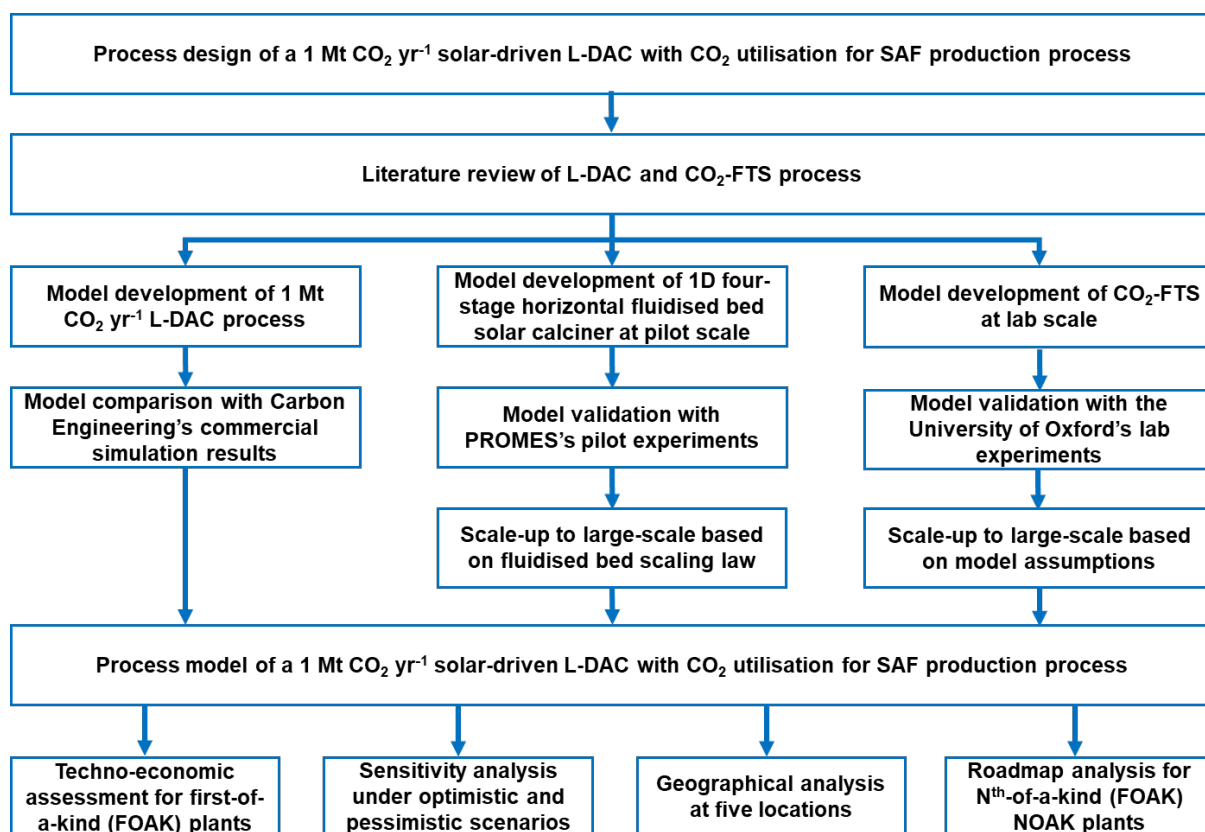


Figure 1.5 Overview of the methodology used in this thesis

1.7 Software tools to be used for this study

1.7.1 Aspen Plus®

Aspen Plus® is a powerful process simulation software widely used in chemical engineering for modelling, designing, and optimising chemical processes (AspenTech, 2024b). It provides comprehensive tools for simulating steady-state and dynamic systems, designing flowsheets, and conducting optimisation and sensitivity analyses. With an extensive database of thermodynamic and physical properties, Aspen Plus® accurately models complex chemical reactions, unit operations, heat and mass transfer, and phase equilibria, making it

essential for process development, optimisation, and troubleshooting in chemical engineering applications. The Aspen Plus® V11 was used for the work presented in Chapters 3, 4, 5 and 6 of this thesis.

1.7.2 Aspen Custom Modeller®

ACM is a specialized process modelling software used in chemical engineering for creating detailed, custom simulations of complex processes that cannot be easily modelled with standard simulation tools (AspenTech, 2024a). ACM allows users to develop custom models of unit operations, reactors, and entire processes using advanced mathematical modelling, including first-principal equations, kinetics, and transport phenomena. It supports both steady-state and dynamic simulations, optimisation, and control strategy development, making it invaluable for detailed process analysis and equipment design. ACM can be linked with Aspen Plus®, allowing for seamless integration of custom models into broader process simulations, enhancing the overall modelling capabilities and enabling a more comprehensive analysis of chemical engineering processes. The ACM V11 was used for the work presented in Chapters 4, 5 and 6 of this thesis.

1.7.3 System Advisor Model

The (SAM) is a comprehensive software tool developed by the National Renewable Energy Laboratory (NREL) for modelling the performance and financial feasibility of renewable energy projects (NREL, 2024c). SAM supports a wide range of technologies, including solar photovoltaics (PV), solar thermal, wind, geothermal, biomass, and energy storage systems. It combines detailed performance modelling with financial analysis, enabling users to evaluate the impact of design and financial parameters on project viability. SAM also includes capabilities for calculating solar field land use, allowing users to estimate the land

area required for solar projects based on system design, layout, and shading considerations. This feature is particularly valuable for optimising site selection and design in solar energy projects, making SAM an essential tool for engineers, project developers, and researchers assessing the technical and economic potential of renewable energy systems. The SAM was used for the work presented in Chapter 7 of this thesis.

1.8 Outline of the thesis

This thesis is organised in eight chapters. The outline of the following chapters is given below.

Chapter 2 provides a comprehensive review of the planned commercial plants, existing pilot plants and lab rigs, liquid sorbents and model-based studies on L-DAC technology. The chapter also explores the experimental work and model-based studies on direct CO₂-FTS technology, to summarise achievements so far and to reveal research gaps.

Chapter 3 focuses on the model development and simulation of the large-scale L-DAC process. It includes detailed model formulation, implementation in Aspen Plus[®], and comparison with CE's DAC. The chapter aims to establish the baseline for the proposed solar-driven DAC process.

Chapter 4 presents the model development, simulation and validation of the pilot-scale air-fluidised solar calciner model. It also provides a new hydrogen-fluidised solar calciner, a key unit of the solar-driven L-DAC process. The scale-up approach for the fluidised bed is introduced and the pilot calciner is scaled up from pilot scale to large scale.

Chapter 5 covers the model development, simulation, and validation of the CO₂-FTS process at the lab scale. Also, the process mode is simulated at a large scale using an ex-situ water removal strategy for process improvement.

Chapter 6 provides the detailed process design of the solar-driven DACCU process. The comprehensive solar-driven DACCU process model is developed based on the individual models developed in previous chapters.

Chapter 7 presents a detailed assessment of the first-of-its-kind solar-driven DACCU plant, including the TEA, sensitivity analysis, geographical analysis and roadmap analysis.

Finally, **Chapter 8** summarises the key findings and contributions from the research. It also discusses the limitations of the current study and proposes directions for future research.

Chapter 2. Literature review

2.1 Overview

This chapter reviews previous research on experimental, modelling and simulation studies of the L-DAC process and CO₂-FTS process. Section 2.2 discusses planned commercial plants, existing pilot plants and rigs, as well as liquid solvents for the L-DAC process. Section 2.3 focuses on model-based studies of the DAC process, including modelling, simulation, power-driven DAC system and performance analyses. Section 2.4 reviews CO₂-FTS studies, covering experiments, modelling and simulation of the CO₂-FTS process. The chapter concluded with a summary of the literature review in Section 2.5.

2.2 Different plants, lab rigs and liquid sorbents for L-DAC

Typically, the study of DAC technology starts with lab-scale experiments for basic chemical and physical properties such as chemical reaction kinetics and mass transfer coefficient for specific capturing CO₂ material. After establishing adequate fundamental knowledge, the technical and economic evaluations for DAC systems are normally studied at pilot scale. Following the research on scale-up and large-scale commercial DAC plants, the mass production of the mature DAC technology can truly achieve the global net-zero emissions target.

2.2.1 Worldwide commercial L-DAC plants

Currently, there are several large-scale commercial L-DAC plants either under construction or in the planning and design stages. Carbon Engineering (CE) is a Canadian company that is at the forefront of L-DAC technology.

In 2022, CE, in collaboration with 1PointFive, began construction of the first large-scale commercial L-DAC plant in Basin, USA. This plant (see Figure 2.1) is expected to capture 0.5 Mt of atmospheric CO₂ annually. The captured CO₂ will be used for enhanced oil recovery (EOR), providing a pathway to carbon-neutral fuels. Plans are in place to expand the project to multiple DAC plants with a combined capacity of capturing 1 Mt of CO₂ per year (Carbon Engineering, 2021).

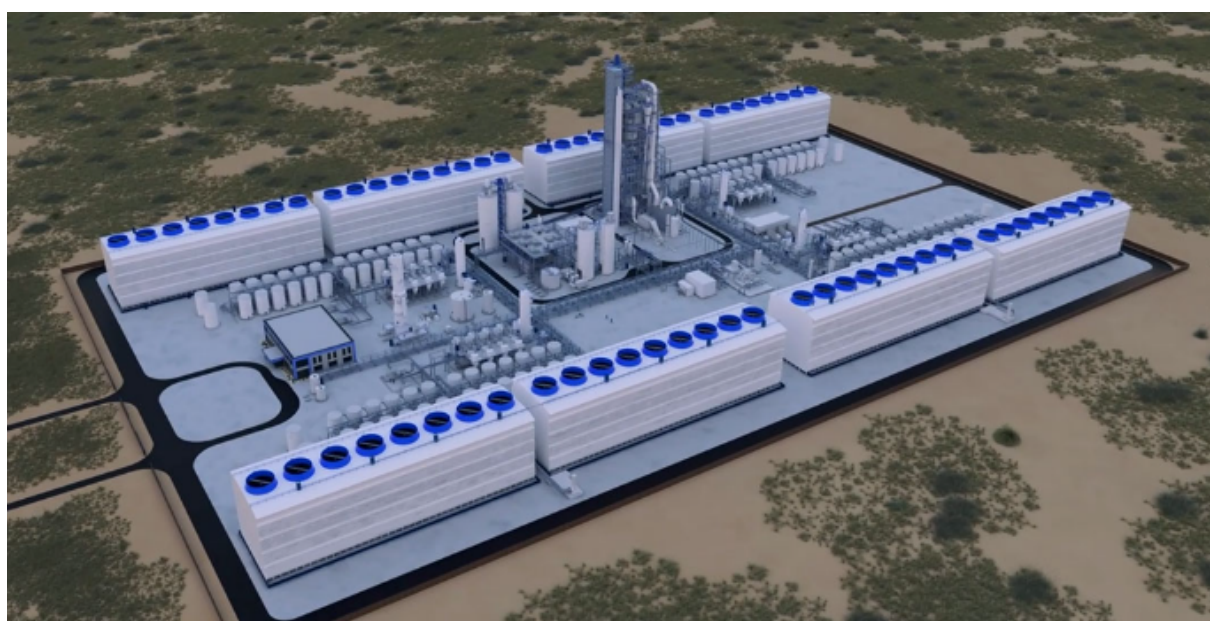


Figure 2.1 Envisioned large-scale L-DAC plant (1PointFive, 2024)

Moreover, the STRATOS DAC Plant in Texas, USA, is being developed by Occidental and 1PointFive. It aims to capture 0.5-1 Mt of CO₂ per year. The facility's primary goal is to provide carbon removal credits and support the production of net-zero transportation fuels. This ambitious project has garnered substantial financial backing, including a significant

US\$550 million investment from BlackRock, highlighting growing investor confidence in the technology and its potential impact on reducing carbon emissions (Credits, 2023).

The first UK commercial-scale L-DAC plant is scheduled for deployment in 2026. This project is led by Storegga, with CE as the technology partner, Petrofac Facilities Management as the engineering partner, and support from the Universities of Cambridge and Edinburgh. It is expected to capture approximately 0.5-1 MtCO₂ per year and will operate entirely on renewable energy (GOV.UK, 2021).

Additionally, a large-scale DAC facility is being developed by CE, Carbon Removal, and Oxy Low Carbon Ventures in Kollsnes, Norway. This plant aims to capture between 0.5-1 MtCO₂ CO₂ per year, with the CO₂ being stored offshore beneath the seabed. Norway's renewable energy capacity, skilled workforce from the oil and gas industry, and emerging carbon capture and storage infrastructure make it an ideal location for DAC deployment (Engineering, 2022).

2.2.2 Pilot plants and experimental data

2.2.2.1 Prototype contactor at the University of Calgary

The Energy and Environmental Systems Group at the University of Calgary in Canada developed and studied a 6.5-meter-tall packed tower prototype for capturing CO₂ from air as shown in Figure 2.2 (Mahmoudkhani et al., 2009). The study evaluated two distinct configurations: a short stack with a height of 4.8 meters and a tall stack with a height of 6.0 meters. The short stack utilised a packing height of 1.5 meters, while the tall stack employed a packing height of 2.6 meters. Both configurations featured an inlet diameter of 0.61 meters and used Sulzer 250X structural packing with a specific surface area (SSA) of 250 m²/m³.

In the experiments, NaOH and KOH solutions were pumped through the packed tower to capture CO₂ from air flowing at a velocity of 0.7 m/s, corresponding to a volumetric flow rate of 3.6 L/m²s. The study also assessed the energy requirements for various components of the system. The results demonstrated that the pump accounted for at least 85% of the total energy consumption of the contactor. Additionally, KOH was found to be more effective than NaOH, capturing a higher amount of CO₂ while consuming less energy.

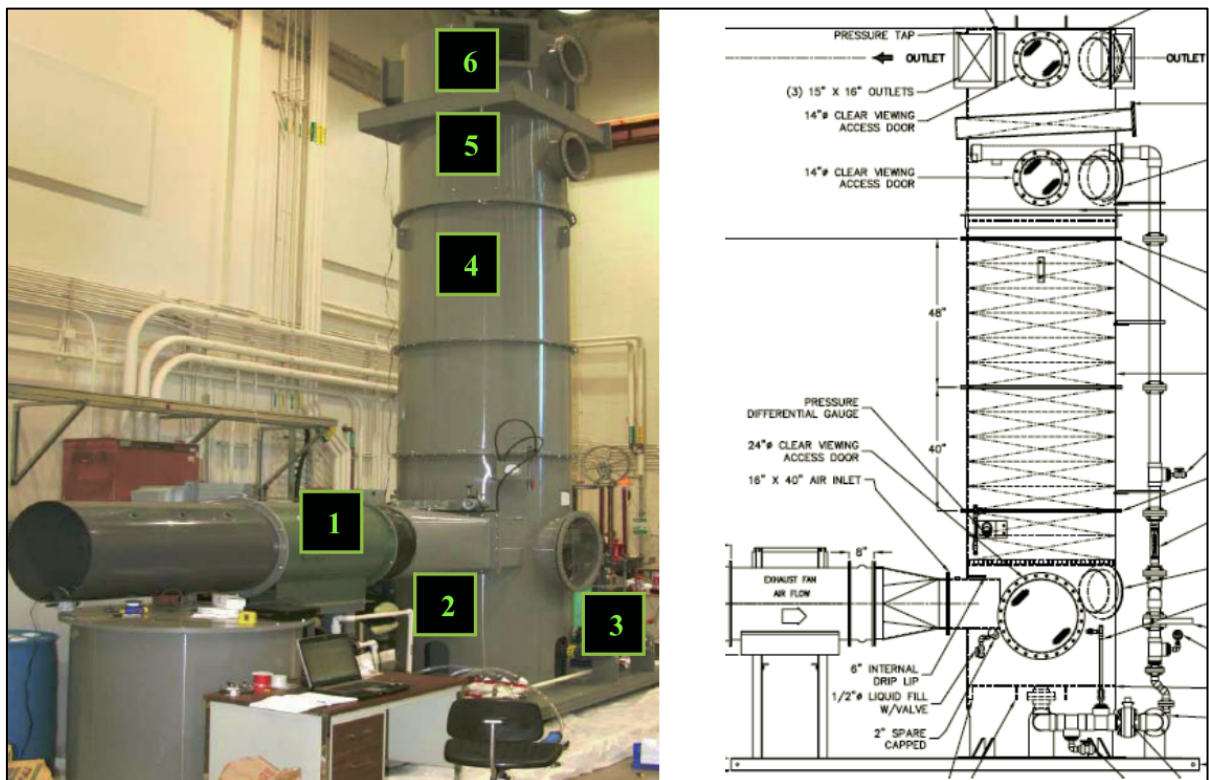


Figure 2.2 CO₂ capture contactor (1. Fan; 2. Fluid Basin; 3. Fluid Pump; 4. Packing; 5. Fluid Distributor; 6. Air Outlet with Demister.) (Mahmoudkhani et al., 2009)

2.2.2.2 Outdoor prototype air contactor

In 2011, CE developed an outdoor prototype air contactor with a packing volume of 10 m³ (Holmes et al., 2013). This slab contactor used Brentwood Industries XF 12560 structured PVC packing and operated in a cross-flow configuration. In this setup, air flowed horizontally through the contactor while the hydroxide solution flowed downward by gravity.

The design incorporated several packing segments (see Figure 2.3), with each segment having dimensions of 1.8 meters in height and 0.9 meters in width. This configuration allowed the total air travel distance (ATD) to be adjusted between 4.5 and 6 meters. Spray nozzles positioned above the packing distributed the hydroxide solution over the packing material, while captured CO₂ was managed and removed through a solution management system. The prototype was operated for over 1000 hours with intermittent liquid flow to evaluate various performance parameters, including pressure drop across the packing, fan energy requirements, CO₂ capture rate, and drift measurements.

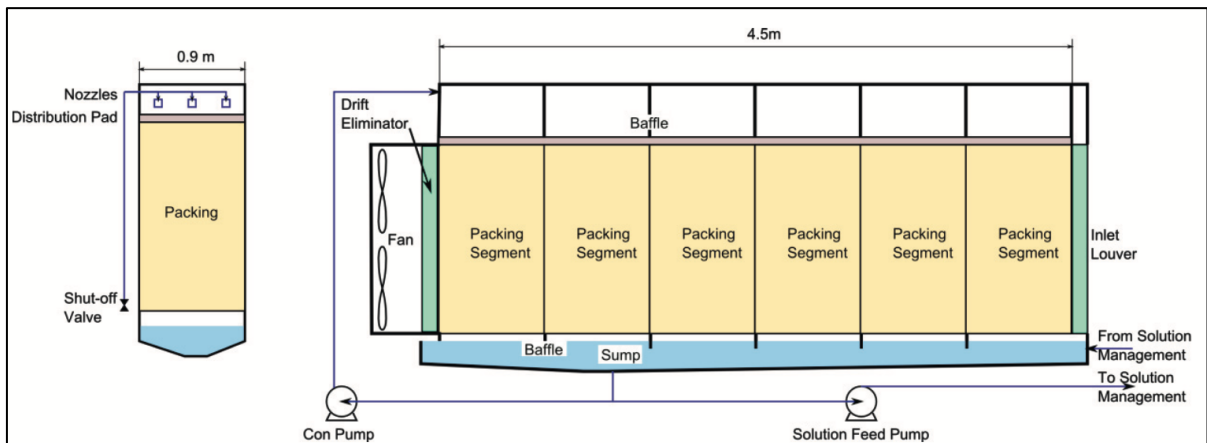


Figure 2.3 Schematic of CE's outdoor prototype air contactor (Holmes et al., 2013)

2.2.2.3 CE's Pilot Plant

In 2015, CE invested US\$ 8.1 million to construct an end-to-end DAC pilot plant (see Figure 2.4) in Squamish, British Columbia, designed to capture approximately 1 ton of CO₂ per day. This pilot plant featured a contactor with two banks of Brentwood XF12560 structured PVC packing, each 3 meters deep, and an inlet cross-section measuring 3 × 5 meters. The pellet reactor in the plant was a steel vessel with an internal height of 12 meters, a diameter of 1.2 meters, and a 60° conical base. For the calciner, an oxy-fired circulating fluidised bed (CFB) was used, which included an 8.5-meter-tall riser with a 0.15-meter interior diameter. The slaker employed a refractory-lined bubbling fluid bed, fluidised by a recirculating steam flow (Keith et al., 2018). The primary objectives of CE's pilot plant were to operate the equipment, study overall process simulation risks, and gather real-world performance data from each unit operation. The data obtained from the pilot plant, combined with process simulation and on-paper engineering designs, was intended to build confidence for scaling up to commercial-scale technologies.



Figure 2.4 CE's pilot DAC plant (Carbon Engineering, 2023)

2.2.3 Lab rigs and experimental data

2.2.3.1 Benchtop Contactor

The University of Calgary's air capture group developed a laboratory-scale benchtop contactor to investigate CO₂ absorption from the air using both steel and PVC packing materials arranged in a cross-flow configuration (Holmes, 2010). This benchtop contactor consists of three main components. The first component is the CO₂ absorption chamber, which is filled with structured packing materials designed to enhance CO₂ absorption. The second component is the air circulation loop, which uses a fan to regulate the air velocity through the CO₂ absorption chamber, ensuring a controlled airflow. The third component is the plumbing network, which delivers a hydroxide solution into the CO₂ absorption chamber, achieving complete flooding of the packing material.

Experiments with this setup involved a structured packing flow channel with a path length of 0.6 meters. The performance of CO₂ absorption and energy consumption were evaluated, and pressure drop curves were generated for the tested packing materials at various air velocities, ranging from 0 to 3 m/s. The study also assessed CO₂ absorption performance under different conditions, including variations in solution chemistry, air flow rate, packing type, and CO₂ inlet concentration.

2.2.3.2 Benchtop Pellet Reactor

At the University of British Columbia, research focused on the CaCO₃ crystallization process for CO₂ recovery in a DAC system using a laboratory-scale fluidised-bed benchtop pellet reactor. This reactor, made from PVC, has a vertical height of 5.20 meters and an inner diameter of 10.16 cm. The main objective of this study was to characterize the dynamics of the fluidised bed and the particle growth rates during a seeded CaCO₃ crystallization process.

The research aimed to optimise the conditions for effective CO₂ capture and recovery within a controlled laboratory environment.

2.2.4 Aqueous sorbents used for L-DAC

2.2.4.1 Aqueous hydroxide solutions

For L-DAC, the CO₂ concentration in the air is significantly lower compared to flue gas from power plants. As a result, using sorbents with strong CO₂-binding affinities is crucial to enhance CO₂ capture efficiency. Early research by Lackner focused on using calcium hydroxide (Ca(OH)₂) due to its high binding energy with CO₂, which forms calcium carbonate (CaCO₃) (Lackner, 2009).

Sodium hydroxide (NaOH) solutions are also employed for CO₂ capture, benefiting from the high solubility of the resulting sodium carbonate (Na₂CO₃) in water. The L-DAC technology uses two interconnected chemical loops: NaOH for CO₂ absorption and calcium hydroxide (Ca(OH)₂) for solvent regeneration. This process, known as causticization, involves the reaction between sodium carbonate (Na₂CO₃) and Ca(OH)₂, resulting in the regeneration of NaOH and the precipitation of CaCO₃ (Sanz-Pérez et al., 2016).

In an exploration of alternative sorbents, Holmes (2010) tested potassium hydroxide (KOH) in a benchtop contactor for CO₂ capture. Subsequent tests in both a CE outdoor contactor and a CE pilot contactor (Holmes et al., 2013, Keith et al., 2018) demonstrated that while KOH is more expensive than NaOH, it offers a higher CO₂ capture rate due to its superior kinetic properties, making it a promising candidate for future commercial applications.

2.2.4.2 Alternative sorbents for causticization process

Beyond traditional methods, alternative causticization processes have been investigated based on the solubility of reaction products. Sodium metaborate (NaBO_2) is a caustic solution used in the autocausticization method, where the reaction product is water-soluble. NaBO_2 reacts with sodium carbonate (Na_2CO_3) to form sodium borate (Na_3BO_3) and release CO_2 , though this method requires high energy to achieve reaction temperatures exceeding 900°C (Hoddenbagh et al., 2001, Yusuf and Cameron, 2004).

Titanium dioxide ($\text{Na}_2\text{O}_3\cdot\text{TiO}_2$) has also been explored as an alternative for the causticization process. When used in place of calcium hydroxide ($\text{Ca}(\text{OH})_2$), titanium dioxide reacts with Na_2CO_3 to produce sodium titanate ($\text{Na}_2\text{O}\cdot 5\text{TiO}_2$) and CO_2 . This method is advantageous as it consumes half the energy required for regeneration compared to the traditional lime-based causticization process.

2.3 Review of model-based studies for L-DAC process

2.3.1 Model development for L-DAC

2.3.1.1 Mass transfer studies for air contractor's structured packing

Numerous studies have been conducted to investigate mass transfer in the structured packing of air contactors, as summarised in Table 2.1 (ATD means air travel distance, V means air velocity, and CF means capture fraction). These studies span a range from laboratory-scale experiments to pilot-scale investigations. CE has been at the forefront of this research, performing a series of experiments aimed at optimising the design and performance of their DAC systems.

Table 2.1 Review of mass transfer studies of structured packing for air contactor

References	Mass transfer coefficient (mm/s)	Packing type	Operation condition	Solvent	CF	Methodology
Baciacchi et al. (2006)	1.2	Sulzer 500Y, cross-flow	ATD=10.3 m, V=4.3 m/s	2 M NaOH	0.5	Theoretical design
Stolaroff et al. (2008)	NA	NA	ATD=3.8 m, V=0.4 m/s	1.3 M NaOH	0.3	Theoretical study
Mahmoudkhani et al. (2008)	NA	Sulzer 250X, counter-flow	ATD= 2.6 m, V=7 m/s	3 M NaOH,	0.68	Experimental study
APS DAC report (2011)	2.0	Sulzer 500Y, cross-flow	ATD=2.8 m, V=2.0 m/s	2 M NaOH	0.5	Theoretical design
Holmes (2010)	2.1	XF12560, cross-flow	ATD=0.6 m, V=1.0 m/s	2 M NaOH	0.23	CE laboratory-scale contactor data
Holmes (2010)	2.4	Sulzer 500Y, cross-flow	ATD=0.6 m, V=1.0 m/s	2 M NaOH	0.49	CE laboratory-scale contactor data
Holmes (2013)	0.8-1.3	XF12560, cross-flow	ATD=4.5-6 m, V=1.4-1.6 m/s	NaOH or KOH (concentration unreported)	>0.8	CE outdoor contactor data
Keith et al. (2018)	1.4	XF12560, cross-flow	ATD=3 m, V=1.4 m/s	2M K ⁺ , 1.1 M OH ⁺ , 0.45 M CO ₃ ²⁻	0.42	CE pilot-scale air contactor data

The mass transfer studies focus on understanding the efficiency and dynamics of CO₂ capture within structured packing materials. These studies are essential for refining models that predict the performance of air contactors and for scaling up the technology to commercial applications. By investigating various parameters such as packing materials, flow dynamics, and chemical reactions, researchers aim to enhance the overall effectiveness of L-DAC systems and support the transition from pilot projects to full-scale implementations.

2.3.1.2 Air contactor design

CE designed an intermittently-wetted air contactor featuring a cross-flow slab geometry (Heidel et al., 2011). In this design, “cross-flow” refers to the air flow being orthogonal to the gravity-driven downward flow of the liquid. The “slab geometry” indicates that the contactor is relatively thin along the air flow axis compared with its height and length (Holmes and Keith, 2012).

The foundational design principles of this air contactor were grounded in a thorough study of CO₂ absorption, including both chemical and physical aspects. Researchers used reaction-diffusion and advection-diffusion equations to model CO₂ capture, validated by laboratory experiments (Holmes, 2010). The reaction-diffusion equation provides a way to calculate the liquid phase CO₂ absorption flux, which in turn determines the minimum liquid film surface area required for a specified CO₂ absorption rate.

A robust and straightforward approximation of CO₂ capture flux was given in Equation 2.1.

$$F = f_{op} \rho_{CO_2} V (1 - e^{\frac{-\epsilon SSA D K_L}{V}}) \quad (2.1)$$

Where, f_{op} is the assumed annual operation fraction; ρ_{CO_2} is the mass density of CO₂ in air; V is the air velocity; ε is the packing efficiency; D is the packing depth; and K_L is the mass transfer coefficient.

The pressure drop for XF12560 packing is given in Equation 2.2.

$$\Delta P = D 7.4 V^{2.14} \quad (2.2)$$

Traditionally, carbon capture processes employed packed towers with structured packing made from stainless steel. However, after testing various materials, Holmes opted for Brentwood XF12560 PVC packing due to its comparable CO₂ absorption performance and cost advantages over stainless steel (Holmes, 2013).

The air velocity is a key factor influencing the mass of CO₂ captured per unit area of packing and over time. CE conducted cost optimisation studies and determined that the optimal air velocities for the air contactor should range between 1.4 and 1.6 m/s.

2.3.1.3 CE's DAC plant design

CE pioneered the detailed design of a large-scale DAC plant using a KOH solvent coupled with a calcium caustic recovery loop (Keith et al., 2018). This DAC plant is designed to capture approximately 1 million tons of CO₂ per year from the atmosphere (see Figure 2.5).

The air contactor in this design is engineered to handle a solution with a concentration of 1.1 M OH⁻, 0.45 M CO₃²⁻, and 2.0 M K⁺. This solution flows downward through PVC packing to capture CO₂ at a concentration of 400 ppm, interacting with a 50 μ m film of liquid phase. The packing depth is set at 7 meters, with a pressure drop of 9.7 Pa/m.

In the fluidised bed-based pellet reactor, the carbonate ions are removed from the solution through the causticization process. A 30 wt% Ca(OH)_2 slurry is injected into the bottom of the reactor, while small seed pellets (CaCO_3) are introduced at the top of the bed, growing into calcite pellets up to 0.9 mm in diameter. The large pellets are discharged at the bottom of the bed.

The calciner employs an oxygen-fired CFB with a bed height of 4.5 meters for the decomposition of CaCO_3 particles and produces CO_2 at 900°C and ambient pressure. The calciner is heated by the natural gas combustion with oxygen as the fluidisation medium. Incoming solids are preheated using two heat recovery cyclones arranged in a counter-current configuration. The first cyclone heats solids from the steam slaker from 300°C to 450°C by using cooling gas steam from 650°C to 450°C . The second cyclone further heats the pellets to 650°C using cooling steam from 900°C .

The steam slaker uses a fluidised bed with a fluidisation velocity of 1 m/s to dry and preheat the CaCO_3 pellets to 300°C . In addition to these major units, CE's design also incorporates other units such as a natural gas turbine, a heat recovery steam generator (HRSG), a CO_2 absorber, a four-stage CO_2 compressor, and a cryogenic air separation unit (ASU).

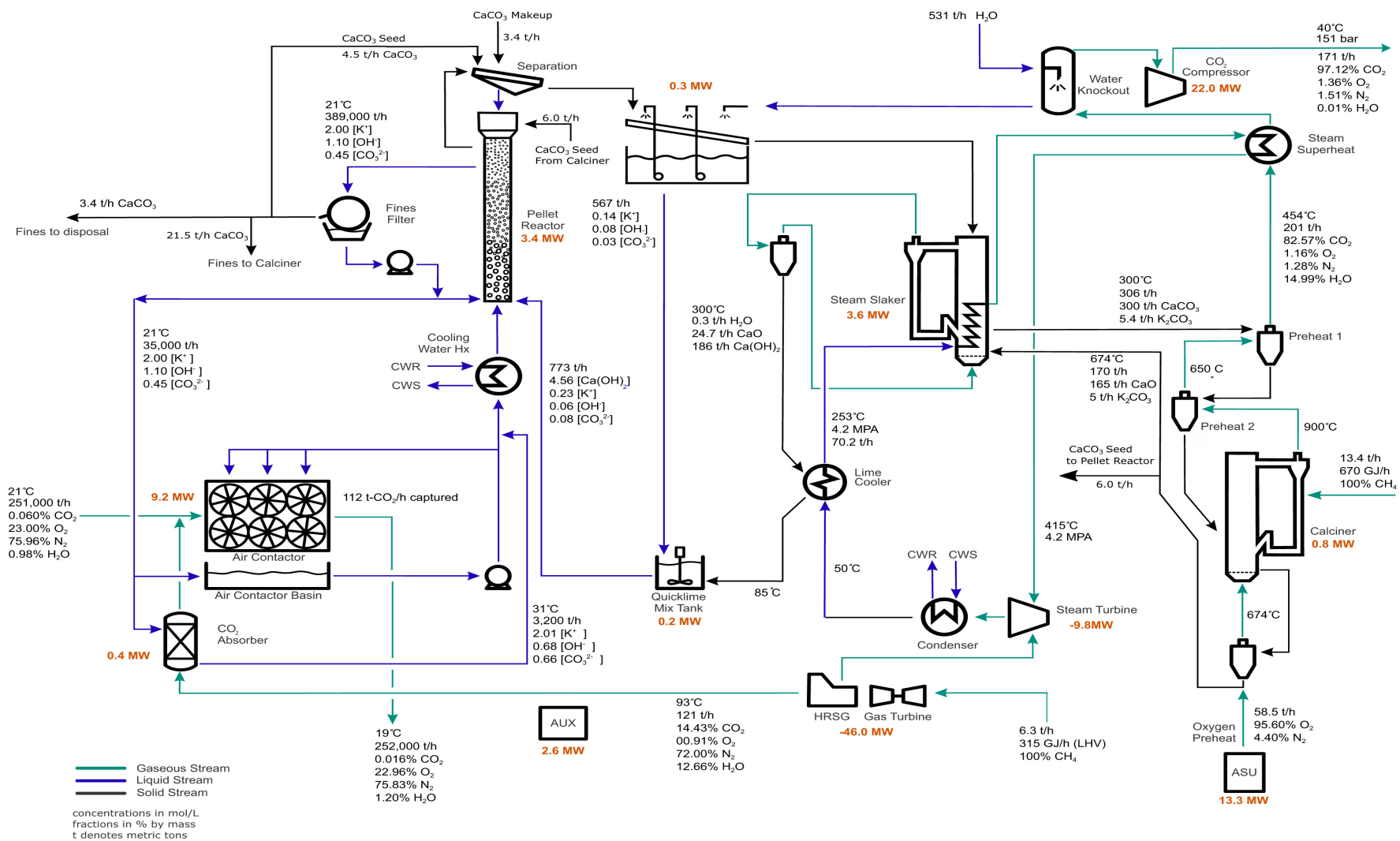


Figure 2.5 Process design of a CE's commercial DAC plant (Keith et al., 2018)

Table 2.2 Summary of literature review on modelling and simulation of L-DAC

References	Tool	Process simulation	Validation data	Comments
Manhamoudkhani et al. (2009)	VMGsim™	Simulation of CO ₂ capture and caustic recovery	Pilot contactor experiments	Experimental results in agreement with theoretical values
Holmes (2010)	Unreported	Simulation of CO ₂ absorption in a small pipe-flow geometry	Lab-scale experiments for CO ₂ absorption performance	Theoretical results link with experimental data
Keith et al. (2018)	Aspen Plus® V8.0	Energy and material balance for 1 MtCO ₂ /year DAC plant	CE pilot plant and vendor data	Simulation depends on performance models of individual unit operations
Sabatino et al. (2021)	Aspen Plus® V11 with Matlab (R2018b)	Energy and material balance for 1 MtCO ₂ /year DAC plant	Validation of air contactor based on Manhamoudkhani et al. (2009) and Keith et al. (2018)	The process design and unit operations based on Keith et al. (2018)
An et al. (2022)	Aspen Plus® V11	Energy and material balance for 1 MtCO ₂ /year DAC plant	Validation based on CE's 1 MtCO ₂ /year air contactor	DAC process was modelled in two separate open loops
Prats-Salvado et al. (2024)	Aspen Plus® V12.1 and HFLCAL VH13	Energy and material balance for 0.1 MtCO ₂ /year DAC plant	NA	A solar-powered L-DAC process-a modified version of CE's DAC process

2.3.2 Modelling and simulation studies of L-DAC

Several studies have developed models for L-DAC systems, with validation based on real-world data from laboratory experiments and pilot plants or mature process design. Specifically, six papers are reviewed here, as detailed in Table 2.2.

2.3.3 Studies of the L-DAC process based on different energy sources

2.3.3.1 Wind-driven DAC system

Li et al. (2015) explored a wind-driven DAC system as an alternative to conventional energy sources. Their study investigated the intermittency and variability of wind power, particularly its seasonal fluctuations, and evaluated how wind energy could meet the CO₂ capture requirements. The research specified the energy needs for each component of the system and analysed their characteristics. An optimal operation model was developed to assess the flexibility of CO₂ capture in response to varying wind power availability.

Globally, the annual potential offshore wind energy is estimated to be 150,000 TWh, assuming turbines operate with capacity factors of 20% or higher (Lu et al., 2009). In contrast, capturing CO₂ from air requires approximately 243 kJ per mole of CO₂ (equivalent to 1535 kWh per ton of CO₂) (Keith et al., 2018). If the entire available offshore wind energy were utilised for CO₂ capture, it could theoretically remove about 97.8 Gt of CO₂ per year. Thus, harnessing even a moderate fraction of offshore wind energy could significantly mitigate global CO₂ emissions and contribute to climate change targets.

2.3.3.2 Solar-driven DAC system

Solar energy is recognized for its high production potential, and solar thermal plants offer two significant advantages as a combined heat and power (CHP) source for DAC systems.

Firstly, solar thermal plants can achieve high dispatch factors due to their ability to store heat, enabling continuous power supply over several days without reliance on costly battery storage (Nassar et al., 2017). Secondly, these plants can provide highly efficient thermal energy alongside electricity, making them a versatile and effective energy source for DAC applications (Belcher, 2005).

2.3.3.3 Other power-driven DAC systems

Other potential power sources for DAC systems include bioenergy, geothermal energy, and nuclear energy. Bioenergy-driven DAC systems can use various feedstocks (e.g., woody biomass) to generate power. Geothermal energy offers a challenge due to its typically low-temperature heat output, which may be less suitable for some DAC processes. In contrast, nuclear power-driven DAC systems are particularly advantageous in remote areas where renewable energy resources are limited, providing a stable and reliable energy source for CO₂ capture (Simon et al., 2011).

2.3.4 Technical, economic and environmental evaluation studies of L-DAC

2.3.4.1 Technical evaluation studies

The technical specifications of previous studies are presented in Table 2.3. L-DAC plants require both thermal energy and electrical power. Electricity is used for air compression, aqueous solution spraying across various units, and CO₂ compression, while heat is primarily needed for the calciner. Research has shown that the electrical power required for capturing each ton of CO₂ ranges from 77 to 764 kWh, while the heat demand is between 5.1 and 9.2 GJ per ton of CO₂ captured (Fasihi et al., 2019). Natural gas power plants commonly supply the necessary heat, but this process results in additional CO₂ emissions. For the L-DAC system fully powered by natural gas, the process emits 0.48 tons of CO₂ per ton of CO₂

captured, meaning the net captured CO₂ is 0.52 tons unless additional CO₂ capture from the combustion process is implemented. Using carbon-neutral renewable synthetic natural gas (RE-SNG) could improve net CO₂ capture; however, the energy required for converting fuel-based CO₂ to SNG presents significant challenges. Therefore, the total operating cost of a DAC system is closely related to both the CO₂ captured from power generation and the net CO₂ captured. A preferred DAC system should consider sustainable and affordable factors.

2.3.4.2 Economic evaluation studies

Previous economic assessment studies of L-DAC systems have been summarised in Table 2.4. Keith (2006) reported an initial cost of US\$444 per ton of CO₂ captured. Later, Holmes and Keith (2012) revised the contactor design, reducing costs to US\$304 per ton of CO₂. Socolow (2011) presented a benchmark DAC system with detailed energy balance and economic analysis, indicating costs between US\$365/t_{CO2} and US\$466/t_{CO2}, depending on the scenario and installation factors. Mazzotti (2013) further optimised the air contactor unit with new packing materials, reducing costs to US\$334-354 per ton of CO₂. Zeman (2014) recalculated costs and energy demands based on the Socolow model, finding a 2.4% reduction in equipment investment costs and a decrease in annual operational expenditures from 4% to 3%. Keith et al. (2018) from CE provided the techno-economic assessment of their DAC systems, where both capital expenditures and final costs of the have been significantly lowered in comparison to the American Physical Society (APS) model, through a new design and choice of material. CE's results indicated that their DAC systems significantly lower costs compared to earlier models, with levelized costs ranging from US\$94 to 232 per ton of CO₂. For their base configuration, the capital expenditures for the first plant were reported at US\$1336/t_{CO2}, with the Nth plant expected to be 31% cheaper at

US\$842/t_{CO2} due to improved constructability and supply chain efficiencies. Further cost reductions are possible with alternative configurations, such as using grid electricity or avoiding CO₂ compression. More recently, some renewable energy-powered DAC systems have been studied and the cost ranges from US\$ 100-600/t_{CO2} depending on different plant configurations, model assumptions and financial account parameters.

2.3.4.3 Environmental evaluation studies

Life cycle assessments (LCA) are essential for understanding the environmental impacts of DAC systems. De Jonge (2019) conducted an LCA on L-DAC system and found that more CO₂ was captured than emitted in the baseline scenario. The carbon efficiency of a DAC system, calculated using Equation 2.3, determines whether the system effectively captures and stores CO₂. Liu (2020) performed an LCA on CE's 1 MtCO₂ baseline DAC system combined with FTS for diesel production. The study revealed that carbon intensity (CI) is highly sensitive to the electricity emissions factor, with a factor of less than 139 g CO₂e/kWh required to achieve a climate benefit over conventional diesel fuel.

$$E_c = \frac{CO_{2,cap} - GHG_{lc}}{CO_{2,cap}} * 100 \quad (2.3)$$

Where $CO_{2,cap}$ is the total amount of kg CO₂ stored over the lifetime of the system and GHG_{lc} is the total amount of greenhouse gasses emitted over the whole life cycle of the system in kg CO₂ equivalents.

Table 2.3 Reported technical specifications of L-DAC

References	Solvents	CO ₂ con.	Absorption	Desorption	Energy demand			Outlet pressure	CO ₂ purity
		ppm	T (°C)	T (°C)	Electricity (kWh/t)	Heat (GJ _h /t)	Power source	bar	%
Keith et al. (2006)	NaOH, Ca(OH) ₂	NA	ambient	900	NA	NA	NG	100	NA
Bacocchi et al. (2006)	NaOH, Ca(OH) ₂	500	ambient	900	440	6.1	NG	NA	NA
Zeman (2007)	NaOH, Ca(OH) ₂	380	ambient	900	764	5.1	NG/coal	NA	NA
Stolaroff et al. (2008)	NaOH, Ca(OH) ₂	NA	NA	900	1199-2461		NA	NA	NA
Mahmoudkhani and Keith (2009)	NaOH, Na ₂ O·3TiO ₂	NA	ambient	850	NA	NA	NA	15	pure
Socolow et al. (2011)	NaOH, Ca(OH) ₂	500	NA	900	494	8.1	NG	100	NA
Li et al. (2015)	NaOH, Ca(OH) ₂	NA	ambient	900	2790		wind + battery	NA	NA
Keith et al. (2018)	KOH, Ca(OH) ₂	400	ambient	900	NA	8.81	NG	150	97.1
Keith et al. (2018)	KOH, Ca(OH) ₂	400	ambient	900	366	5.25	NG + elec	150	97.1
Keith et al. (2018)	KOH, Ca(OH) ₂	400	ambient	900	77	5.25	NG + elec	1	97.1
Fasihi et al. (2019)	KOH, Ca(OH) ₂	400	ambient	900	1535		elec	1	>97
An et al. (2022)	KOH, Ca(OH) ₂	NA	ambient	900	NA	8.3-11.1	NG	150	NA

Table 2.4 Reported economic evaluation of L-DAC

References	Capacity (tCO ₂ /year)	Lifetime (years)	Energy consumption per ton CO ₂	Electricity price (US\$/MWh)	Energy source	Indicated year of cost	Reported cost (US\$/tCO ₂)
Keith et al. (2006)	280,000	20	NA	NA	NA	2005	444
Holmes and Keith (2012)	1,000,000	NA	NA	67	NA	NA	304
Socolow et al. (2011)	1,000,000	20	494 kWh + 8.1 GJ	60	NG + elec	2011	365, 466
Mazzotti et al. (2013)	1,000,000	NA	1840 kWh	60	NG	2013	343-354
Keith et al. (2018)	1,000,000	25	8.81 GJ	NA	NG	2016	168-232
Keith et al. (2018)	1,000,000	25	366 kWh + 5.25 GJ	30-60	NG + elec	2016	113-163
Keith et al. (2018)	1,000,000	25	77 kWh + 5.25 GJ	30-60	NG + elec	2016	94-130
Fasihi et al. (2019)	1,000,000	25	1535 kWh	55.5	elec	2020	206
Sabatino et al. (2021)	1,000,000	20	6.21-6.48 GJ	0-100	NG + elec	NA	<200
An et al. (2022)	1,000,000	25	8.3-11.1 GJ	60	NG	2021	240-409
Young et al. (2023)	980,000	25	1.32 GJ elec + 5.3 GJ heat	14-72	Solar, wind, hydro, geothermal, nuclear	2019	100-600
Prats-Salvado et al. (2024)	100,000	25	NA	NA	Solar thermal, PV, battery	2022	260-320
Sievert et al. (2024)	1,000,000,000	25	1.32 GJ elec + 5.3 GJ heat	29-79	PV, wind, nuclear, geothermal	2022	226-544

2.4 Review of CO₂-FTS technology

2.4.1 Experimental work

The products from the modified CO₂-FTS process can be wide since a variety of catalysts can be used. Hence, this review focuses on the synthesis of jet fuel from the CO₂-FTS process. To date, the modified CO₂-FTS process for CO₂ conversion into jet fuel has only been reported at a laboratory scale. A summary of a few studies on the CO₂-FTS process to jet fuel (C₈-C₁₆) is presented in Table 2.5. Most studies reported Fe and Co-based catalysts and achieved up to 64% selectivity to jet fuel whereas, CO₂ conversion varies from 10% to 55% (Zhang et al., 2021, Choi et al., 2017a, Choi et al., 2017b, Hwang et al., 2021, Yao et al., 2020). The largest jet fuel yield of 18.3% can be found in Yao et al. (Yao et al., 2020).

2.4.2 Model-based studies

Table 2.6 presents an overview of previous studies on modelling and simulation for the modified CO₂-FTS process to liquid fuels. Meier et al. (2017) developed a kinetic model comprising 20 reactions to study CO₂-FTS plant performance through periodical removal of water for C₅⁺ hydrocarbons. The authors looked into ex-situ water removal to improve CO₂-FTS reaction rates and C₅⁺ selectivity. Zang et al. (2021a) assessed the synthesis of liquid fuels (C₅⁺) through a techno-economic assessment (TEA) of the CO₂-FTS process and predicted the minimum selling price (MSP) of the FT fuel is US\$5.4–5.9/gal. Fernandez-Torres et al. (2022) applied Aspen-HYSYS® to design and optimise CO₂-FTS to gasoline at a commercial-scale. For a gasoline production rate of 23.65 ton/hr, their results indicated a CAPEX and OPEX between 73 to 128 USM\$ and 244 to 1951 USM\$/yr, respectively. Kamkeng and Wang (2023) studied the performance improvement of the CO₂-FTS process for gasoline (C₅-C₁₁) production using ex-situ water removal. The authors developed a CO₂-

FTS model based on first principles and a modified Anderson-Schulz-Flory (ASF) distribution, which was implemented in Aspen Plus® using Fortran® Routines and validated with laboratory data. The results demonstrated that the use of ex-situ water removal technique can increase CO₂ conversion and gasoline yield by up to 34% and 70%, respectively. The single CO₂-FTS reactor with recycle and three-stage CO₂-FTS reactors in series showed a similar process efficiency of 66.4%. However, economic analysis was not evaluated to indicate the feasibility of commercial deployment. Colelli et al. (2023) carried out the comparative TEA for the indirect and direct production of synthetic kerosene (C₁₀-C₁₄) via FTS. They predicted the productivity of the plant (66.18 bbl/d and 38.46 bbl/d) and product cost (460 to 1435 €/bbl and 752 to 2364 €/bbl) for the indirect and direct process. However, their simulation results based on kinetic model present very large relative errors (-38.6-77.8%) compared with experimental data.

Table 2.5 Summary of studies performed for CO₂-FTS process to jet fuel at lab-scale

Catalyst	Operating pressure (bar)	Operating temperature (°C)	H₂/CO₂ (mol/mol)	CO₂ conversion (%)	Jet fuel (C₈-C₁₆) selectivity in HC (%)	Jet fuel (C₈-C₁₆) yield (%)	Reference
CoFe-0.81Na	30	240	3	10.2	63.5	6.5	Zhang et al. (2021)
Fe-Cu	10	300	3	16.7	~37	6.2	Choi et al. (2017a)
Fe-Zn	10	340	3	34	~49	16.7	Choi et al. (2017b)
FeK/Co-NC	25	300	3	54.6	~30	16.4	Hwang et al. (2021)
Fe-Mn-K	10	300	3	38.2	47.8	18.3	Yao et al. (2020)

Table 2.6 Previous studies on modelling and simulation of CO₂-FTS process to liquid fuels

Targeted liquid fuel carbon ranges	Model	Software for model development	Assessment	Reference
C ₅ +	Kinetic model of CO ₂ -FTS	CHEMCAD	Process analysis	Meiri et al. (2017)
FT fuel (carbon ranges NA)	Chemical Equilibrium model	Aspen Plus [®]	TEA	Zang et al. (2021a)
Gasoline (carbon ranges NA)	Thermodynamic model	Aspen HYSYS [®]	Economic and environmental assessment	Fernández-Torres et al. (2022)
Gasoline (C ₅ -C ₁₁)	Steady-state CO ₂ -FTS model based on a modified ASF distribution	Aspen Plus [®] using Fortran [®] Routines	Technical analysis	Kamkeng and Wang (2023)
Kerosene cut (C ₁₀ -C ₁₄)	Kinetic model of CO ₂ -FTS	Aspen Plus [®]	TEA	Colelli et al. (2023)

2.5 Summary

The literature review of the L-DAC process and CO₂-FTS process in this chapter has shown that:

- Currently, several large-scale commercial L-DAC plants are under construction or in the planning and design stages globally, particularly in the US and Europe. These projects highlight the growing impact of L-DAC technology in CO₂ removal.
- Pilot plants and lab-scale experiments play a crucial role in advancing L-DAC technology by providing valuable data and insights.
- Aqueous alkaline sorbents are essential in L-DAC technology due to their strong CO₂-binding affinities, necessary for capturing CO₂ from the low concentrations present in ambient air.
- Model-based studies for L-DAC processes focus on optimising CO₂ capture efficiency through detailed simulations of mass transfer, air contactor designs, and system performance. These studies provide critical insights that support the scaling of L-DAC technology from pilot to commercial applications.
- The technical, economic, and environmental evaluation of L-DAC systems reveals key insights into their performance and feasibility. L-DAC requires significant thermal and electrical energy. While natural gas often supplies the required heat, it introduces additional CO₂ emissions impacting the net capture rate, which emphasize the need for low-carbon energy sources to maximize climate benefits.
- The review of CO₂-FTS technology focuses on converting CO₂ into jet fuel (C₈-C₁₆) at the laboratory scale. Model-based studies have developed kinetic models and simulations to

optimise the CO₂-FTS process, improve reaction rates, and assess the techno-economic viability of liquid fuel production. Key findings include increased CO₂ conversion and fuel yield with ex-situ water removal, though commercial feasibility remains uncertain due to limited economic analysis.

Chapter 3. Model development, simulation and comparison of liquid-based DAC process

3.1 Overview

In this chapter, the L-DAC process was developed at a commercial scale in Aspen Plus® V11. The process model was established based on the commercially available design from CE and literature-reported modelling and simulation studies. Section 3.2 presents the detailed model development procedures for the L-DAC process at a commercial scale in terms of thermodynamics, process flows and unit operations. Section 3.3 compares the developed L-DAC process model with CE's commercial-scale L-DAC design. Finally, the conclusions of this chapter are drawn in section 3.4.

3.2 Model development of L-DAC at commercial scale

The process model of the L-DAC system was developed based on the commercially available CE's design (Keith et al., 2018). The L-DAC process was modelled in a continuous flowsheet encompassing the K-cycle for CO₂ absorption and the Ca-cycle for CO₂ desorption. KOH was selected for CO₂ absorption due to its faster kinetic performance and lower energy consumption compared to other alkaline solvents such as NaOH (Mahmoudkhani et al., 2009), as well as its ability to effectively handle low CO₂ concentrations, outperforming amine-based solvents like Monoethanolamine (MEA). The choice of calcium looping for CO₂ desorption was motivated by its low cost and high technological maturity, particularly in the cement industry.

The mass and energy balance are performed through process simulation in Aspen Plus®. It was designed to annually capture roughly 1 Mt of CO₂ from the atmosphere and eventually deliver 1.48 Mt of dry CO₂ (1 Mt of air-captured CO₂ and 0.48 Mt of on-site CO₂ emitted from natural gas combustion) for storage or utilisation.

3.2.1 Thermodynamic model and chemical reactions

The model employed the **RK-SOAVE**, **ENRTL-RK** and **SOLIDS** thermodynamic property packages for the gaseous phase, aqueous phase and solid phase, respectively. The selection of physical property methods in the Aspen simulation was based on the targeted modelling environment and methods referenced in previous literature (Keith et al., 2018; Sabatino et al., 2021; An et al., 2022). The gaseous phase is modelled using **RK-SOAVE** (Redlich-Kwong-Soave) to predict vapour-liquid equilibrium (VLE) of gaseous species, chosen for its reliability in handling non-ideal gas mixtures at moderate pressures and temperatures. The liquid phase employs **ENRTL-RK** (unsymmetrical electrolyte Non-Random Two-Liquid) for binary interaction parameters, electrolyte pair parameters, and the equilibrium constant of the precipitation reaction. The **SOLIDS** method is used to handle the thermodynamic behaviour of solid phases and is easy for convergence.

It should be noted that the CO₂ absorption is based on the two-film rate-based approach and the CO₂ desorption is based on equilibrium chemical reactions. For the CO₂ absorption process, the KOH and Ca(OH)₂ salts are regarded as K⁺, Ca²⁺ and OH⁻ in the environment.

The chemical reactions between aqueous KOH and CO₂ are described by the set of equilibrium reactions and the kinetic reactions. The equilibrium reactions in Table 3.1

represent the dissociation of water, the formation of bicarbonate and the formation of carbonate.

Table 3.1 Chemistry settings of equilibrium reactions for rate-based air contactor model

Equilibrium Reactions	A	B	C	D
$\text{CO}_2 + 2\text{H}_2\text{O} \leftrightarrow \text{HCO}_3^- + \text{H}_3\text{O}^+$	231.465	-12092.1	-36.7816	0
$\text{HCO}_3^- + \text{H}_2\text{O} \leftrightarrow \text{H}_3\text{O}^+ + \text{CO}_3^{2-}$	216.05	-12431.7	-35.4819	0
$2\text{H}_2\text{O} \leftrightarrow \text{OH}^- + \text{H}_3\text{O}^+$	132.899	-13445.9	-22.4773	0

The temperature-dependent equilibrium constants (K_{eq}) for these reactions are defined on a molar concentration scale and have been determined from Equation 3.1. The coefficients of the equilibrium constant (A, B, C and D) for these reactions were taken from Sabatino et al. (2021).

$$\ln K_{eq} = A + \frac{B}{T} + C \ln T + DT \quad (3.1)$$

The kinetically controlled reactions are presented in Table 3.2. These sets of reactions control the rate of absorption and enhance mass transfer from the gas phase to the liquid phase. The reaction rates (r) of the kinetic reactions are determined using the power-law expressed as follows:

$$r = kT^n e^{-\frac{E}{RT}} \prod_{i=1}^N C_i^{a_{ij}} \quad (3.2)$$

Where k is the pre-exponential factor, E is the activation energy, T is the system temperature, R is the universal gas constant, C_i is the concentration of species, a_{ij} is the reaction order of

component i in reaction j. Kinetic parameters used in the power-law to calculate the rate of reactions are presented in Table 3.2.

Table 3.2 Chemistry settings of kinetic reactions for rate-based air contactor model

Kinetic Reactions	k	n	E (J/kmol)
$\text{CO}_2 + \text{OH}^- \rightarrow \text{HCO}_3^-$	4.32e+13	0	5.54709e+07
$\text{HCO}_3^- \rightarrow \text{CO}_2 + \text{OH}^-$	2.38e+17	0	1.23305e+08

The chemical reactions for salt formation of CaCO_3 , Ca(OH)_2 and decomposition of CaCO_3 are modelled as equilibrium reactions based on their stoichiometry. The mass and energy balance of them is determined from reaction conversions and Aspen default Gibbs free energy.

3.2.2 Process model development

Figure 3.1 depicts the block flow diagram (BFD) of the L-DAC process. The green arrow lines represent gaseous streams, the blue arrow lines represent liquid streams, and the black arrow lines represent solid streams. The streams numbered 1-8 in red are the input streams, while the streams numbered 9-15 in purple are the outputs from the simulation to which our results are compared. The modelled key units of the L-DAC process include an air contactor, pellet reactor, steam slaker, calciner and CO_2 absorber.

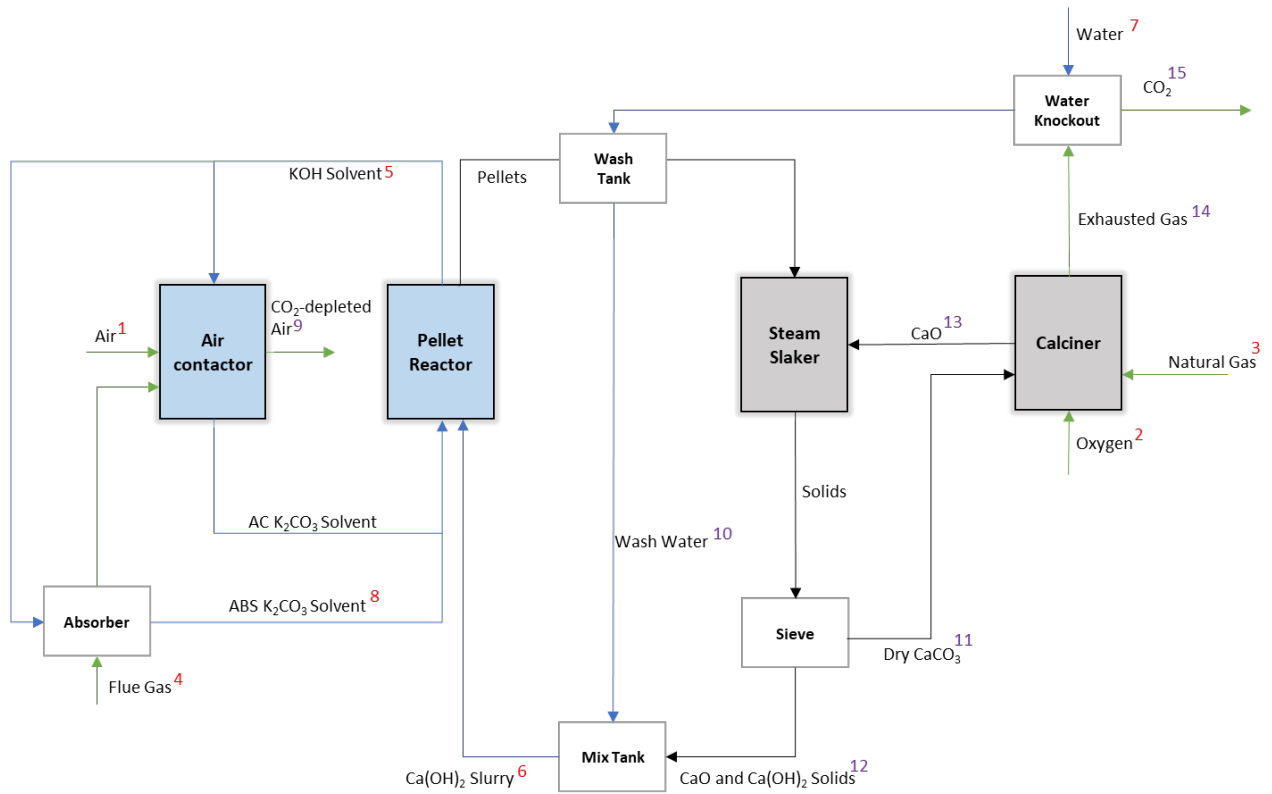


Figure 3.1 Block flow diagram of L-DAC process

3.2.2.1 Air contactor model

The air contactor is the beginning and the most essential unit for the DAC plant. CE established an outdoor prototype and a pilot air contactor to investigate the key parameters such as air velocity, pressure drop and CO₂ capture rate. The model of the air contactor is based on the practical design, as illustrated in Figure 3.2. Figure 3.3 presents the model development approach for the commercial-scale air contactor. Hundreds of modules are stacked and ordered as 4m × 40m (4 modules vertical and 40 modules horizontal) in a bank (20m × 200m × 7m) to obtain the 100 kt/year CO₂ capture capacity (Holmes and Keith, 2012, Heidel et al., 2011, Holmes et al., 2013). Tens of such banks can achieve the 1 MtCO₂/year capacity.

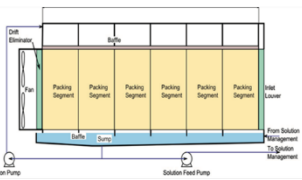
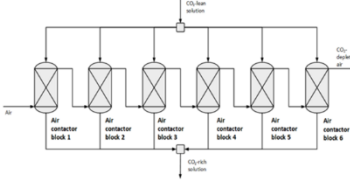
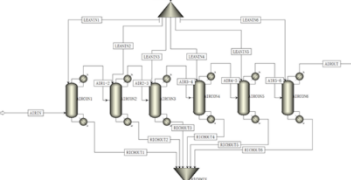
name	CE's air contactor prototype	Sabatino's air contactor model	Developed air contactor model
Schematic diagram			
Scale	0.9x1.8 m cross section area with 4.5-6 m air travel distance (ATD)	25 m ² cross section area with 7 m ATD	Six continuous linked blocks (5.64 packing diameter with 1.17 m height)
Packing type	Brentwood XF12560 structured PVC packing	Sulzer 250 X and Sulzer 250 Y structured packing	Modified Sulzer 250 Y structured PVC packing
Comment	Test prototype performance	Kinetic model	rate-based RadFrac model
Ref.	Holmes et al., 2013	Sabatino et al., 2021	

Figure 3.2 Model development for one air contactor module




Schematic diagram			
Scale	One air contactor unit 5x5 m cross section area with 7 m ATD	One bank (160 air contactor units) 20 m tall, 7 m deep, and 200 m long	Commercial scale air contactor (10 banks)
Contacting area	25 m ²	4,000 m ²	40,000 m ²
Capture level	610 t/yr CO ₂ captured	100 kt/yr CO ₂ captured	1 Mt-CO ₂ /yr captured

Figure 3.3 Model development for commercial-scale air contactor

The simulation of one modular unit of air contactor adopted an approach from Sabatino et al. (2021) to represent the real-world design presented by Keith et al. (2018). The rate-based model is further improved using modified packing properties and correlated pressure drop. Since the Brentwood XF12560 packing is not a built-in packing in Aspen Plus®, a modified Sulzer 250Y PVC packing is used instead. The Brentwood XF12560 packing parameters

including specific surface area (SSA), void fraction and liquid holdup presented in Table 3.3 was used to replace the default value of Sulzer 250Y PVC packing.

Table 3.3 Modified Sulzer 250Y PVC packing setting in Aspen Plus®

Parameter	Settings	Reference
Material	PVC	Holmes (2010)
SSA	210 m ² /m ³	
Liquid holdup	35 g/m ²	
Void fraction	0.95	Cooling Tower Depot® (2023) and Fair et al. (2000)

The packing pressure drop is correlated with the pilot experiments and used for calculating the fan energy requirement. The correlations were made for the pressure drop of Brentwood XF12560 packing. The pressure drop Equation 3.3 provided by Brentwood Industries Inc. (Heidel et al., 2011) was adapted from the pilot experimental (Keith et al., 2018).

$$\Delta P = (7.4v_{air}^{2.14a} + 4.3Q_l \times v_{air}^{0.4b}) \times ATD^{0.95c} \quad (3.3)$$

Where, ΔP is the pressure drop in Brentwood XF12560 packing (Pa); v_{air} is the air velocity driven by the air contactor (m/s); Q_l is the average liquid flow rate on the unit packing area (L/m² s); ATD is the air travel distance (m); a, b, and c are fitting parameters (a=1.06, b=3.31, c=0.79).

The mechanical energy requirement of fans in the air contactor (E_{fans} , J/h) is calculated from Equation 3.4 (Holmes and Keith, 2012).

$$E_{fans} = ATD * \frac{7.4V_{air}^{2.14}}{\eta_{fan}} * t_{op} * A_{module} * N_{modules} \quad (3.4)$$

Where η_{fan} is the fan efficiency (%), t_{op} is the operating time (s), A_{module} is the cross-section area of each air contactor module (m²), and $N_{modules}$ is the number of air contactor modules.

The mechanical energy requirement of pumps in the air contactor (E_{pumps} , J/h) is calculated from Equation 3.5 (de et al., 2019).

$$E_{pumps} = \frac{w * ATD * \rho_{Sorbent} * f * g * h}{\eta_{pumps}} * t_{op} * N_{modules} \quad (3.5)$$

Where w is the width of a module (m), $\rho_{Sorbent}$ is the density of the sorbent (kg/L), f is the sorbent flow rate (m²/s), g is 9.81 m/s² and h is the height of a module (m).

3.2.2.2 L-DAC process model

For the whole L-DAC process, the main unit components and their operating conditions are listed in Table 3.4. The blocks and physical properties of each component are shown in Table 3.5. The air contactor processes 251 kt/h CO₂ in the air at 400 ppm. The CO₂ absorber also processes 121 t/h flue gas from the natural gas power plant. For simplicity, note that the power plant is not simulated in the L-DAC process. To capture CO₂ in the air contactor and CO₂ absorber, the lean KOH solvent concentration is assumed to be 2 M K⁺, 1.1 M OH⁻, and 0.45 M CO₃²⁻ based on CE's commercially available design. The energy requirement of the plant is determined from the Aspen simulation. However, it should be noted that the energy consumption for air contactors is calculated separately.

Table 3.4 Specifications of unit operations for L-DAC process

Parameter	Value	Source
Air Contactor		
Number of banks	10	Holmes et al. (2013)
Number of air contactor units in each bank	160	
Number of blocks in each air contactor unit	6	Sabatino et al. (2021)
Number of stages per block	20	
Diameter	5.64 m	
Height	1.16 m	
Packing	Modified Sulzer 250Y PVC (representing Brentwood XF12560 packing)	Holmes (2010)
Solvent recovery rate	99.93%	Madhu et al. (2021)
Operating temperature	21 °C	Sabatino et al. (2021)
Operating pressure	1 bar	
Pellet Reactor		
Operating temperature	21 °C	Sabatino et al. (2021)
Operating pressure	1 bar	
Calcium retention	90%	Keith et al. (2018)
Steam Slaker		
Pellet water carryover	11.7 wt%	Adapted from process model mass balance
Operating temperature	300 °C	Keith et al. (2018)
Operating pressure	1 bar	
CaO conversion	85%	
Calciner		
Operating temperature	900 °C	Keith et al. (2018)
Operating pressure	1 bar	
CaCO ₃ conversion	98%	
CO ₂ Absorber		
Diameter	7.5 m	Keith et al. (2018)
Height	12 m	
Packing	BERL Ceramic packing	

Table 3.5 The simulated L-DAC components in Aspen Plus®

Components	Blocks	Physical Property
Air contactor	RADFRAC	RK-SOAVE, ENTRTL-RK
Pellet reactor	RSTOIC	RK-SOAVE, ENTRTL-RK
Steam slaker	RGIBBS	SOLIDS
Calcliner	RSTOIC	SOLIDS
CO ₂ absorber	RADFRAC	RK-SOAVE, ENTRTL-RK
Water pump	PUMP	RK-SOAVE, ENTRTL-RK

3.3 Model comparison of L-DAC at commercial scale

To validate the developed L-DAC process in terms of model accuracy, the simulation results were compared with CE's commercial design. To make the whole simulation work, the required stream inputs are provided in Table 3.6. The comparison of output streams is detailed and presented in Table 3.7. The steam temperature, flow rate and components are compared. The validation results show great agreement with absolute relative errors below 6.03%.

The CO₂ capture rate is calculated based on the CO₂ mass flow difference between upstream and downstream of gas streams, as shown in Equation 3.6. The comparison of unit performance is given in Table 3.8. The CO₂ capture rate of the air contactor and CO₂ absorber can achieve the same capture rate (around 75%) as CE designed. The energy consumption for major units is also compared, and the relative error is less than 0.56%.

$$CO_2 \text{ capture rate} = \frac{mCO_{2in} - mCO_{2out}}{mCO_{2in}} \quad (3.6)$$

Table 3.6 Stream inputs into the 1MtCO₂/year L-DAC process model

Stream Number	Stream ID	Parameters	Value
1	Air	Temperature (°C)	21
		Flow rate (kt/h)	251
		CO ₂ (wt%)	0.06
		O ₂ (wt%)	23.00
		N ₂ (wt%)	75.96
		H ₂ O (wt%)	0.98
2	Oxygen	Temperature (°C)	21
		Flow rate (t/h)	58.5
		O ₂ (wt%)	95.60
		N ₂ (wt%)	4.4
3	Natural Gas	Temperature (°C)	21
		Flow rate (kt/h)	13.4
4	Flue Gas	Temperature (°C)	40
		Flow rate (kt/h)	121
		CO ₂ (wt%)	14.43
		O ₂ (wt%)	0.91
		N ₂ (wt%)	72
		H ₂ O (wt%)	12.66
5	KOH Solvent	Temperature (°C)	21
		Flow rate (kt/h)	35
		K ⁺ (mol/L)	2
		OH ⁻ (mol/L)	1.1
		CO ₃ ²⁻ (mol/L)	0.45
6	Ca(OH) ₂ Slurry	Temperature (°C)	21
		Flow rate (t/h)	777
		CaOH (wt%)	28.7
7	Water	Temperature (°C)	21
		Flow rate (t/h)	531
8	ABS K ₂ CO ₃ Solvent	Temperature (°C)	31
		Flow rate (t/h)	3200
		K ⁺ (mol/L)	2.01
		OH ⁻ (mol/L)	0.68
		CO ₃ ²⁻ (mol/L)	0.66

Table 3.7 Model stream results and comparison with stream results from CE's DAC process

Stream ID	Name	Parameters	CE's DAC process	Process model simulation results	Relative error (%)
9	CO ₂ -depleted Air	Temperature (°C)	19	18.47	-2.79
		Flow rate (kt/h)	252	251.55	-0.18
		CO ₂ (wt%)	0.016	0.01542	-3.63
		O ₂ (wt%)	22.96	22.95	-0.04
		N ₂ (wt%)	75.83	75.8295	0
		H ₂ O (wt%)	1.2	1.2	0
10	Wash Water	Temperature (°C)	NA	54	NA
		Flow rate (t/h)	567	566.998	0
		K ⁺ (kg/h)	3089	3080	-0.29
		OH ⁻ (kg/h)	768	740	-3.65
		CO ₃ ²⁻ (kg/h)	1016	1062	4.53
11	Dry CaCO ₃	Temperature (°C)	300	300	0
		Flow rate (t/h)	300	300.58	0.19
12	CaO and Ca(OH) ₂ Solids	Temperature (°C)	300	300	0
		Flow rate (t/h)	211	210.11	-0.42
		CaO (t/h)	24.7	24.76	0.24
		CaOH (t/h)	186	185.35	-0.35
13	CaO	Temperature (°C)	674	674	0
		Flow rate (t/h)	165	165.04	0.02
14	Exhausted Gas	Temperature (°C)	454	450	-0.88
		Flow rate (t/h)	201	201.41	0.20
		CO ₂ (wt%)	82.57	82.553	-0.02
		O ₂ (wt%)	1.16	1.227	5.78
		N ₂ (wt%)	1.28	1.278	-0.16
		H ₂ O (wt%)	14.99	14.942	-0.32
15	CO ₂	Flow rate (t/h)	171	171.33	0.19
		CO ₂ (wt%)	97.12	97.046	-0.08
		O ₂ (wt%)	1.36	1.442	6.03
		N ₂ (wt%)	1.51	1.502	-0.53
		H ₂ O (wt%)	0.01	0.0098	-2.00

Table 3.8 Comparison of simulated unit performance with CE's design

Parameter	CE's DAC process	Simulation results	Relative error (%)
Air Contactor			
CO ₂ captured rate (%)	74.5	74.54 ^a	0.05
Pumping energy (kWh/tCO ₂)	21	20.9 ^b	0.13
Fan energy (kWh/t-CO ₂)	61	61.2 ^c	0.56
Pellet Reactor			
Ca ²⁺ to CaCO ₃ conversion (%)	100 ^d	100	0
Discharged pellets (%)	~90	90	0
Pumping energy (kWh/tCO ₂)	27	26.9 ^b	0.14
Steam Slaker			
CaO conversion (%)	85	85	0
Slaking heat (kJ/mol)	105.2 ^e	105.03 ^f	-0.16
Calciner			
CaCO ₃ conversion (%)	98	98	0
Thermal energy consumption (GJ/tCO ₂)	5.25	5.23 ^f	-0.44
CO₂ absorber			
CO ₂ absorber capture level (%)	90	89.99 ^a	-0.01
^a Obtained from rate-based absorption model			
^b Calculated from the liquid flow rate (82% pump efficiency)			
^c Calculated from fan energy equation (70% fan efficiency)			
^d Ca ²⁺ as a limiting reagent mentioned in Keith et al. (2018)			
^e Obtained from CE's patent (Heidel and Rossi, 2017)			
^f Aspen Plus [®] simulation results			

3.4 Conclusion

- (1) The methodology for the model development of the steady-state L-DAC process at commercial scale is presented. The L-DAC process was successfully implemented in Aspen Plus[®].
- (2) The L-DAC process model is more advanced compared with previous work (Sabatino et al., 2021) An et al., 2022), especially in terms of air contactor modelling. A

modified built-in packing representing the Brentwood XF12560 packing was incorporated, and the packing pressure drop was adjusted based on correlations derived from pilot experiments.

- (3) The commercial scale L-DAC process model is well-established, and the relative errors are less than ~6% compared with the literature-reported results. Therefore, it demonstrates significant agreement on material and energy balance. This strong agreement provides the confidence for following model development of solar-driven L-DAC process where the natural gas combustion-based calciner is replaced with solar calciner.

Chapter 4. Model development, simulation, validation and scale-up of solar calciner

4.1 Overview

In this chapter, a novel hydrogen-fluidised solar calciner was proposed and developed at a commercial scale based on the design, model development, validation and scale-up of a pilot solar calciner. Initially, section 4.2 introduces the pilot air-fluidised solar calciner and then proposes a hydrogen-fluidised solar calciner for application in the L-DAC process. Section 4.3 presents the detailed model development procedures for the air-fluidised solar calciner at the pilot scale in terms of model assumptions and model implementation. Section 4.4 validates the developed solar calciner model with pilot experiments from the French PROMES laboratory. Section 4.5 provides a scale-up approach for fluidised bed reactor from pilot scale to commercial scale using literature-reported scaling laws. Finally, the conclusions of this chapter are drawn in section 4.6.

4.2 Pilot solar calciner and newly-proposed solar calciner

4.2.1 Pilot air-fluidised solar calciner

The solar calcination process depicted in Figure 4.1 is realized at the world's largest solar furnace in the French PROMES laboratory (Esence et al., 2020b). It integrates three sub-systems: (1) heliostat field, (2) parabolic mirror and (3) solar furnace. The heliostat field consists of 63 heliostats that receive direct normal irradiation (DNI) and reflect solar energy on the parabolic mirror. The parabolic mirror collects solar energy and delivers the concentrated solar power (CSP) to the solar furnace's front wall which is coated with high-

temperature paint Pyromark® 2500 for increasing solar absorptivity. This solar reactor was built with high-temperature durable nickel-chromium-iron alloy Incoloy® 800HT which can sustain up to 1100 °C. The heat is transferred from the front wall to the particles through radiation, conduction and convection to provide the sensible heat and the endothermic calcination reaction enthalpy.

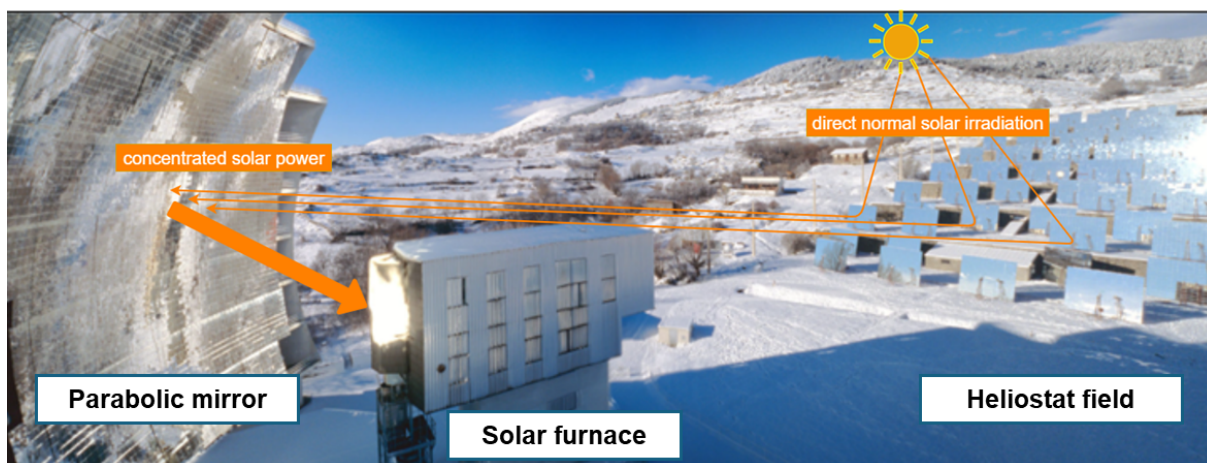


Figure 4.1 Photograph of the 1-MW Odeillo's solar furnace

The intermittent solar radiation on the heliostat field is controlled by aiming strategy and movable aperture. Despite the direct normal irradiation on the heliostats in the range of 777-1000 W/m² during the test campaign, the concentration factor on the solar furnace's front wall is averagely controlled at 220 suns (1 sun equivalent to a solar radiative flux of 1 kW/m²). At steady state operation, the global average temperature of the reactor is between 790-831 °C, for which the mean solar radiative power input (P_{in}) received by the solar furnace was between 45.4-67.4 kW.

This pilot-scale solar reactor manufactured by COMESSA was implemented as the focus of the solar furnace. As shown in Figure 4.2, it is a four-stage fluidised bed reactor fluidised by

air from the bottom and the particles cross-flow from the 1st stage to the 4th stage. The solar reactor is 1 m in length and contains 4 compartments. Each has a 25 cm length, and 8 cm width and is separated from each other by 40 cm height baffles. So, the height of the fluidised bed is 40 cm and above the 40 cm height, a disengaging zone (conical part in Figure 4.2) limits the particle entrainment. Theoretically, the solar reactor can process 48 kg particles (assuming a density of 2700 kg/m³ and a void fraction of 0.5). The experiments showed the highest conversion at 95.2%, which was conducted at a 20 kg/h particle flow rate and high air fluidisation flowrate of 30 Nm³/h. In this case, the highest thermochemical efficiency (17%) and highest thermal efficiency (29%) were achieved.

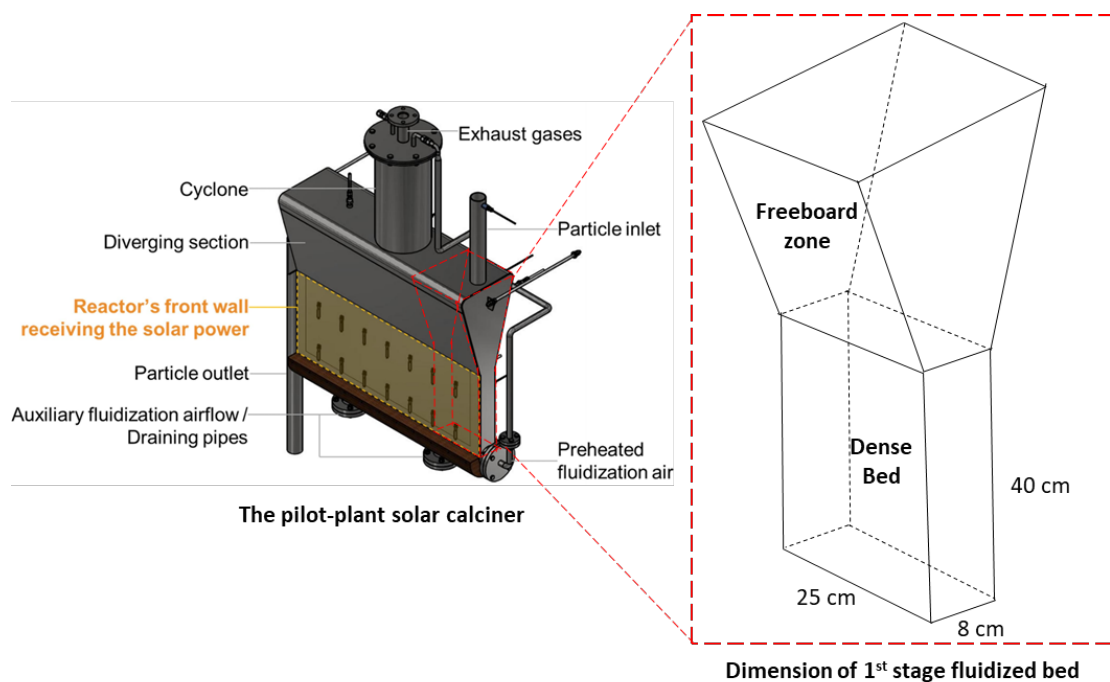


Figure 4.2 Schematic diagram of the pilot-scale solar reactor and the dimension of 1st stage fluidised bed

4.2.2 Newly-proposed hydrogen-fluidised solar calciner

Considering this pilot solar calciner cannot be directly used for L-DAC because the presence of fluidised air during the CO₂ desorption stage would make CO₂ capturing from air meaningless. Therefore, an alternative fluidisation medium needs to be identified. Taking inspiration from the hydrogen direct reduction (HDR) process applied in the steel industry (Wang et al., 2021), hydrogen is proposed as an alternative fluidisation medium in the solar calciner for the L-DAC process. In the steel industry, hydrogen has been successfully implemented as an innovative solution for achieving a low-carbon emissions process. Projects such as MIDREX H2™, which utilises 100% hydrogen as a reducing agent to manufacture iron, demonstrate the feasibility and effectiveness of hydrogen-based fluidised beds (MIDREX, 2022). Drawing from this industrial application, this work has compelling evidence to use hydrogen as a fluidisation medium for solar calciner. The schematic diagram of a hydrogen-fluidised solar calciner for the solar calcination process is shown in Figure 4.3. The hydrogen is fluidised from the bottom of the solar calciner. With the CaCO₃ decomposed using thermal energy from concentrated solar power, the released CO₂ is swept by H₂ and collected from the top of the solar calciner. Based on the pilot calcination process, the hydrogen-fluidised solar calcination process is designed in Figure 4.4, which includes the heliostat field, parabolic mirror and solar calciner.

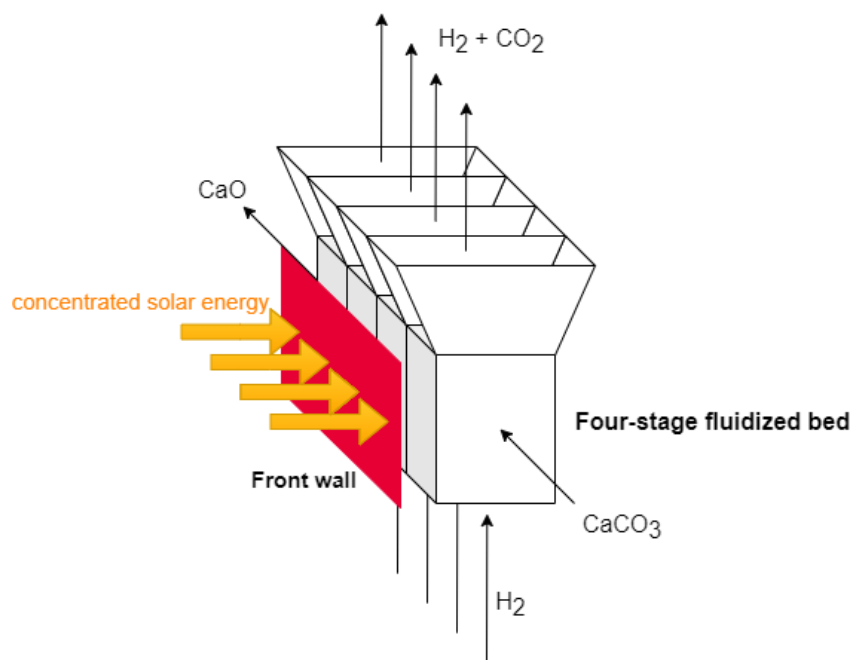


Figure 4.3 Schematic of the solar calciner—a hydrogen-based four-stage horizontal fluidised bed

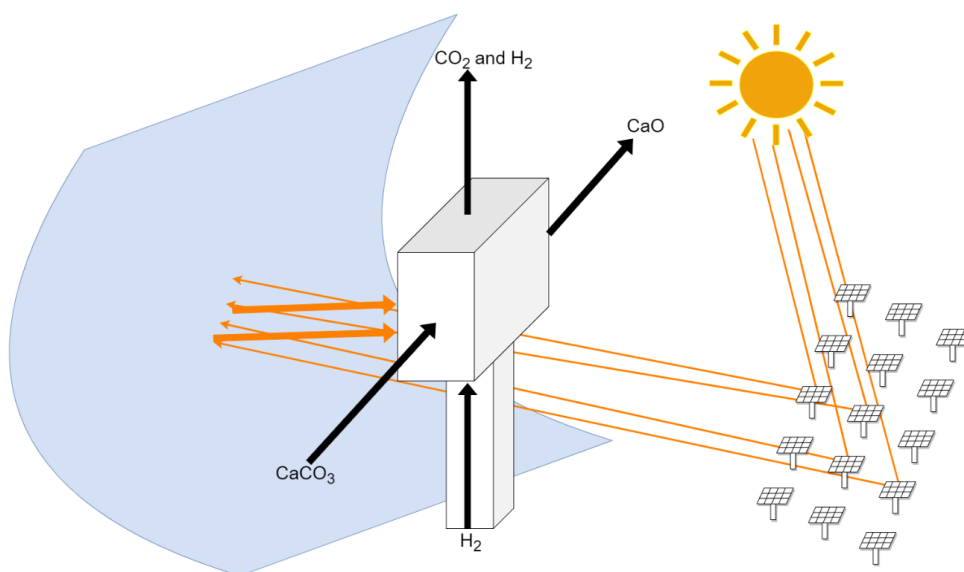


Figure 4.4 Schematic of the solar calcination, encompassing the heliostat field, parabolic mirror and solar calciner

4.3 Model development of solar calciner at pilot scale

Since no study modelled the mass and energy balance of this pilot calciner, this is the first work to develop a four-stage fluidised bed model for the PROMES's pilot reactor.

4.3.1 Assumptions

The following assumptions were made during solar calciner model development:

- The pilot four-stage horizontal fluidised bed is represented by the tandem of four fluidised bed blocks in Aspen Plus®.
- The solar calciner is modelled at steady-state.
- The hydrodynamic of the fluidised bed is only considered in the height axis.
- The freeboard zone was assumed as 40 cm in height.
- The operating temperature of the solar calciner represents the mean reactor temperature.
- Waste heat recovery is not considered in the solar calciner.

4.3.2 Model implementation

To reproduce the four-stage horizontal fluidised bed used for solar calcination, the solar reactor was simulated in four fluidised beds and the process flowsheet was implemented in Aspen Plus® V11 shown in Figure 4.5. The **SOLIDS** physical property method was used to cope with the gas-solid environment. The specifications of each fluidised bed and other settings are presented in Table 4.1.

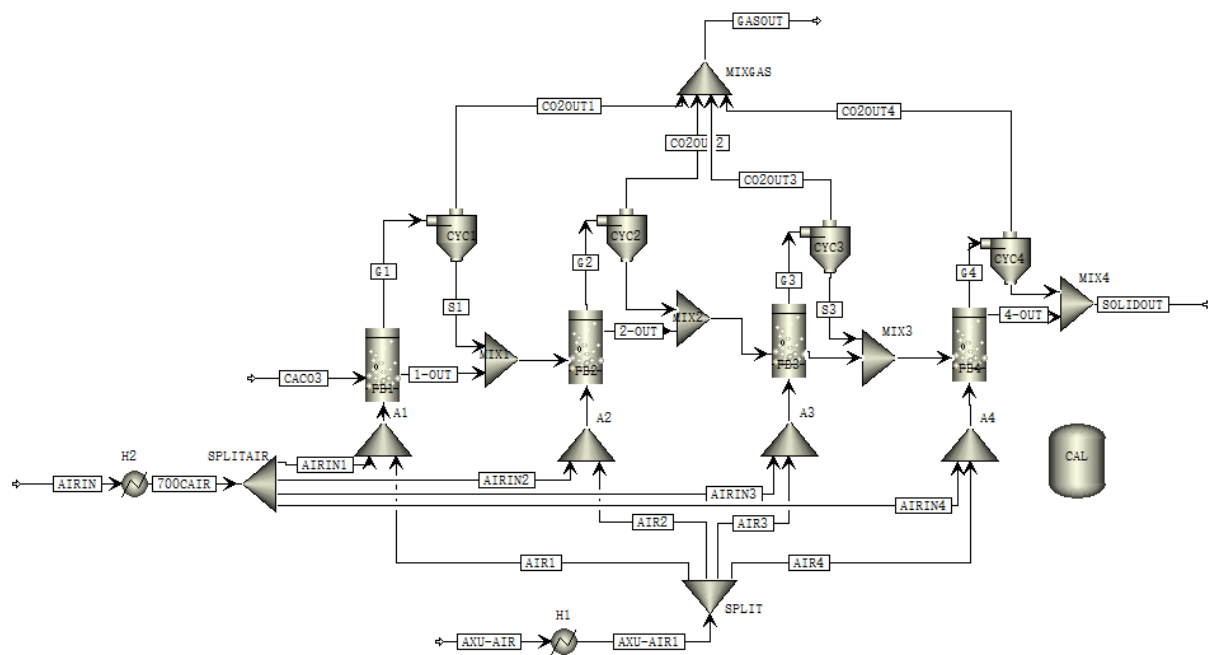


Figure 4.5 Four-stage horizontal solar calciner in Aspen Plus® flowsheet

Table 4.1 Specification of fluidised bed setup in Aspen Plus®

Bed Geometry	
Bed number	4
Width	25 cm
Depth	8 cm
Height (dense bed height)	40 cm
1 st stage solid discharge location	5 cm
2 nd stage solid discharge location	30 cm
3 rd stage solid discharge location	5 cm
4 th stage solid discharge location	40 cm
Bed inventory	
Voidage at minimum fluidisation	0.5
Geldart classification	Geldart A
Other model settings	
Minimum fluidisation velocity correlation	Wen & Yu (1966)
Transport disengagement height	Fung and Hamdullahpur (1993)
Elutriation	Tasirin & Geldart (1998)

It should be noted that Aspen uses the default stream and reaction enthalpy for energy balance calculation. To accurately model the pilot calciner, the Aspen Custom Modeller® V11 (ACM) was used to correlate the enthalpy of reaction and streams as well as the calculation method for thermal efficiency. All the equations for enthalpy correlation and thermal efficiency calculation are given in Table 4.2. These equations were coded in ACM and then exported as an additional calculation block (CAL) in the Aspen flowsheet (see Figure 4.5).

Table 4.2 Equations for enthalpy correlation and thermal efficiency calculation

Parameter	Equation	Reference
Enthalpy of reaction (ΔH)	$\Delta H = -1.447 \times 10^{-6} \times T^3 + 3.323 \times 10^{-3} \times T^2 + 5.882 \times T + 1.810 \times 10^5$	Robie and Hemingway (1995)
Enthalpy of CaCO_3 (h_{CaCO_3})	$h_{\text{CaCO}_3} = 9.963 \times 10^2 \times T + 1.345 \times 10^{-1} \times T^2 + 5.882 \times T + 2.156 \times 10^7 \times T^{-1}$	Robie and Hemingway (1995)
Enthalpy of Air (h_{air})	$h_{\text{air}} = 1.041 \times 10^3 \times T - 1.512 \times 10^{-1} \times T^2 + 2.500 \times 10^{-4} \times T^3 - 9.883 \times 10^{-8} \times T^4 + 6.782 \times 10^{-12} \times T^5 + 2.686 \times 10^{-15} \times T^6$	Hilsenrath (1955)
Thermochemical efficiency (η_{thch})	$\eta_{\text{thch}} = \frac{P_{\text{reaction}}}{P_{\text{in}}} = \frac{x_{\text{CaCO}_3} \times m_p \times \alpha_{\text{out}} \div M_{\text{CaCO}_3} \times \Delta H}{P_{\text{in}}}$	Esence et al. (2020b)
Thermal efficiency (η_{th})	$\eta_{\text{th}} = \frac{P_{\text{reaction}} + m_p \times h_{\text{CaCO}_3}^{T_{\text{in}} \rightarrow T_{p,\text{mean}}} + m_{\text{air}} h_{\text{air}}^{T_{\text{in}} \rightarrow T_{p,\text{mean}}}}{P_{\text{in}}}$	Esence et al. (2020b)

In Table 4.2, the enthalpy of reaction ΔH is calculated as Joule per mole and the temperature T is expressed in Kelvin. T_{in} is inlet stream temperature. $T_{p,\text{mean}}$ is the average temperature of the particle in the reactor. m_p is the mass flowrate of inlet CaCO_3 particles and m_{air} is the

mass flowrate of fluidised air. M_{CaCO_3} is the molar mass of $CaCO_3$. α_{out} is the $CaCO_3$ conversion. x_{CaCO_3} is the mass fraction of $CaCO_3$ in the inlet.

4.4 Validation of solar calciner at pilot scale

Two sets of pilot experimental data in Table 4.3 were used for model validation. Both cases are at the same particle flowrate of 20 kg/h. Case 1 was at a low air fluidisation flow rate, while case 2 was at a high fluidisation flowrate.

Table 4.3 Process specifications of solar calcination process at pilot scale

	Case 1: low fluidisation flowrate	Case 2: high fluidisation flowrate
Mass flow rate of $CaCO_3$ (kg/h)	20	20
Air flow rate (Nm^3/h)	10.1	19.3
Auxiliary air (Nm^3/h)	3	4
Global temperature in calciner ^a ($^{\circ}C$)	831	813
Solar power in (kW)	67.4	57.8
Inlet $CaCO_3$ purity ^b (wt%)	98.5%	98.5%
^a Global temperature represents the reactor temperature in each specific case		
^b Other impurities include 0.085% CaO and 0.065% unreactive materials such as SiO, MgO, and MnO		

It can be found in Table 4.4 that the validation results are in line with expectations. Case 1 shows the absolute relative errors in the range of 0.08-8.16%. While case 2 shows the absolute relative errors in the range of 0.03-2.81%.

Table 4.4 Validation of two representative experimental data of solar calcination

	Case 1: low fluidisation flow rate			Case 2: high fluidisation flow rate		
	Pilot data	Simulation result	Relative errors	Pilot data	Simulation result	Relative errors
Mass balance						
CaCO ₃ conversion (α_{out})	88.50%	88.57%	-0.08%	95.20%	95.43%	-0.24%
CaCO ₃ weight fraction in solids outlet	18.60%	18.26%	1.80%	7.62%	7.68%	-0.75%
CaO weight fraction in solids outlet	80.65%	80.92%	-0.34%	91.24%	91.22%	0.03%
Unreactive materials weight fraction in solids outlet	0.75%	0.81%	-8.16%	1.14%	1.11%	2.81%
Energy balance						
Thermochemical efficiency (η_{thch})	14%	13.62%	2.70%	17%	17.10%	-0.60%
Thermal efficiency (η_{th})	23%	23.42%	-1.85%	29%	29.13%	-0.46%

Figure 4.6 presents the hydrodynamics in the solar calciner from the 1st stage to the 4th stage. It was found most of solids are fluidised by air in the dense bed zone (under 40 cm bed height). The CO₂ fraction could reflect the extent of the calcination reaction. The CaCO₃ particles continuously flow from 1st stage to 4th stage of the fluidised bed and the CaCO₃ conversion is further extended. The most CaCO₃ particles are decomposed in the 1st stage while the 4th stage present smallest extent conversion.

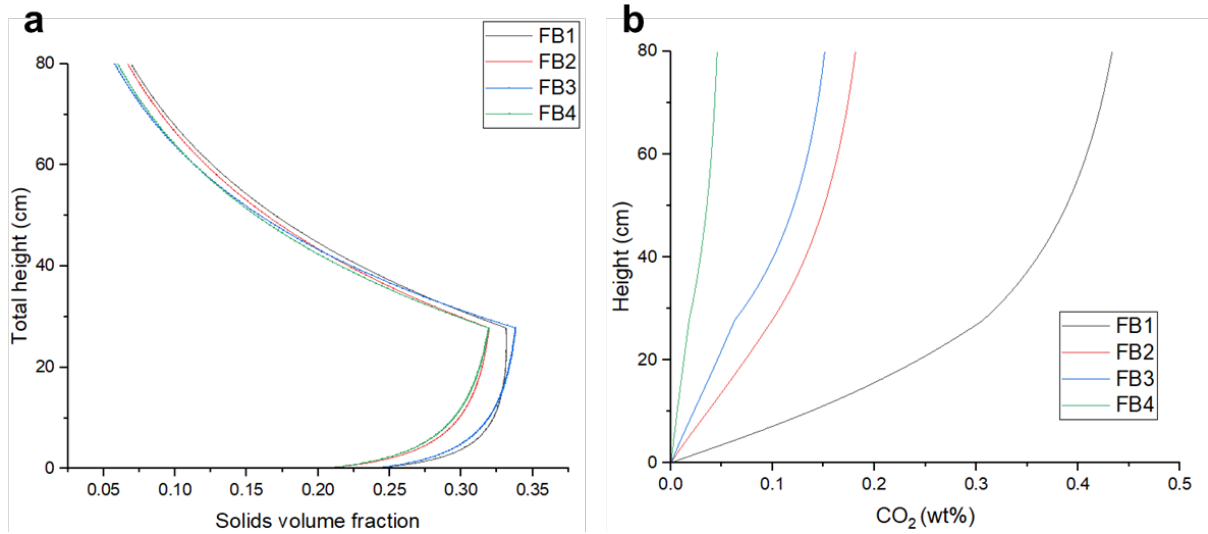


Figure 4.6 Hydrodynamics in the solar calciner. (a) Solids volume fraction along height. (b) CO₂ mass fraction along height (FB: fluidised bed)

4.5 Scale-up of solar calciner from pilot scale to commercial scale

The scale-up of solar calciner is based on the scaling law in open literature which is considered as the most efficient and cost-effective method for determining the hydrodynamics of a hot fluidised bed system (Knowlton et al., 2005, Rüdisüli et al., 2012). It should be noted that rare studies considered the scaling effect on the reaction conversion (Chew et al., 2022). Here, the scale-up approach used for the solar calciner considers both hydrodynamic similarity and chemical conversion (Kelkar and Ng, 2002).

The solar calciner is initially scaled to achieve hydrodynamic similarity. Based on the previous studies on scaling relations for fluidised beds (Glicksman, 1984, Glicksman et al.,

1993), it was found that the independent nondimensional parameters (such as Reynolds number, Froude number and bed geometric ratios) govern the dynamics of fluidised bed.

From Glicksman's study, the gas-to-particle drag can be represented by the Ergun equation (Equation 4.1). The first term represents the viscous contribution to the drag and the second term represents the fluid inertia.

$$\frac{\beta L}{\rho_s u_0} = 150 \frac{\varepsilon(1-\varepsilon)^2}{\varepsilon^3} \frac{\mu L}{\rho_s u_0 (\phi d_p)^2} + 1.75 \frac{\varepsilon^2(1-\varepsilon)}{\varepsilon^3} \frac{|u-v| \rho_f}{\phi d_p u_0 \rho_s} L \quad (4.1)$$

Where ϕ is the particle sphericity, β is the coefficient of drag force, ρ_s is the particle density, ρ_f is the fluid density, u_0 is the superficial velocity, ε is the bed voidage, μ is the fluid viscosity, L is the bed dimension, d_p is the particle diameter, u is the fluid velocity and v is the particle velocity.

For a given reactor type-gas solid bubbling fluidised bed, the Reynolds number is less than 4 ($Re \leq 4$), and viscous forces dominate the fluidisation hydrodynamics. The inertia term can be omitted for a simplified scaling process.

For this case, the similarity between a small bed and a larger bed (scaled up by a factor of n) is maintained by ensuring that the geometric and topological attributes of the bed are scaled proportionally as shown in Equation 4.2. This includes parameters of bed diameter (D_T), height (H), distributor orifice diameter (P_n), and mean bubble diameter (d_b). When scaled up, these attributes maintain a consistent ratio, preserving the hydrodynamic behaviour between the small and large systems.

$$n = \frac{D_T^l}{D_T^s} = \frac{H^l}{H^s} = \frac{P_n^l}{P_n^s} = \frac{d_b^l}{d_b^s} \quad (4.2)$$

Where the superscript s refers to the smaller scale fluidised bed, here is the pilot scale. The superscript l refers to the n times larger scale fluidised bed.

In Equation 4.3, the minimum fluidisation velocity (U_{mf}), gas superficial velocity (U_G) and bubble rise velocity scale as the square root of the scale ratio n .

$$n^{0.5} = \frac{U_{mf}^l}{U_{mf}^s} = \frac{U_G^l}{U_G^s} = \frac{u_b^l}{u_b^s} \quad (4.3)$$

Equation 4.4 gives the scaling rules for solid bed voidage (ϵ_s) and the volume fraction of bubble (ϵ_b).

$$1 = \frac{\epsilon_s^l}{\epsilon_s^s} = \frac{\epsilon_b^l}{\epsilon_b^s} \quad (4.4)$$

The relationship for flow rate of solids (F_s) is presented in Equation 4.5.

$$n^3 = \frac{F_s^l}{F_s^s} \quad (4.5)$$

The scaling of flow rate of gas (F_G) is given by Equation 4.6.

$$n^{2.5} = \frac{F_G^l}{F_G^s} \quad (4.6)$$

For achieving the same reaction conversion at different scales, the scaling principle is illustrated in Figure 4.7.

With the assistance of scaling law, the design and operating parameters were calculated in Table 4.5. Initially, the design and operating parameters for the hydrogen-fluidised bed were calculated at pilot scale. Subsequently, the scaling factor was set as 10 to determine the parameters of the hydrogen-fluidised bed at a large scale.

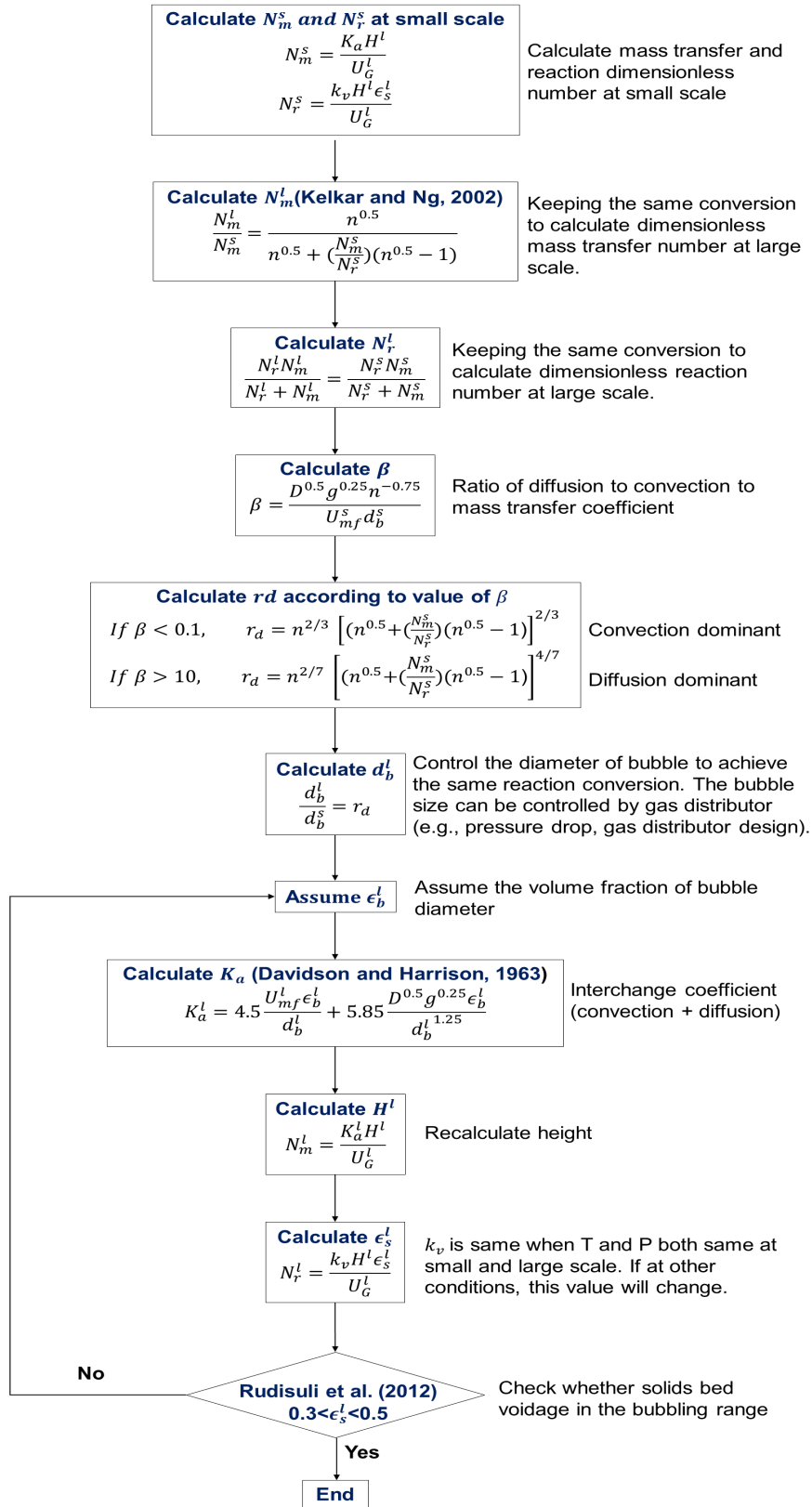


Figure 4.7 Scale-up principle of solar calciner for achieving the same reaction conversion

Based on the scaling law, the bubble size of the fluidised bed is controlled in a suitable range to achieve the same reaction conversion at large-scale (see Figure 4.8).

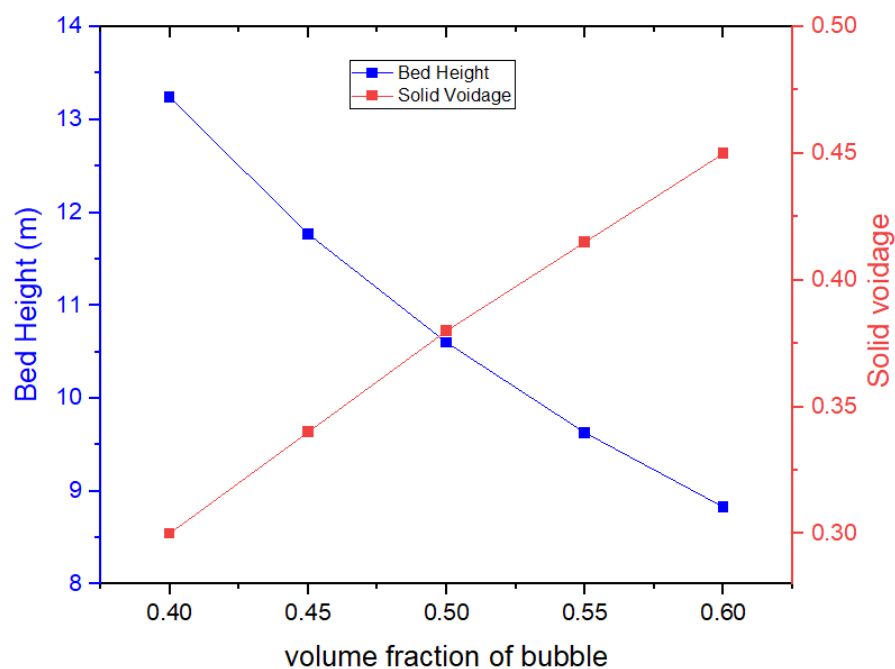


Figure 4.8 Bed height and solid voidage as a function of bubble volume fraction at large-scale

Table 4.5 Design and operating parameters of large-scale hydrogen-based solar calciner through scaling approach

Symbol	Description	Unit	Pilot-scale (Air-fluidised bed)	Pilot-scale (H ₂ -fluidised bed)	Large-scale (H ₂ -fluidised bed)
n	Scaling factor	-	1		10
Reactor Geometry and Phase Flows					
L	Length	m	0.08	0.08	0.8
W	Width	m	0.25	0.25	2.5
H	Height	m	0.8	0.8	10.73
F _S	Solids flow rate	kg/h	20	20	20,000
F _G	Gas flow rate	kg/h	30	2.077	656.8
U _{mf}	Minimum fluidisation velocity	mm/s	4	8.1	25.5
U _G	Superficial fluidisation velocity	m/s	0.4	0.404	1.28
u _b	Bubble velocity	m/s	0.95	0.94	2.97
Phase distribution					
d _p	Mean particle diameter	μm	100	100	178
d _b	Bubble diameter	m	0.053	0.05	0.7
ε _b	Volume fraction of bubble	-	0.415	0.42	0.5
ε _s	Voidage of solids	-	0.5	0.5	0.37
Transport attributes					
K _a	Interchange coefficient	s ⁻¹	0.64	0.01	0.69
Dimensionless No. and Reactor Performance					
N _r	Reaction numbers	-	1.28	1.49	4.69
N _m	Mass transfer numbers	-	0.1	1.37	0.84
X _{CaCO3}	CaCO ₃ conversion	-	0.95	0.95	0.95

4.6 Conclusion

- (1) A hydrogen-fluidised solar calciner is proposed based on the pilot solar calciner design. This newly-proposed solar calciner is suitable for application in the L-DAC process. The fluidised H_2 could sweep the air-captured CO_2 for collection, therefore the mixed gas (H_2 and CO_2) from the solar calciner has the potential to be used in the downstream processing.
- (2) The solar calciner model was successfully developed at pilot scale in Aspen Plus[®], in which ACM was used for the correlation of enthalpy and calculation of thermal efficiency.
- (3) The pilot fluidised bed model was validated using two sets of pilot data from the French PROMES laboratory and the absolute relative errors in the range of 0.03-8.16%.
- (4) The scale-up approach for solar calciner achieving hydrodynamic similarity and same reaction conversion was developed based on the scaling law of fluidised bed. It was used to replace the fluidised air with new fluidisation medium-hydrogen and to scale up the fluidised bed from the pilot scale to commercial scale.

Chapter 5. Model development, simulation and validation of direct CO₂-FTS process

5.1 Overview

In this chapter, a CO₂ conversion into jet fuel route is provided through direct CO₂-FTS. A CO₂-FTS model was developed in Aspen Plus® linking with ACM based on first principles and modified ASF distribution. Section 5.2 presents the detailed model development procedures for the CO₂-FTS process at the lab scale in terms of assumptions, modelling of hydrocarbon distribution and model implementation. Section 5.3 validates the developed CO₂-FTS process model with lab experiments from the University of Oxford. Section 5.4 further simulates the CO₂-FTS process model at commercial scale using assumptions and provides an ex-situ water removal approach via gas recycling for further process improvements. Finally, the conclusions of this chapter are drawn in section 5.5.

5.2 Model development of CO₂-FTS process at lab scale

5.2.1 Assumptions

The following assumptions were made during CO₂-FTS model development:

- The CO₂-FTS process operates at steady-state conditions. Hence, the accumulation of heat and mass was not considered.
- Only reactant conversion and specific products are considered based on material balance and stoichiometric reactions.
- The type of HCs depends on the nature of catalyst. Since the selectivity towards oxygenated compounds was below 1.0% during experiments (Yao et al., 2020), they

were neglected in this model. Hence, only olefins and paraffins were considered in this model.

- The chain growth probability of hydrocarbons was based on the given ASF plot from experiments (Yao et al., 2020).
- The infinite number of CO₂-FTS reactions was handled by the lumping technique. It is simply defined as grouping several components into a smaller number of components to represent the whole group (Hillestad, 2015).

5.2.2 Modelling of hydrocarbon distribution

A model for the prediction of hydrocarbon distribution was developed in ACM. This model combines modified ASF theory and kinetic modelling of the CO₂-FTS process to accurately predict the hydrocarbon distributions. Based on the previous modified ASF model, the weight fraction of hydrocarbon (W_n) was calculated from Equation 4.1 (Donnelly et al., 1988) based on two chain growth probabilities (α_1 and α_2) and two fractions of hydrocarbons (f_1 and f_2).

$$W_n = f_1 \times \alpha_1^{n-1} + f_2 \times \alpha_2^{n-1} \quad (4.1)$$

The C₃ hydrocarbon is considered a deviation from the standard ASF distribution due to the complex reaction mechanisms of the Fe-Mn-K catalyst used. Consequently, specific experimental conditions and kinetic values were employed to accurately model the chain growth probability and weight fraction for C₃ hydrocarbons. The chain growth probability of C₃ (α_{C_3}), as shown in Equation 4.2, was calculated using the specific experimental conditions (P_{CO_2} and P_{H_2}) and kinetic values (k_1, k_5 and $k_{6,0}$) suggested by Kamkeng and Wang (2023).

$$\alpha_{C_3} = \frac{k_1 P_{CO_2}}{k_1 P_{CO_2} + k_5 P_{H_2} + k_{6,0} e^{3c}} \quad (4.2)$$

The weight fraction of C₃ compounds (W_3) can be calculated from Equation 4.3 using the chain growth probability of C₃.

$$W_3 = 3 \times (1 - \alpha_{C_3})^2 \times \alpha_{C_3}^2 \quad (4.3)$$

Two fractions of hydrocarbons (f_1 and f_2) related to α_1 and α_2 are derived from Equations 4.4 and 4.5 based on carbon number at break point (b) and fitting parameter (λ).

$$f_1 = \lambda \frac{1 - W_3}{\frac{1}{1 - \alpha_1} - \frac{\alpha_1}{1 + \alpha_1} + \left[\frac{1}{1 - \alpha_2} - \frac{\alpha_2}{1 + \alpha_2} \right] \left(\frac{\alpha_1}{\alpha_2} \right)^{b-1}} \quad (4.4)$$

$$f_2 = f_1 \times \left(\frac{\alpha_1}{\alpha_2} \right)^{b-1} \quad (4.5)$$

The mass fraction of hydrocarbons obtained from ASF theory is converted into the corresponding selectivity (S_n) by applying Equations 4.6 to 4.8.

$$\frac{1}{\bar{M}} = \sum_{n=1}^{50} \frac{W_n}{M_n} \quad (4.6)$$

$$x_n = \frac{W_n}{M_n} \times \bar{M} \quad (4.7)$$

$$S_n = \frac{x_n \times n}{\sum_{n=1}^{50} x_n \times n} \quad (4.8)$$

Where M_n is the molecular weight of hydrocarbon n, \bar{M} is the average molecular weight, and x_n is the mole fraction of hydrocarbon.

With the obtained selectivity of hydrocarbons, the molar flowrate for each carbon compound (n_{HC_n}) are calculated based on Equations 4.9 and 4.10.

$$N_{HC} = n_{CO_{2in}} \times X_{CO_2} \times X_{CO} \quad (4.9)$$

$$n_{HC_n} = N_{HC} \times \frac{S_n}{n} \quad (4.10)$$

Where N_{HC} is the total molar flowrate of produced hydrocarbons, X_i is the conversion of reactant i , and n_i is molar flowrate of reactant i .

5.2.3 Model implementation of CO₂-FTS process using Aspen Plus® and Aspen Customer Modeller®

The CO₂-FTS process was implemented in Aspen Plus® linking with Aspen Customer Modeller® (ACM). Initially, the modified ASF distribution model was calculated in ACM® for every carbon number ranging from 1 to 50. The CO₂-FTS reactions and lumping components used for process modelling are presented in Table 5.1. For simplicity, the wax category represents hydrocarbons with carbon numbers greater than 17, encompassing both waxes and any minimal higher-carbon components such as diesel. Based on the olefin to paraffin ratio specified in the experimental study, the flowrate of the corresponding carbon number can determine each product.

Table 5.1 Products and chemical reactions implemented for the CO₂-FTS model

Carbon range	Product category	Carbon number	Component	Chemical reaction
n=1	CO	1	CO	$\text{CO}_2 + \text{H}_2 \rightarrow \text{CO} + \text{H}_2\text{O}$
	Methane		CH ₄	$\text{CO} + 3\text{H}_2 \rightarrow \text{CH}_4 + \text{H}_2\text{O}$
$2 \leq n \leq 4$	Light Hydrocarbon (C ₂ -C ₄)	2, 3 and 4	C ₂ H ₆	$2\text{CO} + 5\text{H}_2 \rightarrow \text{C}_2\text{H}_6 + 2\text{H}_2\text{O}$
			C ₂ H ₄	$2\text{CO} + 4\text{H}_2 \rightarrow \text{C}_2\text{H}_4 + 2\text{H}_2\text{O}$
			C ₃ H ₈	$3\text{CO} + 7\text{H}_2 \rightarrow \text{C}_3\text{H}_8 + 3\text{H}_2\text{O}$
			C ₃ H ₆	$3\text{CO} + 6\text{H}_2 \rightarrow \text{C}_3\text{H}_6 + 3\text{H}_2\text{O}$
			C ₄ H ₁₀	$4\text{CO} + 9\text{H}_2 \rightarrow \text{C}_4\text{H}_{10} + 4\text{H}_2\text{O}$
			C ₄ H ₈	$4\text{CO} + 8\text{H}_2 \rightarrow \text{C}_4\text{H}_8 + 4\text{H}_2\text{O}$
$5 \leq n \leq 7$	Light Naphtha (C ₅ -C ₇)	5, 6 and 7	C ₅ H ₁₂	$5\text{CO} + 11\text{H}_2 \rightarrow \text{C}_5\text{H}_{12} + 5\text{H}_2\text{O}$
			C ₅ H ₁₀	$5\text{CO} + 10\text{H}_2 \rightarrow \text{C}_5\text{H}_{10} + 5\text{H}_2\text{O}$
			C ₆ H ₁₄	$6\text{CO} + 13\text{H}_2 \rightarrow \text{C}_6\text{H}_{14} + 6\text{H}_2\text{O}$
			C ₆ H ₁₂	$6\text{CO} + 12\text{H}_2 \rightarrow \text{C}_6\text{H}_{12} + 6\text{H}_2\text{O}$
			C ₇ H ₁₆	$7\text{CO} + 15\text{H}_2 \rightarrow \text{C}_7\text{H}_{16} + 7\text{H}_2\text{O}$
			C ₇ H ₁₄	$7\text{CO} + 14\text{H}_2 \rightarrow \text{C}_7\text{H}_{14} + 7\text{H}_2\text{O}$
$8 \leq n \leq 16$	Jet Fuel (C ₈ -C ₁₆)	12	C ₁₂ H ₂₆	$12\text{CO} + 25\text{H}_2 \rightarrow \text{C}_{12}\text{H}_{26} + 12\text{H}_2\text{O}$
			C ₁₂ H ₂₄	$12\text{CO} + 24\text{H}_2 \rightarrow \text{C}_{12}\text{H}_{24} + 12\text{H}_2\text{O}$
$n \geq 17$	Wax	20	C ₂₀ H ₄₂	$20\text{CO} + 41\text{H}_2 \rightarrow \text{C}_{20}\text{H}_{42} + 20\text{H}_2\text{O}$

Figure 5.1 illustrates the CO₂-FTS process flowsheet implemented in Aspen Plus® using the physical property method **Peng-Robinson**. The ACM model was exported as a calculation block (FLOWRATE) to the Aspen Plus® flowsheet for calculating the flowrate of hydrocarbons presented in Table 5.1. With the help of Fortran® Routines, the PRODUCT stream is correlated to the ACM model. The feedstock H₂ and CO₂ were assumed to be at 25°C and 1 bar. They are first compressed at 10 bar with a 2-stage compressor featuring intercooling. Afterwards, they were mixed and heated at 300°C in a heater (HEATER). The CO₂-FTS reactor which performs the RWGS and FTS reactions is represented by a stoichiometry reactor block (CO₂-FTS) in Aspen Plus®.

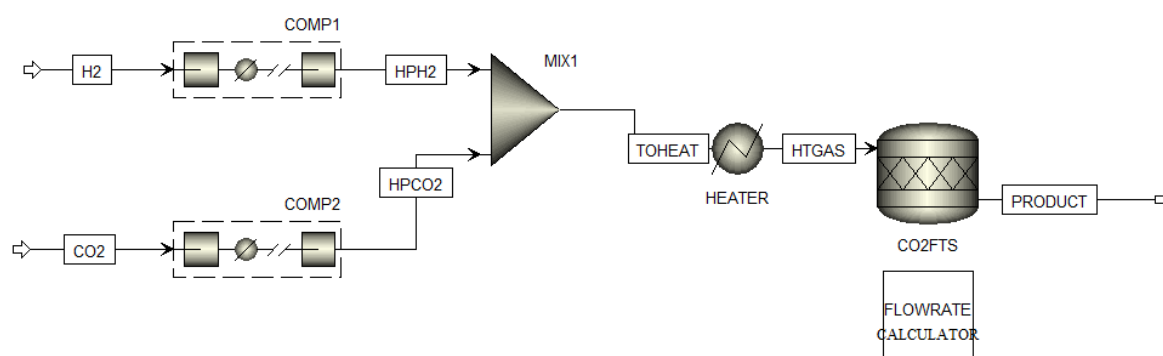


Figure 5.1 Flowsheet diagram of CO₂-FTS process implemented in Aspen Plus® using Fortran® Routines

5.3 Model validation at lab scale

To validate the developed CO₂-FTS model, lab-scale experiments conducted at the University of Oxford were used. The experiments provide ASF plots and selectivity for

different carbon categories for model validation. The ratio of olefin to paraffin for each hydrocarbon is obtained from experiments (Yao et al., 2020, Zhang et al., 2021). The input process conditions and parameters used for the CO₂-FTS model validation are presented in Table 5.2. Process conditions were available from Yao et al. (Yao et al., 2020), and other parameters were reasonably assumed based on the literature.

Table 5.2 Input parameters used for model validation

Parameter		Value	Reference
Reactor type		fixed bed	(Yao et al., 2020)
Reactor diameter (cm)		1	
Reactor temperature (°C)		300	
Reactor pressure (MPa)		1	
H ₂ /CO ₂ ratio		3	
Flow rate (mL/min)		40	
CO ₂ conversion (%)		38.2	
Chain growth probability	α_1	0.79	(Donnelly et al., 1988, Yao et al., 2020)
	α_2	0.57	
Carbon number at breakpoint		12	
Kinetic constants	k_1	1.66×10^{-2}	(Todic et al., 2013, Kamkeng and Wang, 2023)
	k_5	6.99×10^{-5}	
	$K_{6,0}$	2.02×10^{-2}	
Constant c		-0.26	
Fitting parameter λ	$n \leq 7$	$0.15e^{0.35n}$	
	$8 \leq n \leq 12$	$0.29e^{0.39n}$	
	$n \geq 13$	$2.7e^{36n^{-1}}$	

Figure 5.2 compares the model prediction results of the ASF plots with the experimental data given from carbon numbers 1 to 16. The ASF plots agree with the experimental trend and model values. On the other hand, the hydrocarbon distributions were validated based on the experimental selectivity of CO, C₁, C₂-C₄, C₅+, and C₈-C₁₆. Figure 5.3 compares five product categories of model prediction results with experimental data. All the relative errors shown in Table 5.3 are below 2.5%. Therefore, Figure 5.2 and Figure 5.3 show great agreement of the developed model with experimental work.

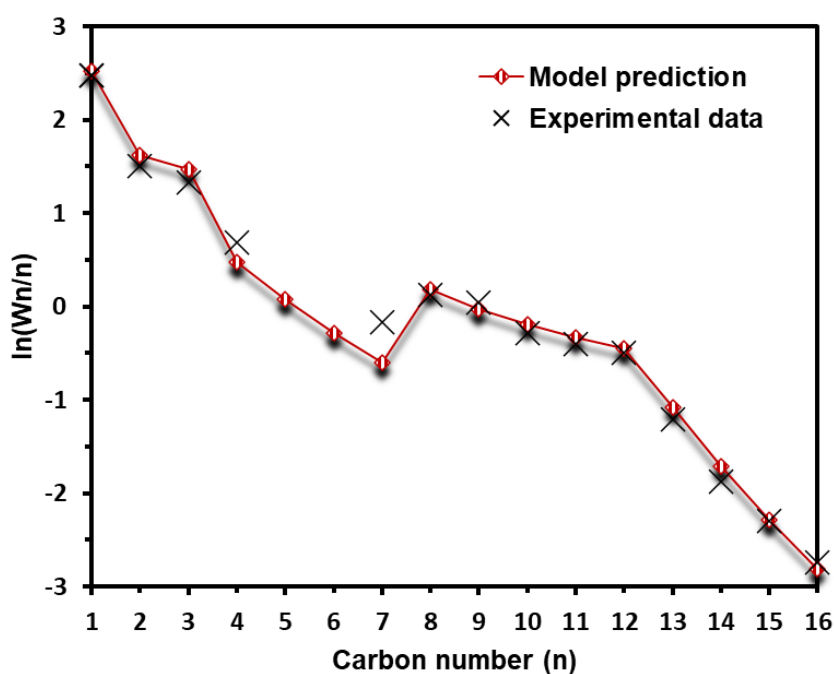


Figure 5.2 Model prediction of ASF plot compared with experimental data

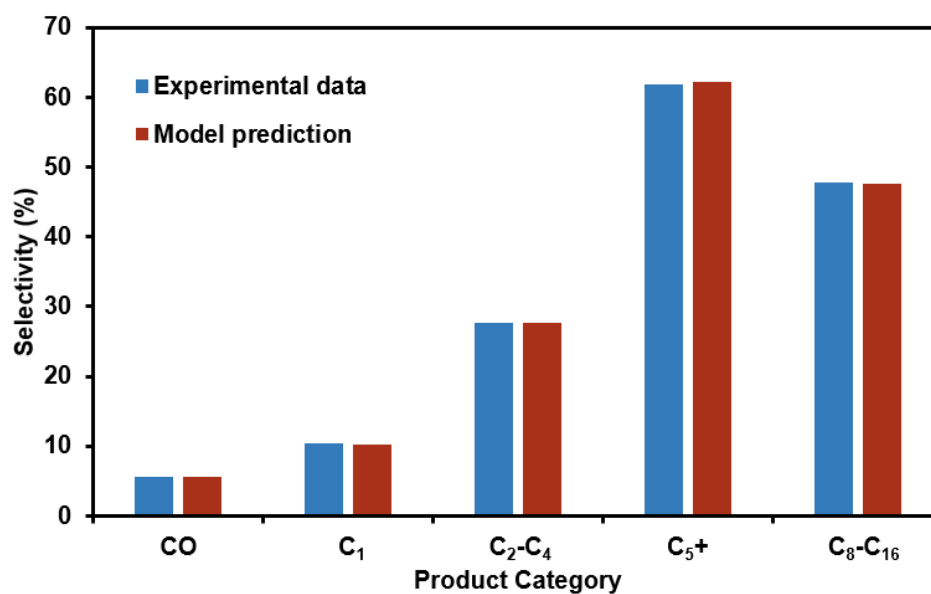


Figure 5.3 Model prediction and experimental values of CO₂-FTS product selectivity

Table 5.3 Model validation results of selectivity for different product categories

Product category	Selectivity (%)		Relative error (%)
	Experimental data	Model prediction	
CO	5.6	5.60	0.00
C ₁	10.4	10.14	-2.51
C ₂ -C ₄	27.7	27.60	0.34
C ₅ +	61.9	62.26	0.58
C ₈ -C ₁₆	47.8	47.64	-0.34

5.4 Simulation of the modified CO₂-FTS process for jet fuel production at commercial scale

5.4.1 Assumptions

The scale-up of the CO₂-FTS model is based on assumptions from previous studies investigated by Kamkeng and Wang (2023). The CO₂-FTS reactor and Fe-Mn-K catalyst are assumed to behave the same way at lab-scale and large-scale. Also, it was assumed that there is no pressure drop in the heaters and coolers. Therefore, the operating conditions are the same at different scales and the impact on the reactor dimensions to reactions is neglected. The material and energy flow of the large-scale CO₂ utilization process is simulated based on validated and scaled models. CO₂ conversion (X_{CO_2}) and jet fuel yield ($Y_{jet\ fuel}$) are calculated based on Equations 4.11 and 4.12.

$$X_{CO_2} = \frac{nCO_{2in} - nCO_{2out}}{nCO_{2in}} \quad (4.11)$$

$$Y_{jet\ fuel} = X_{CO_2} \times S_{jet\ fuel} \quad (4.12)$$

5.4.2 CO₂-FTS process for jet fuel production

Figure 5.4 shows the CO₂-FTS process using a single reactor. The process features an open-loop configuration without the recirculation or upgrade of unconverted reactants, water removal and/or reactor design. The process flow diagram of the base case scenario developed in Aspen Plus® linking with ACM. The inlet flowrate of CO₂ and H₂ could be determined from the previous commercial CO₂ utilization plant (Kamkeng and Wang, 2023, Fernández-Torres et al., 2022) or it could be determined from the feedstock production plants. It should be noted that the products leaving the reactor are cooled down to 40 °C based on industry operation for syncrude oil separation. Followed by the cooler, a three-phase separator divides the stream into light gas, jet fuel and water. The jet fuel stream mainly contains C₈-C₁₆ range

hydrocarbons and lighter and heavier hydrocarbons are also included in this stream. To get the pure jet fuel for commercial standard, further operations such as distillation and separation are required.

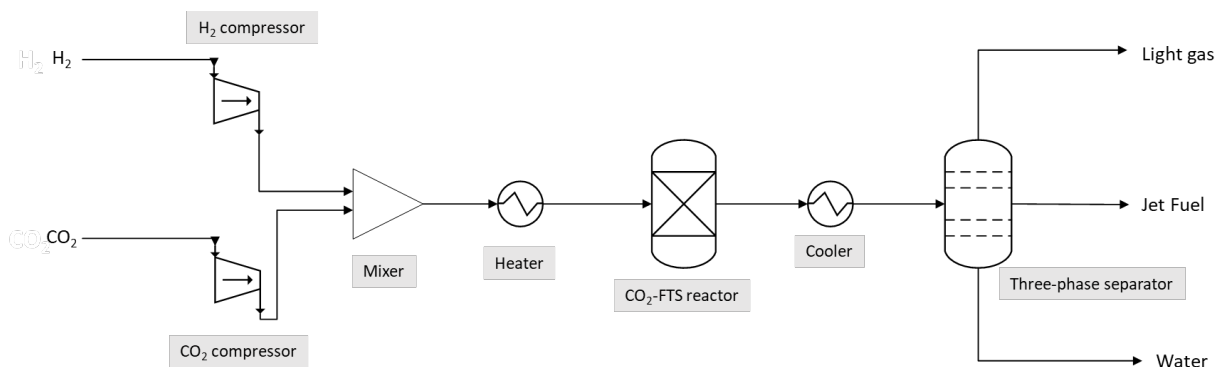


Figure 5.4 Commercial CO₂-FTS process for jet fuel production

5.4.3 Ex-situ water removal through gas recycling

Previous studies (both experimental and modelling) have demonstrated that water formation during the CO₂-FTS process significantly inhibits CO₂ conversion due to a decrease in the driving force of the RWGS reaction. Therefore, continuous water removal is essential to improve RWGS reaction rate hence, CO₂ conversion. The ex-situ water removal for the CO₂-FTS process through gas recycling was simulated in Aspen Plus[®] linking with ACM (see Figure 5.5). The unreacted gas including H₂, CO, and CO₂ is separated from the light gas stream and recycled to the mixer. The recycled gas flowrate depends on the gas recycling ratio set in the splitter. The unreacted gas is controlled with an H₂ to CO₂ ratio of 3 to meet the strict operating conditions in the lab. Since only the ratio of 3 is studied in the experiments, the other ratio of the reaction circumstance is unknown. The study of different gas recycling ratios can be further carried out by sensitivity analysis in Aspen Plus[®].

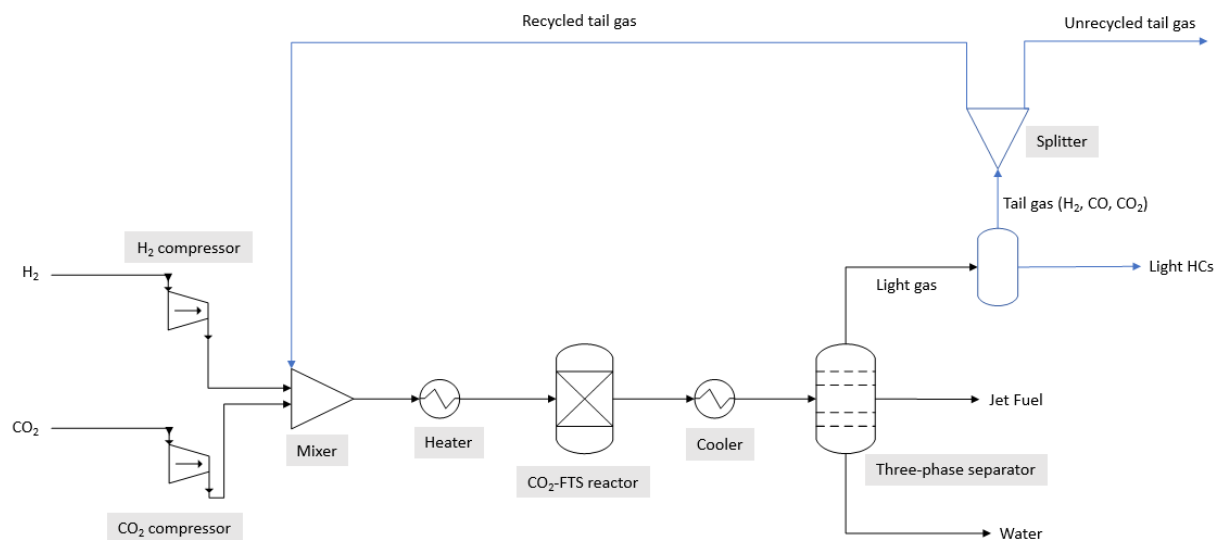


Figure 5.5 Commercial CO₂-FTS with gas recycling for jet fuel production

5.5 Conclusion

- (1) A model for predicting the hydrocarbon distribution of the CO₂-FTS process using Fe-Mn-K catalyst is successfully developed in ACM, which combines the modified ASF theory and kinetic modelling of CO₂-FTS.
- (2) The CO₂-FTS process model for jet fuel production was implemented at lab scale in Aspen Plus[®] linking with ACM and validated using experimental ASF plots and hydrocarbon selectivity.
- (3) The CO₂-FTS process model for jet fuel production was simulated at commercial scale based on literature-reported assumptions. The ex-situ water removal approach through gas recycling has the potential for performance improvement, which can be regarded as an operating strategy for converting CO₂ into jet fuel at commercial scale.

Chapter 6. Process design, model development and simulation of solar-driven DACCU process for SAF production

6.1 Overview

In this chapter, a process design of 1 MtCO₂/year solar-driven DAC and CO₂ utilisation (solar-driven DACCU) to produce SAF is proposed. The novel process is based on three processes namely CE's DAC process (Keith et al., 2018), solar calcination process (Esence et al., 2020a, Esence et al., 2020b), and direct CO₂-FTS process (Yao et al., 2020, Kamkeng and Wang, 2023). Section 6.2 describes the innovations, material flow, process flow diagram and unit design and operations. Section 6.3 presents the detailed model development procedures for solar-driven DACCU process at commercial scale based on the models developed in Chapters 3, 4 and 5. Section 6.4 presents the simulation results of process model at commercial scale which can be used for further plant performance assessment. Finally, the conclusions of this chapter are drawn in section 6.5.

6.2 Process design

6.2.1 Innovations

The proposed solar -driven DACCU process is the result of the innovation and integration of three existing processes. These three processes involve CE's L-DAC process (Keith et al., 2018), solar calcination process (Esence et al., 2020a, Esence et al., 2020b), and CO₂-FTS process (Yao et al., 2020). Each process is redesigned in tandem with each other to eventually achieve this large-scale air-to-fuel process. The innovation for each process can be summarised as L-DAC driven by solar energy, hydrogen-based solar calcination, and direct CO₂-FTS for jet fuel production.

6.2.1.1 L-DAC driven by solar energy

Conventional CE's DAC process has been discussed in literature (Keith et al., 2018, Heidel et al., 2011, Holmes and Keith, 2012, Holmes et al., 2013). The key difference between the proposed DAC design and that of the CE is that it applies a specially designed solar calciner with hydrogen as the fluidisation medium. This is in contrast to CE's design which uses a natural gas-based calciner with oxygen as the fluidisation medium (Keith et al., 2018). Here, we innovatively employ hydrogen as the fluidisation medium in the solar calciner. Thereby, the thermal energy source is changed from fossil fuel (e.g. natural gas) to solar energy (i.e. CSP). The solar calciner enables liquid solvent-based DAC fully driven by renewable energy and continuous CO₂ utilisation in the downstream process.

6.2.1.2 Hydrogen-based solar calcination

Conventional oxy-fuel combustion-based calciner uses oxygen for fluidisation, which requires an air separation unit (ASU) to separate oxygen from air. Previous solar calcination process uses air to fluidise CaCO₃ particles, which is meaningless for CO₂ air capture. This work innovated to use hydrogen as the fluidisation media in solar calciner. Applying hydrogen to fluidise calcite particles will not affect its decomposition, but more importantly, it is in favour of CO₂ mixing with H₂ acting as feedstock for CO₂ utilisation.

6.2.1.3 Direct CO₂-FTS for jet fuel production

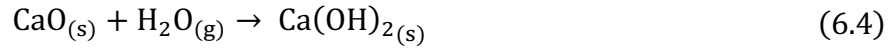
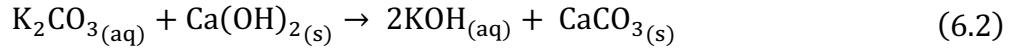
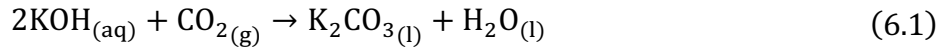
The previous DACCU process uses two-step FTS-based CO₂ conversion to fuel, where CO₂ is firstly converted to CO and then hydrocarbons. In this work, the CO₂ is directly converted to jet fuel via one-step CO₂-FTS using Fe-Mn-K catalyst. Therefore, the syngas preparation step is eliminated. In terms of feedstock used for CO₂ utilisation, the CO₂ is directly from DAC plant and the purity is very high (nearly 100%) while most required H₂ is directly from the fluidised

H₂ used in solar calciner. Thus, additional steps such as CO₂ purification and H₂ preparation could be avoided.

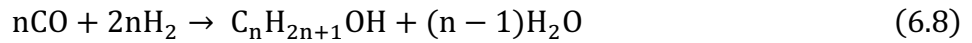
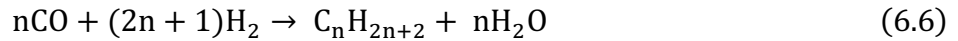
6.2.2 Process description

6.2.2.1 Process chemistry

The material flow is shown in Figure 6.1. The solar-driven DAC section is based on two closed chemical loops of K-cycle absorption (Equation 6.1-6.2) and Ca-cycle desorption (Equation 6.3-6.4).



The direct CO₂-FTS process consists of the RWGS reaction (Equation 6.5) and FTS reactions (Equations 6.6-6.8) in a single CO₂-FTS reactor to produce jet fuel (C₈-C₁₆) and by-products such as gaseous hydrocarbons (C₁-C₄), liquid hydrocarbons (C₅-C₇) and wax (C₁₇₊).



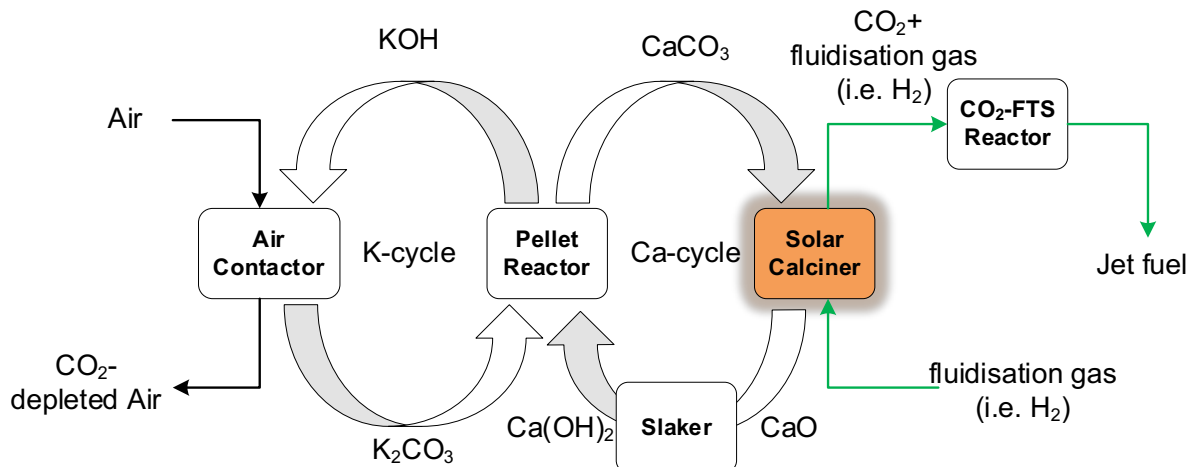


Figure 6.1 Process chemistry of solar-driven DACCU process

6.2.2.2 Process flow diagram

Figure 6.2 depicts a simplified process flow diagram of the 1 Mt CO₂ per year solar-driven DACCU process for SAF production which consists of two major sections: (a) solar-driven DAC and (b) CO₂-to-SAF. The first section represents CO₂ capture from the air and consists of four major units namely the air contactor, the pellet reactor, the slaker and the solar calciner. Notably, solar calcination is regarded as a subsection mainly containing the solar calciner and it plays a vital role in combining DAC with CO₂ utilisation. The second section CO₂-to-SAF enables continuous CO₂ utilisation to produce SAF through CO₂-FTS and separation process. Major units are indicated with graphical representations that suggest a real-world schematic physical design. Some units (e.g. heaters, pumps, and compressors) and streams (e.g. CaCO₃ seed recovery and hydrogen makeup) are not shown for the sake of simplicity. The detailed process flow diagrams of the whole process and simulation results are presented in Figure 6.3-6.5.

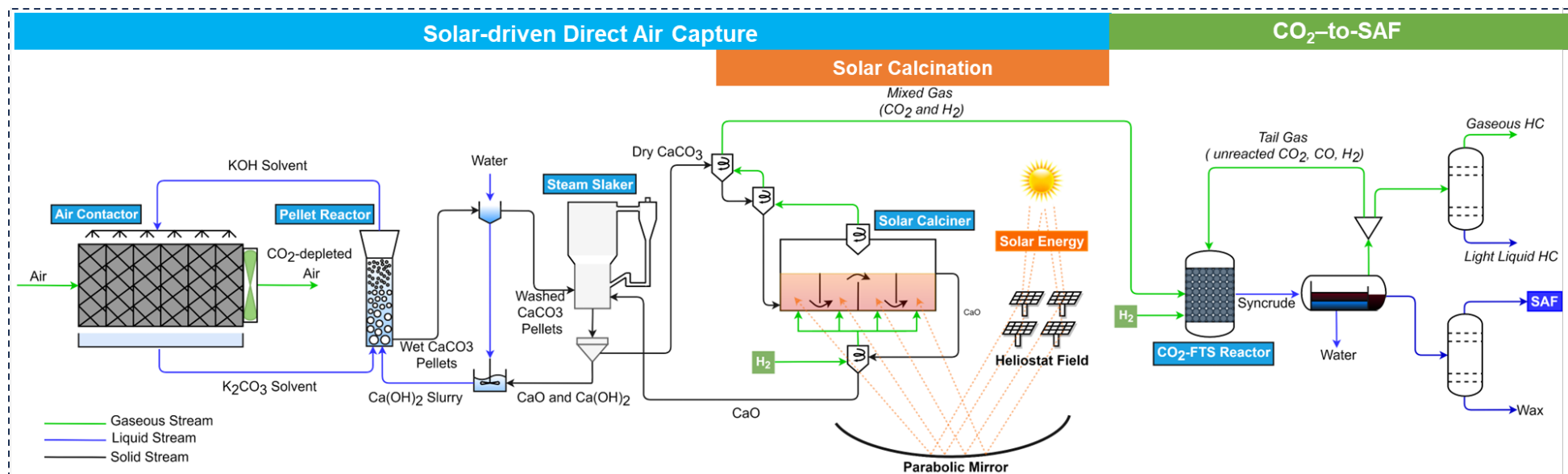


Figure 6.2 Simplified process flow diagram of the solar -driven DACCU process, incorporating the solar-driven DAC and CO₂-to-SAF sections.

6.2.2.3 Unit design and operations

This proposed CSP-driven DACCU process encompasses five major units (1) air contactor, (2) pellet reactor, (3) steam slaker, (4) solar calciner and (5) CO₂-FTS reactor. The detailed design specifications for each major unit are summarised in Table 6.1.

6.2.2.3.1 Air contactor

The function of the air contactor is to capture CO₂ in the air using solvent sorbent typically KOH solvent owing to its high CO₂ uptake and low cost. The air contactor unit is made of thousands of modules. One air contactor module is indeed a structured packing tower where a series of segments of Brentwood XF12560 packing is contained and wetted with KOH solvent. Hundreds of modules are stacked and ordered as 4*40 (4 in vertical and 40 in horizontal) in a bank (20m*200m*7m) to obtain the 100 kt/year CO₂ capture capacity. Tens of banks achieve the 1 Mt-CO₂/year capacity. Fan drives air cross flow from one side of packing to another side to enable CO₂ absorbed by KOH solvent.

6.2.2.3.2 Pellet reactor

The function of the pellet reactor is to regenerate CO₂ absorption solvent and recycle it to air contactor and transform captured CO₂ from CO₂-rich solvent to solid form (CaCO₃). The pellet reactor adopts a bubbling fluidised bed fluidised by liquid solvent. Typically, 30 wt% Ca(OH)₂ slurry reacts with potassium carbonates from air contactors to form calcite pellets. Pellet seeds are input from the top of the bed, so the pellets are grown from the top until finished and discharged as large spherical pellets at the bottom.

6.2.2.3.3 *Steam slaker*

The function of the steam slaker is to dry the wet pellets and transform CaO into Ca(OH)_2 . The steam slaker applies a circulating fluidised bed fluidised by steam and discharge solids at the bottom. This reactor can be self-sustained because high-temperature CaO recycles back from solar calciner and the steam hydration of CaO generates a large amount of slaking heat. The slaking heat is mainly used for drying the washed wet pellets and heating the recirculating steam.

6.2.2.3.4 *Solar calciner*

The solar calciner adopted a hydrogen-based four-stage horizontal fluidised bed to decompose CaCO_3 and release captured CO_2 for subsequent utilization. Calcite particles are fluidised by hydrogen and decomposed with the heat from solar energy. Then, CO_2 is carried by H_2 and discharged at the top of the reactor. Heat is transferred from solar to the particles through radiation, conduction and convection. The inlet calcite particles recover the heat from the mixture gas through two cyclones, on the other hand, the hydrogen recovers the heat from discharged high-temperature CaO .

6.2.2.3.5 *CO_2 -FTS reactor*

The CO_2 -FTS reactor is achieved by a fixed bed reactor packed with catalyst and transform mixture gas (CO_2 and H_2) to jet fuel through the CO_2 -FTS approach. Usually, a good catalyst should have high CO_2 conversion and high hydrocarbon selectivity in desired products. Here, the Me-Fe-K catalyst is selected and could achieve 38.2% CO_2 conversion and 47.8% selectivity of $\text{C}_8\text{-C}_{16}$ in hydrocarbons.

Table 6.1 Design specification of major units of 1 MtCO₂/year solar-driven DACCU plant

Parameter	Value	Unit
Air contactor		
Reactor type	Packed bed (Brentwood XF12560 structured packing)	N/A
Dimensions of the single air contactor unit (length×breadth×hight)	5×7×5	m
Dimensions of the air contactor bank (length×breadth×hight)	20×7×200	m
CO ₂ capture rate	74.5	%
Plant capture productivity	119.4	tCO ₂ /h
Fan electricity	57.4	kWh/tCO ₂
Pumping electricity	18.3	kWh/tCO ₂
Pellet reactor		
Reactor type	Bubbling fluidised bed	N/A
Ca ²⁺ conversion	100	%
Pumping electricity	23.8	kWh/tCO ₂
Steam slaker		
Reactor type	Circulating fluidised bed	N/A
Operating temperature	300	°C
CaO conversion	85	%
Solar calciner		
Reactor type	Four-stage horizontal fluidised bed	N/A
Dimensions of the solar calciner (length×breadth×hight)	13.4×1.1×5.3	m
Hydrogen fluidisation velocity	1.28	m/s
Operating temperature	813	°C
Reactor thermal efficiency	60	%
CaCO ₃ conversion	95.2	%
Solar energy requirement	7.16	GJ/tCO ₂
CO₂-FTS reactor		
Reactor type	Fixed bed	N/A
Catalyst type	Fe-Mn-K	N/A
H ₂ to CO ₂ ratio	3	N/A
Operating temperature	300	°C
Operating pressure	10	bar
CO ₂ conversion	38.2	%
SAF (C ₈ -C ₁₆) selectivity	47.8	%
Electricity consumption	732.7	kWh/tCO ₂

6.3 Model development of solar-driven DACCU at commercial scale

The material and energy balance of the 1 MtCO₂/year solar-driven DACCU process is based on the first principles modelling approach, which was performed using a combination of an equation-oriented model developed in ACM and a block-oriented model developed in Aspen Plus® V11. This model is justified by validation of different key streams and units and subsequent scaling-up as aforementioned in Chapter 3, 4 and 5.

6.3.1 Model development of solar-driven DAC process at commercial scale

The L-DAC process has been simulated and compared at commercial in Chapter 3. Here, for the solar-driven DAC, by incorporating the solar calciner, some units are eliminated which includes air separation unit (ASU), CO₂ absorber, and water knockout. Despite the retrofitting of the calciner, the new solar-driven DAC process maintains the same capacity of 1 MtCO₂/year. This is due to the retention of the air contactor unit and the air inlet area is not changed. The simulation of the solar-driven DAC process is conducted based on the proposed design wherein the solar calciner model replaces the calciner model in the simulated L-DAC process.

6.3.2 Model development of solar calcination at commercial scale

In Chapter 4, the pilot-scale air-fluidised solar reactor was modelled and validated at the pilot scale and followed by scaling up to commercial scale hydrogen-fluidised solar calciner. Note that the scaling factor is based on the required commercial size of the solar calciner. At a specific size, the design and operating parameters when using hydrogen as a fluidisation medium are determined with the scaling law.

6.3.3 Model development of CO₂-to-SAF at commercial scale

The CO₂-FTS process was modelled, validated at lab scale and simulated at commercial scale in Chapter 5. Here, for this commercial-scale CO₂-to-SAF process, the syncrude obtained from the CO₂-FTS reactor requires upgrading through separations and distillations to yield commercial products. For simplicity, the hydrocracking of heavy hydrocarbons is not considered in the work, while process improvement is employed through ex-situ water removal coupled with recirculation of unreacted CO₂, CO and H₂ to CO₂-FTS reactor (Kamkeng and Wang, 2023).

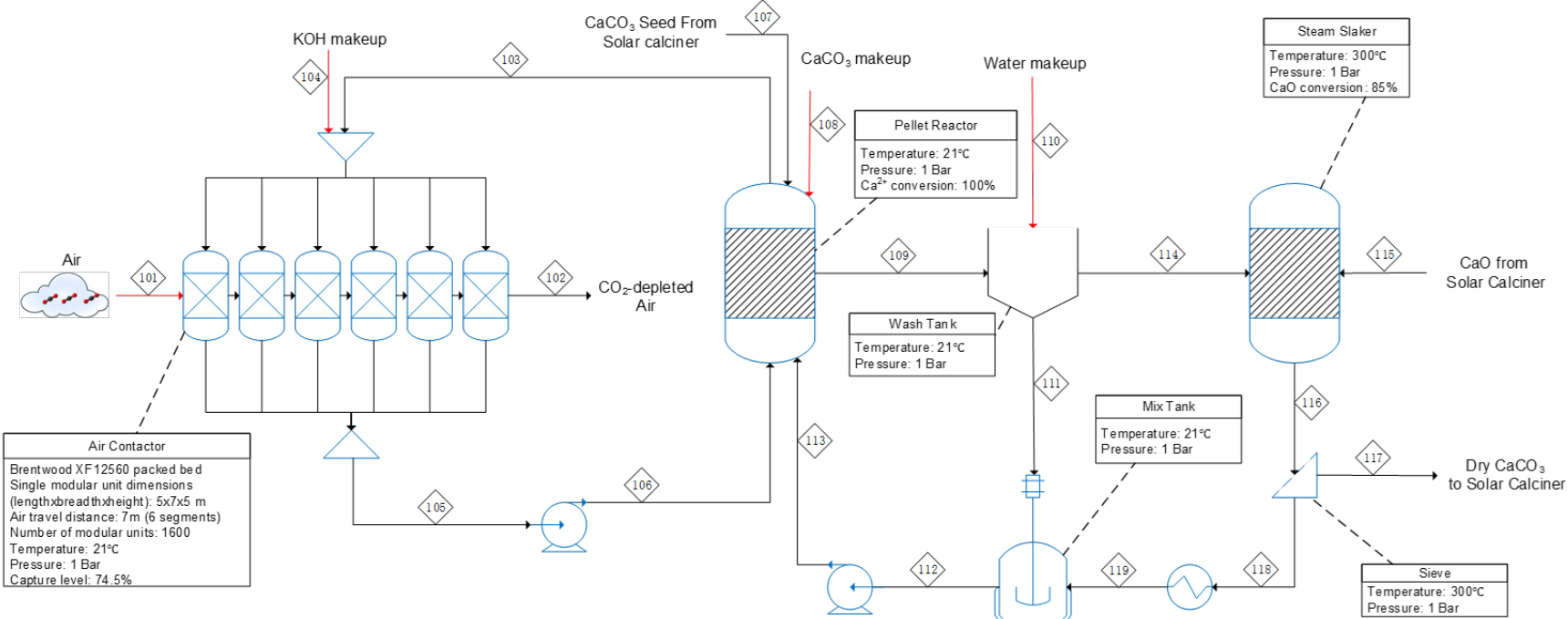
6.4 Simulation of solar-driven DACCU at commercial scale

The simulation results of 1 MtCO₂/year solar-driven DACCU process are presented in Figures 6.3, 6.4 and 6.5.

6.5 Conclusion

- (1) A novel design for the large-scale solar-driven DACCU process to produce SAF was proposed based on L-DAC, solar calcination and CO₂-FTS processes.
- (2) The proposed process has been developed at 1 MtCO₂/year scale based on the models developed in Chapter 3, 4 and 5 via modelling, simulation, comparison/validation and scale-up.
- (3) The simulation results of 1 MtCO₂/year solar-driven DACCU process model are given in details, which could be used for further performance evaluations such as techno-economic assessment.

Solar-driven Direct Air Capture



Component	Units	101	102	103	104	105	106	107	108	109	110	111	112	113	114	115	116	117	118	119
Total Flow	t/hr	251,000	251,456	32,630	10	32,174	32,174	14	27	330	516	523	716	716	323	152	479	285	194	194
Temperature	°C	21	19	21	21	18	18	21	21	21	21	21	21	21	21	450	300	300	300	85
Pressure	bar	1	1	1.4	1	1	1.8	1	1	1	1	1	1	1.8	1	1	1	1	1	1
CO ₂	t/hr	160	41			0	0			0		0	0	0	0					
N ₂	t/hr	190,650	190,650			0.3	0.3			0		0	0	0	0					
O ₂	t/hr	57,730	57,730			0.2	0.2			0		0	0	0	0					
H ₂ O	t/hr	2,460	3,025	28,950		28,434	28,434			39	516	518	511	511	37					
K ⁺	t/hr		7	2,322		2,315	2,315			3		3	3	3	0					
OH ⁻	t/hr		1	556		462	462			1		1	1	1	0					
CO ₃ ²⁻	t/hr		3	802		962	962			1		1	1	1	0					
HCO ₃ ⁻	t/hr		0	0		0	0			0		0	0	0	0					
H ₃ O ⁺	t/hr		0	0		0	0			0		0	0	0	0					
KOH	t/hr				10				27											
Ca(OH) ₂	t/hr												201	201						
CaCO ₃ (S)	t/hr							14		285					285		285	285		
Ca(OH) ₂ (S)	t/hr																		171	171
CaO(S)	t/hr															152	23		23	23

Figure 6.3 Process flow diagram and stream results of solar-driven DAC section excludes solar calcination

Solar-driven Direct Air Capture

Solar Calcination

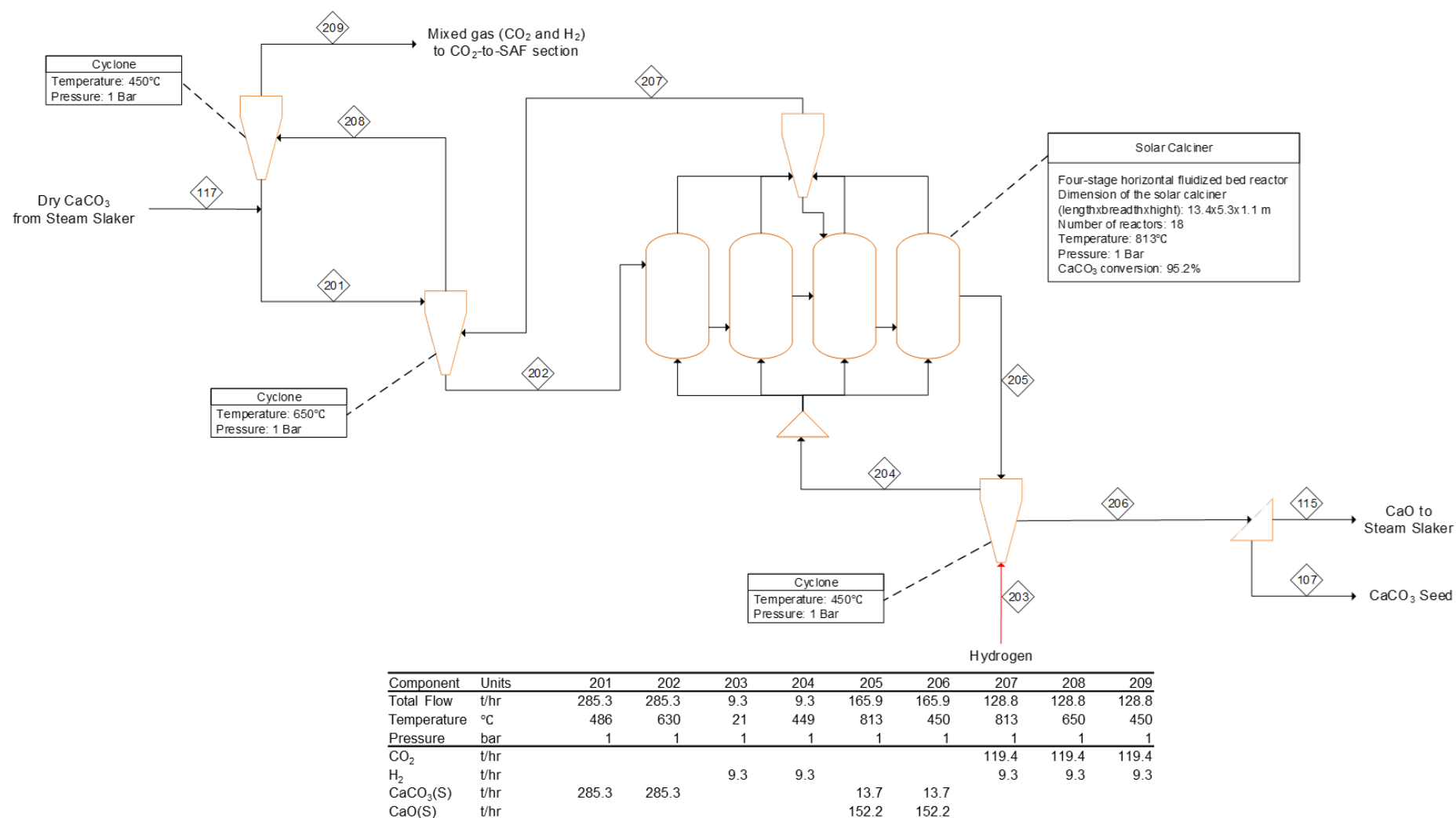
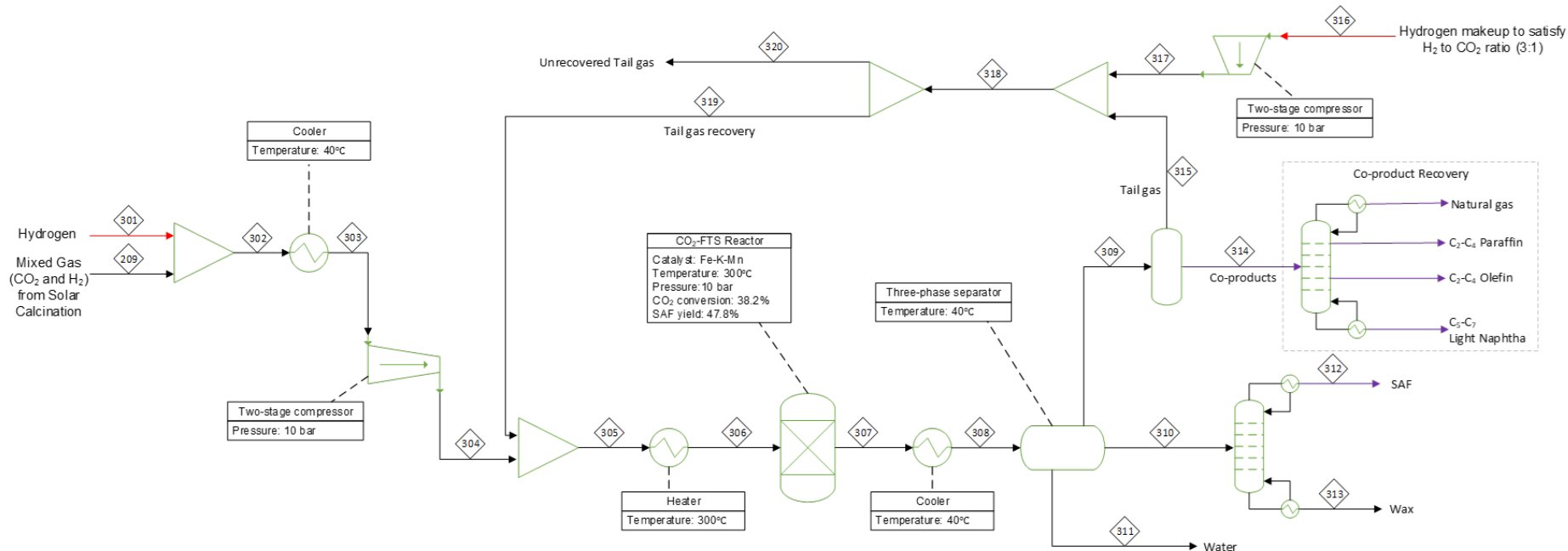


Figure 6.4 Process flow diagram and stream results of solar calcination subsection in solar-driven DAC section

CO₂-to-SAF



Component	Units	301	302	303	304	305	306	307	308	309	310	311	312	313	314	315	316	317	318	319	320
Total Flow	t/hr	7.1	135.8	135.8	135.8	309.8	309.8	309.8	309.8	210.9	17.0	81.9	15.4	1.6	18.6	192.4	0.9	0.9	193.3	173.9	19.3
Temperature	°C	21	331	30	40	40	300	300	40	40	40	40	40	40	40	40	21	40	40	40	40
Pressure	bar	1	1	1	10	10	10	10	10	10	10	10	10	10	10	10	1	10	10	10	10
CO	t/hr				3.47	3.47	3.85	3.85	3.85	0.00	0.00			0.00		3.85			3.85	3.47	0.39
H ₂	t/hr	7.07	9.34	16.41	16.41	37.67	37.67	22.70	22.70	22.70	0.00	0.00		0.00		22.70	0.91	0.91	23.62	21.25	2.36
CO ₂	t/hr		119.42	119.42	119.42	268.65	268.65	166.03	166.03	165.81	0.21	0.01		0.21		165.81			165.81	149.23	16.58
H ₂ O	t/hr							83.77	83.77	1.87	0.04	81.85		0.04	1.87						
CH ₄	t/hr							3.77	3.77	3.77	0.00	0.00		0.00	3.77						
C ₂ H ₆	t/hr							1.41	1.41	1.41	0.00	0.00		0.00	1.41						
C ₂ H ₄	t/hr							1.74	1.74	1.74	0.00	0.00		0.00	1.74						
C ₃ H ₈	t/hr							1.63	1.63	1.62	0.01	0.00		0.01	1.62						
C ₃ H ₆	t/hr							2.41	2.41	2.40	0.01	0.00		0.01	2.40						
C ₄ H ₁₀	t/hr							1.06	1.06	1.04	0.02	0.00		0.02	1.04						
C ₄ H ₈	t/hr							0.93	0.93	0.91	0.02	0.00		0.02	0.91						
C ₅ H ₁₂	t/hr							0.94	0.94	0.89	0.05	0.00		0.05	0.89						
C ₅ H ₁₀	t/hr							0.70	0.70	0.67	0.03	0.00		0.03	0.67						
C ₆ H ₁₄	t/hr							0.94	0.94	0.73	0.09	0.00		0.09	0.73						
C ₆ H ₁₂	t/hr							0.70	0.70	0.48	0.08	0.00		0.08	0.48						
C ₇ H ₁₆	t/hr							0.73	0.73	0.50	0.23	0.00		0.23	0.50						
C ₇ H ₁₄	t/hr							0.44	0.44	0.30	0.14	0.00		0.14	0.30						
C ₁₂ H ₂₆	t/hr							14.36	14.36	0.21	14.15	0.00	14.15	0.00	0.21						
C ₁₂ H ₂₄	t/hr							1.30	1.30	0.02	1.28	0.00	1.28	0.00	0.02						
C ₂₀ H ₄₂	t/hr							0.63	0.63	0.00	0.63	0.00		0.63	0.00						

Figure 6.5 Process flow diagram and stream results of CO₂-to-SAF section

Chapter 7. Evaluation of solar-driven DACCU process for SAF production: techno-economic assessment, sensitivity analysis, geographical analysis and roadmap analysis

7.1 Overview

In this chapter, a comprehensive TEA has been conducted for a 1 MtCO₂/year DACCU process based on the process model developed in Chapter 6. Section 7.2 presents the framework and research methodology for TEA. Section 7.3 presents the TEA results at the base case scenario and compares the proposed process with the previous processes. Section 7.4 conducts the sensitivity analysis using pessimistic and optimistic parameters to highlight key research directions for future process improvements and optimisations. Section 7.5 tests the plant's feasibility through geographical analysis at five selected locations (i.e., USA, Chile, Spain, South Africa and China). Section 7.6 provides a roadmap analysis predicting the cost reduction potential in the future. Finally, the conclusions of this chapter are drawn in section 7.7.

7.2 TEA framework and methodology

In this study, the high-level TEA is carried out to highlight the cost drivers and geographical impacts toward the successful deployment of the proposed process. Figure 7.1 summarises the key input and out parameters of the 1Mt CO₂/year DACCU process model. Parameters such as DNI, solar multiple (SM) and weighted average cost of capital (WACC) are more regionally dependent, whereas parameters such as scaling factors, and reactor efficiency are technology-dependent in the model. In practice, some of these factors would show regional

variation as well, for instance, the cost of PV electricity price according to the risk premium of countries, but this global TEA does not consider these regional influences. The TEA was initially carried out for solar-driven DACCU at base case scenario. The parameters in base case are based on the previous literature (Prats-Salvado et al., 2024, Sabatino et al., 2021, Keith et al., 2018, IEAGHG, 2021). Some parameters such as CO₂ capture rate and gas recovery ratio were determined from process model. The parameters given in optimistic and pessimistic scenarios were used for sensitivity analysis.

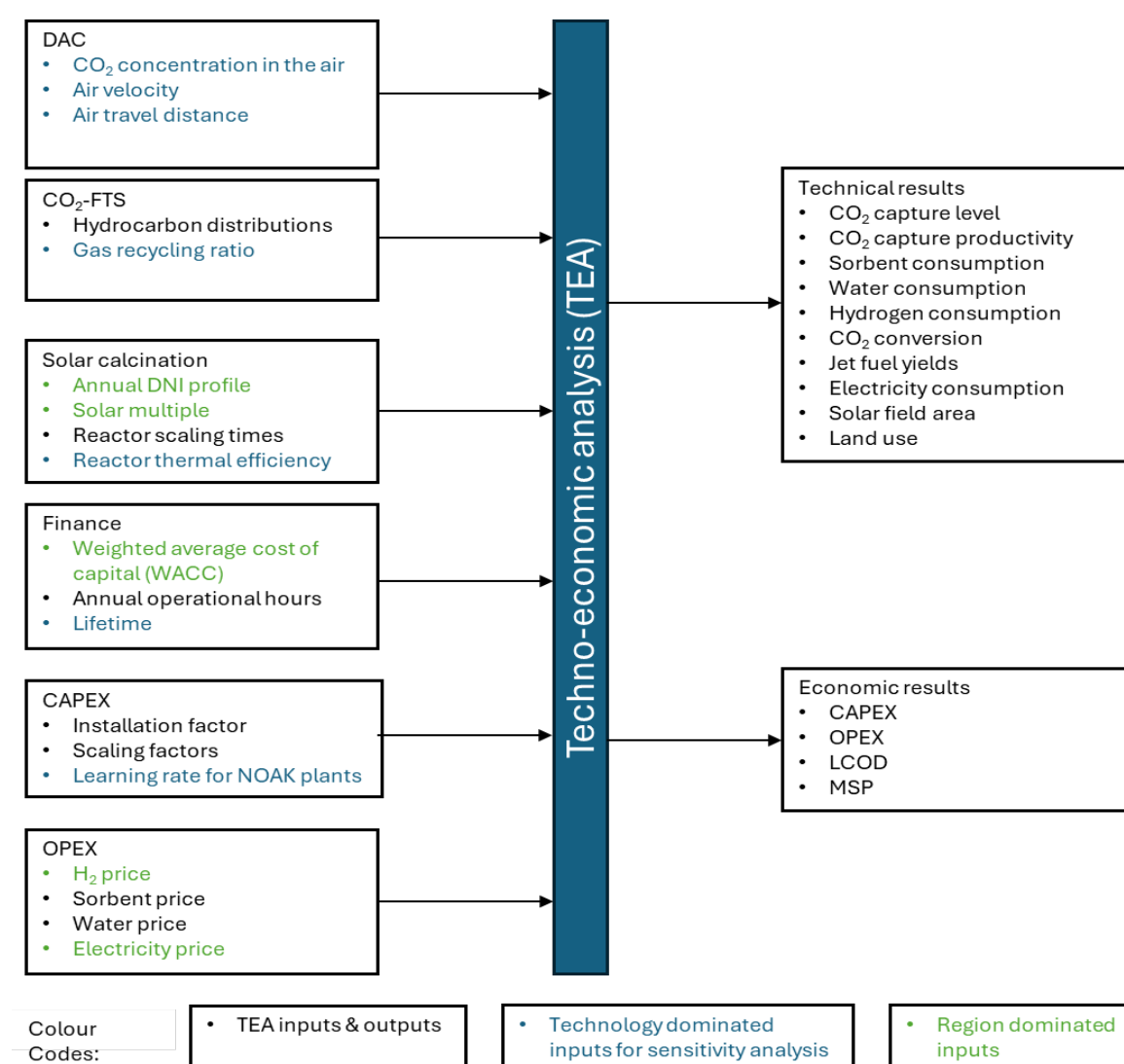


Figure 7.1 Schematic overview of techno-economic input and output parameters

Table 7.1 Technical parameters for the solar-driven DACCU plant for the base case, optimistic and pessimistic scenarios

Technical and design parameters	Units	Optimistic scenario ^a	Base Case scenario	Pessimistic scenario ^a	Source
CO ₂ capture capacity	Mt/yr	0.96	0.96	0.96	^b
SAF productivity	kt/yr	141.8	123.4	52.1	^b
Plant lifetime	year	40	30	20	(Fasihi et al., 2019)
Yearly operating hours	hr	8000	8000	8000	(Fasihi et al., 2019)
Weighted average cost of capital	%	5	10	15	(IEAGHG, 2021)
CO ₂ capture rate	%	~90%	~75%	~50%	^b
CO ₂ concentration in the air	ppm	450	420	400	(Keith et al., 2018)
Air velocity	m/s	2	1.4	1	(Keith et al., 2018)
Air travel distance	M	11.7	7	3.5	(Keith et al., 2018)
Dimensions of single air contactor (length x width x depth)	M	5 x 5 x 11.7	5 x 5 x 7	5 x 5 x 3.5	(Keith et al., 2018)
Solar multiple	N/A	2.5	3	3.5	^b
Thermal efficiency of solar calciner	%	80%	60%	40%	(Bellos, 2023)
Dimensions of single solar calciner (length x depth x bed height)	M	13.4 x 5.3 x 1.1	13.4 x 5.3 x 1.1	13.4 x 5.3 x 1.1	^b
Maximum size of single solar calciner	MW _{th}	40	40	40	(Esence et al., 2020b)
Number of solar calciners	N/A	15	18	21	^b
CAPEX of CSP	US\$M	198.5	397	595.5	^b
Gas recovery ratio	%	99	90	80	^b
Total CO ₂ conversion	mol %	98.2	85.8	75.4	^b

Total jet fuel yield	mol %	44.2	38.6	33.9	^b
SAF market price	US\$/kg	1.24	2.47	3.71	(IATA, 2024)
Catalyst cost	US\$/g	3.98	3.98	3.98	^c
Total land use	km ²	6.44	7.64	8.84	^b
Land cost	US\$/m ²	1.37	2.74	54.82	^b
H ₂ production cost	US\$/kg	1	2	3	(Department of Energy, 2023)
H ₂ transportation cost	US\$/kg	0.18	0.18	0.18	(GOV.UK Department for Energy Security & Net Zero, 2023)
Pipeline required to transport H ₂	km	50	50	50	(GOV.UK Department for Energy Security & Net Zero, 2023)
Electricity demand for DAC	MW	18.5-27.9	11.9	6.4-6.6	^b
Electricity demand for CO ₂ use	MW	97.6	99.0	81.5	^b
PV electricity price	US\$/MWh	10	30	60	(IEAGHG, 2021)
^a Optimistic and pessimistic scenarios are used for sensitivity analysis					
^b Value calculated based on process model					
^c Cost of Fe-Mn-K catalyst is estimated based on the cost of elements					

Table 7.1 illustrates the technical parameters of proposed DACCU process under base case, optimistic and pessimistic scenarios. These parameters are obtained either from literature, process model or assumptions.

7.2.1 Capital expenditure

Based on the material flow and energy requirement, the equipment size and cost are determined, from which, the total capital expenditure (CAPEX) is estimated based on the literature-reported method (Keith et al., 2018, An et al., 2022, Fernández-Torres et al., 2022).

The CAPEX of the DAC plant and CO₂-to-SAF plant are calculated based on Equations 7.1-7.5.

$$\text{Total field cost} = \text{Field cost} + \text{Non-field cost} \quad (7.1)$$

$$\text{Direct field cost} = \sum \text{Installed equipment cost} \quad (7.2)$$

$$\text{Installed equipment cost} = \text{Equipment cost} \times \text{Installation factor} \quad (7.3)$$

$$\text{Equipment installed cost} = \text{Purchased equipment cost} \times \text{Installation factor} \quad (7.4)$$

$$\text{Purchased equipment cost} = \text{Basecost} \times \left(\frac{\text{Newsize}}{\text{Basesize}} \right)^{\text{Scaling exponent}} \times \left(\frac{\text{CEPCI}_{\text{New}}}{\text{CEPCI}_{\text{Base}}} \right) \quad (7.5)$$

Where, the Chemical Engineering Plant Cost Index (CEPCI) is an essential tool for chemical-process-industry projects to adjust equipment prices from year to year.

Studies in the literature do not emphasize the economics of CSP-based solar calcination. Considering that this technology is at the preliminary design stage, the cost of CSP is estimated based on literature-reported CSP technologies such as the parabolic trough, concentrated solar power tower and beam-down solar technology (Bellos, 2023, Kincaid et al., 2018, Segal and Epstein, 2001, Zayed et al., 2021, Tregambi et al., 2021). The evaluated equipment of CSP includes the heliostat field, parabolic mirror, solar calciner and tower. Based on the estimation from previous work (Kurup et al., 2022, Buck and Sment, 2023), the installed cost for the heliostat field was US\$75 /m² and the parabolic mirror was US\$95.6/m².

The installed cost for the solar calciner and tower was estimated from CSP plants. The CAPEX of the CSP plant is calculated based on Equation 7.6-7.8 (Buck and Sment, 2023).

$$CAPEX = Direct\ cost + Indirect\ cost \quad (7.6)$$

$$Direct\ cost = Contingency + Factor \times Direct\ cost \quad (7.7)$$

$$Indirect\ cost = Land\ cost + Factor \times Indirect\ cost \quad (7.8)$$

7.2.2 Operational expenditure

The TEA assumes 8000 operating hours per year for economic evaluation (IEAGHG, 2021). The fixed operational expenditure (OPEX) includes maintenance, labour, administration, and other costs. The annual fixed OPEX is assumed to be 3% of the CAPEX (Otitoju et al., 2021). The variable OPEX covers electricity consumption, co-product credits, and material inputs (i.e., sorbent, water, catalyst and hydrogen). The input information obtained from the model on raw material (e.g. KOH and CaCO₃), hydrogen, electricity, etc., was used to estimate the annual variable operational expenditure. For TEA analysis under base, optimistic and pessimistic scenarios, the green hydrogen is produced offsite in an alkaline electrolyser (AE) plant located 50 km away from the DAC plant and transported through a 10-inch diameter pipeline. Considering the hydrogen is purchased for use, the cost of hydrogen including production and transportation is US\$2.18/kg (GOV.UK Department for Energy Security & Net Zero, 2023, Department of Energy, 2023). The electricity demand for fans, pumps, compressors and heaters is assumed supplied by the PV system to minimise environmental impact. Makeup materials such as KOH, CaCO₃, and water are added based on the mass balance of the process model. The sorbent price is assumed at US\$750/t KOH and US\$/200t CaCO₃. The industrial water price is assumed at US\$1/m³ (Marchese et al., 2021, An et al.,

2022, IEAGHG, 2021). Note that the Fe-Mn-K catalyst is recently used in the lab, and the cost is uncertain thereby the cost of it is estimated based on the cost of elements.

7.2.3 Levelized cost and minimum selling price

The prediction of the CAPEX and OPEX enables the calculation of two cost metrics: (a) the levelized cost and (b) the minimum selling price (MSP). The equation for the levelized cost is provided as Equation 7.9 (IEAGHG, 2021).

$$\text{Levelized cost} = \frac{(\text{CAPEX} \times \text{CRF} + \text{annual variable OPEX} + \text{annual fixed OPEX})}{\text{annual CO}_2 \text{ capture}} \quad (7.9)$$

With capital recovery factor (CRF) represents the portion of the initial CAPEX that needs to be paid every year. CRF is based on the WACC and plant lifetime (Lifetime) as shown in Equation 7.10 (IEAGHG, 2021).

$$\text{CRF} = \frac{\text{WACC} \times (1 + \text{WACC})^{\text{Lifetime}}}{(1 + \text{WACC})^{\text{Lifetime}} - 1} \quad (7.10)$$

This levelized cost calculated this way represents the cost of capturing and processing one tonne of CO₂ from the atmosphere. However, the construction or operation procedures emit CO₂ or other GHG. The net levelized cost can be estimated based on carbon removal efficiency as defined in Equation 7.11 (IEAGHG, 2021).

$$\text{Net levelised cost} = \frac{\text{Levelized cost}}{\text{carbon removal efficiency}} \quad (7.11)$$

The carbon removal efficiency (de Jonge et al., 2019) defined in Equation 7.12 is the percentage of net CO₂ captured from air in the lifecycle.

$$\text{Carbon removal efficiency} = 1 - \frac{\text{total LCA emissions}}{\text{total CO}_2 \text{ captured from air}} \quad (7.12)$$

The equation for the MSP of SAF is provided as Equation 7.13.

$$MSP = \frac{(CAPEX \times CRF + \text{annual variable OPEX} + \text{annual fixed OPEX})}{\text{annual SAF production}} \quad (7.13)$$

7.2.4 Sensitivity analysis

To understand the impact of key parameters on overall solar-driven DACCU cost, a sensitivity analysis on TEA is carried out. The impact of different operating and design variables on each sector (i.e. solar-driven DAC, solar calcination and CO₂-to-SAF) and financial accounting parameters was investigated. This cost is not optimised from every variable connected with the final economic analysis which is far beyond the preliminary design stage.

7.2.5 Preliminary LCA

In this paper, the environmental benefits of using solar energy to power DAC are performed by a preliminary LCA. The accounted CO₂ emissions are from plant construction emissions, sorbent production emissions, and energy-related (heat and electricity) emissions (IEAGHG, 2021). Note that this study does not perform a full cradle-to-grave LCA analysis and relies on publicly available sources for estimating emissions. The LCA analysis is only carried out on solar-driven DAC process to have a clear view of CO₂ emissions cut when using renewable energy to replace natural gas. Any potential CO₂ emissions from the CO₂ utilisation plant are not included.

7.2.6 Location screening

The location will technically influence the weather conditions such as DNI and daily solar hours, and thus determine the final solar field area. Economically it will affect the WACC and finally affect the cost metrics such as CAPEX, OPEX, and MSP. The first consideration for location is its ability to operate large-scale CSP plants. Here, countries with existing CSP plants were identified as potential locations and were therefore prioritised in the initial evaluation. In Figure 7.2, the current worldwide large-scale CSP plants (NREL, 2024b) were collected and summarised. It is noticeable that China has the largest total CSP capacity of 901 MW with several 100 MW CSP power plants operating in the Northwest areas like Xinjiang, Gansu and Qinghai. These areas are characterized by vast deserts, arid landscapes, and relatively sparse populations, which are appropriate for constructing solar-based plants.

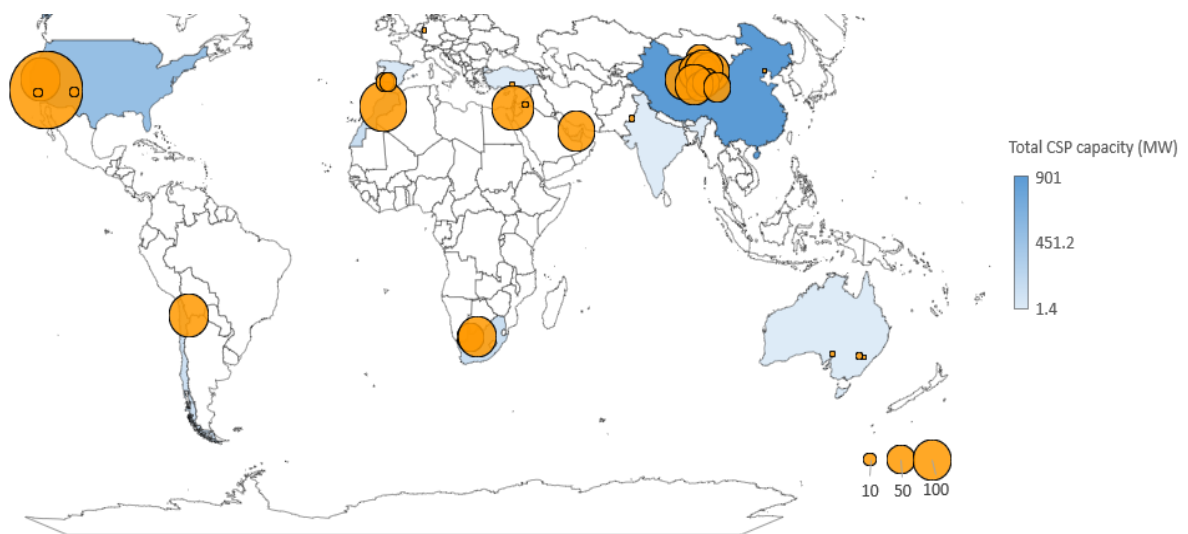


Figure 7.2 Global map of current high-temperature CSP plants with bubble size representing plant scale

Next, with the consideration of location with high DNI, the feasibility of CSP plant implementation and land availability, five locations (NREL, 2024b) were selected in Table 7.2, covering countries in different continents including the USA (North America), Chile (South America), Spain (Europe), South Africa (Africa), and China (Asia). These locations are limited to latitudes below 45 degrees, where the same general regions are feasible for solar PV.

Table 7.2 Five selected CSP project locations used for geographical analysis

Project	Country	Longitude (deg)	Latitude (deg)	Capacity	Technology	SM	Status
Crescent Dunes	USA	39.17	-119.78	110 MW	Solar power tower	3	Operational since 2015
Cerro Dominador	Chile	-22.46	-68.93	110 MW	Solar power tower	2.4	Operational since 2021
Planta Solar 20	Spain	37.45	-6.26	20 MW	Solar power tower	3	Operational since 2009
Redstone CSP Project	South Africa	-28.31	23.38	100 MW	Solar power tower	2.7	Operational since 2023
Shouhang Dunhuang Phase II	China	40.05	94.42	100 MW	Solar power tower	3	Operational since 2018

7.2.7 Calculation of land use

Based on the selected locations, the software System Advisor Model (SAM) was employed to estimate land use requirements based on regional solar irradiation and daily solar hours. The principles for land use calculation are given in Figure 7.3. The imported weather conditions (e.g., annual DNI and wind speed) are from NREL's National Solar Radiation Database (NSRD) (NREL, 2024b).

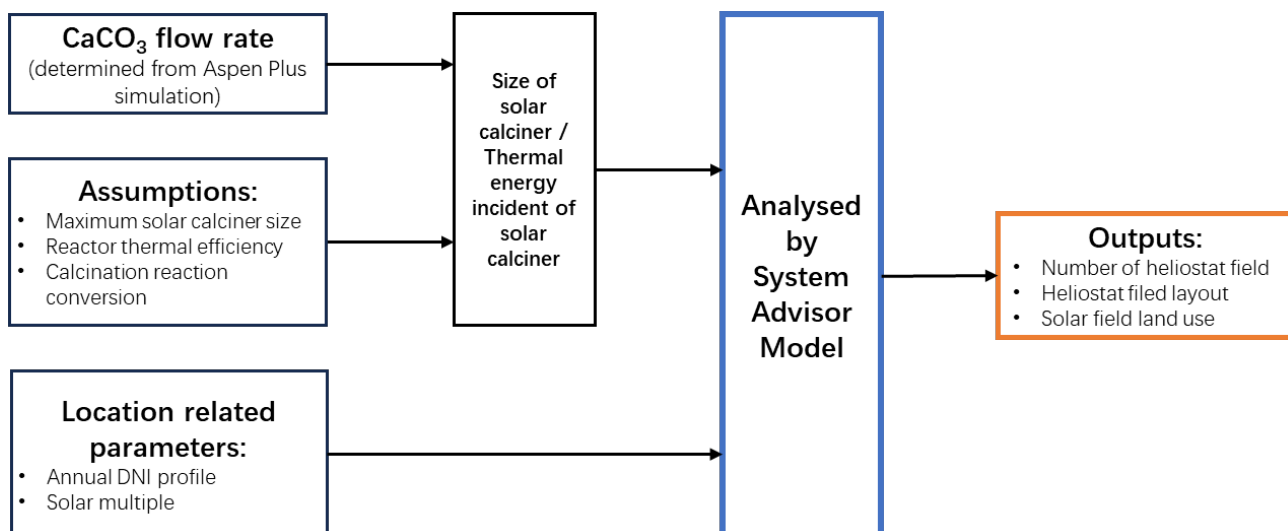


Figure 7.3 Principle of SAM analysis for land use calculation

7.3 TEA

7.3.1 Baseline TEA

In the base case scenario, the 1MtCO₂/year solar-driven DACCU plant can capture approximately 0.96 Mt CO₂ in the air and produce ~0.12 Mt SAF, which equals 50% of global SAF production in 2022 (IATA, 2024). Such large-scale solar-driven DACCU plants will be crucial for the aviation industry to meet its net-zero commitments by 2050 (IEA, 2022). The MSP of SAF is estimated at US\$4.4/kg which is 1.8 times the 2022 market price (US\$2.4/kg) of SAF and 4 times that of conventional jet fuel (US\$1.1/kg) (IATA, 2024). Detailed MSP cost breakdown, illustrating the capital and operational contributions are shown in Figure 7.4a. The levelized cost of solar-driven DACCU (LCOD) is projected at US\$256.8/tCO₂ (see Figure 7.4b), indicating the investment required to capture and convert each ton of atmospheric CO₂ to SAF, serving as a key indicator for policymakers providing

incentives towards market success. However, it remains significantly above the industry target of US\$100/t_{CO2} (IEA, 2024b).

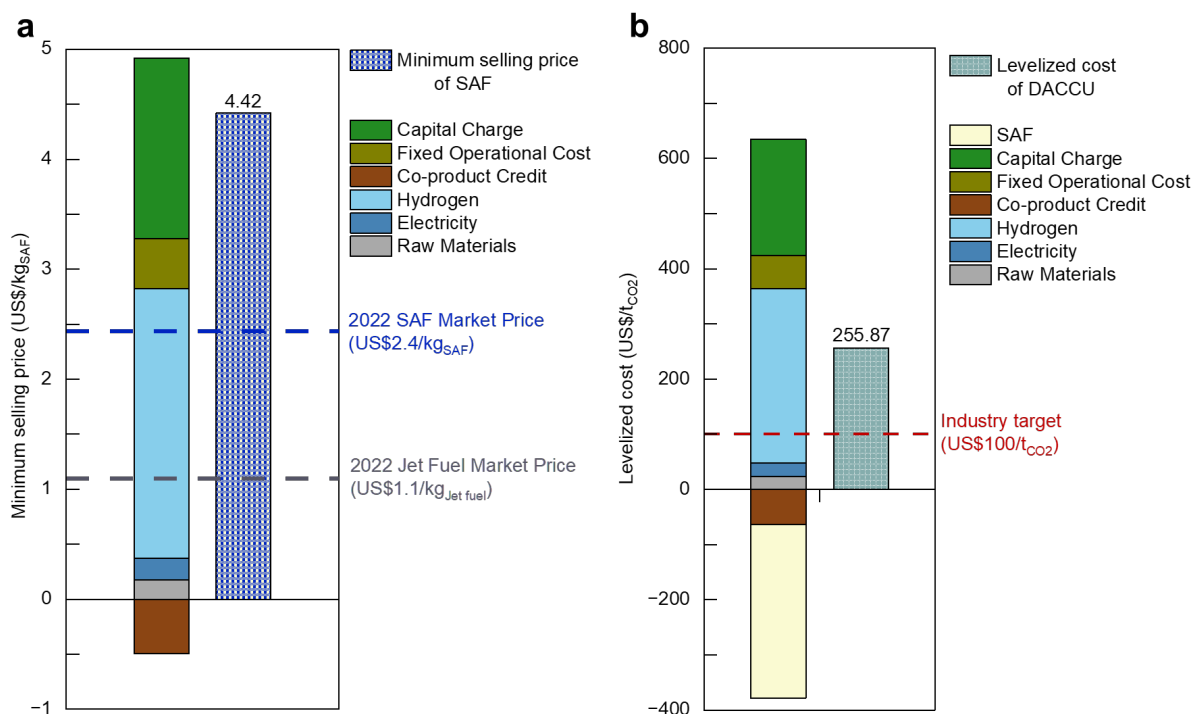


Figure 7.4 The base case results for (a) minimum selling price of SAF and (b) levelized cost of proposed solar-driven DACCU process

It is evident from the results of final cost metrics that OPEX is the primary economic contributor, with CAPEX consisting of 37% of the overall costs. As shown in Figure 7.5, the CAPEX breakdown indicates US\$1376M (72.3%) allocated to the solar-driven DAC plant and US\$506M (26.6%) to the CO₂-to-SAF plant. The major equipment costs include the air contactor and the pellet reactor for DAC, the solar calciner and heliostat field for solar

calcination, and compressors and CO₂-FTS reactor for CO₂-to-SAF. Detailed CAPEX information is summarised in Tables 7.3 and 7.4



Figure 7.5 Detailed CAPEX breakdown of solar-driven DACCU in the base case

Table 7.3 Equipment installed cost breakdown by section at base case

Equipment type	Installation factor	Scaling factor	Reference installed cost (US\$)	Installed cost (2020 US\$)	Source
Direct air capture					
Air contactor	1.86	1	212,200,000	233,549,271	(Keith et al., 2018)
Pellet reactor	1.7	0.675	130,700,000	133,967,959	(Keith et al., 2018)
Steam slaker	1.45	0.675	38,850,000	37,606,988	(Keith et al., 2018)
Steam turbine	NA	0.7	7,510,000	8,265,575	(Keith et al., 2018)
Filter	1.76	NA	30,900,000	31,840,017	(Keith et al., 2018)
Other equipment	NA	NA	102,900,000	89,045,962	(Keith et al., 2018)
Buildings	NA	0.61	6,700,000	6,566,310	(Keith et al., 2018)
Transformer	NA	0.7	19,800,000	19,075,577	(Keith et al., 2018)
Subtotal				559,917,659	
Solar calcination					
Heliostat field	NA	1	NA	126,688,860	(Buck and Sment, 2023)
Parabolic mirror	2.27	1	NA	38,006,658	(Buck and Sment, 2023)
Solar calciner & solar tower	2.27	0.48	NA	211,679,219	(Prats-Salvado et al., 2024)
CaCO ₃ storage tank	NA	NA	NA	376,374,737	(Prats-Salvado et al., 2024)
CaO storage tank	NA	NA	NA	14,166,215	(Prats-Salvado et al., 2024)
Subtotal				397,001,544	
CO₂-to-SAF					
Mix gas compressor	2.47	0.65	NA	134,197,817	Calculated from Aspen
H ₂ compressor	2.47	0.6	2,547,995	631,220	(Zang et al., 2021a)
Preheater	2.47	0.6	6,248,204	8,409,070	(Zang et al., 2021a)
CO ₂ -FTS reactor	2.75	0.8	36,681,585	119,848,154	(Zang et al., 2021a)
Syncrude cooler	1.52	0.7	50,244	742,256	(Zang et al., 2021a)
Three-phase separator	1.69	0.7	6,595,713	9,179,403	(Zang et al., 2021a)
Distillation unit	2.47	0.65	2,547,995	40,303,243	(Zang et al., 2021a)
Subtotal				313,311,162	

Table 7.4 CAPEX summary of 1 Mt_{CO2}/yr solar-driven DACCU plant by section at base case

Parameter	Item	Calculation method	Cost (2020 US\$M)
Direct air capture			
Total direct field costs (TDFC)		Sum of installed cost	559.9
Indirect field costs (IFC)		12.7% of TDFC	71.1
Total field costs (TFC)		TDFC + IFC	631.0
Non-field costs (NFC)	Engineering	12% of TPC	108.4
	Contingency	6% of TFC	126.2
	Other project costs	20% of TFC	37.9
Total non-field costs (TNFC)		Sum of non-field costs	272.5
Total project costs (TPC)		TFC + TNFC	903.5
Solar calcination			
TDFC		Sum of installed cost	397.0
Contingency		10% TDFC	39.7
Direct cost		TDFC + Contingency	436.7
Indirect cost		9% TDFC	35.7
Total capital investment of CSP		Direct cost + Indirect cost	472.4
CO₂-to-SAF			
TDFC		Sum of installed cost	313.3
IFC		12.7% of TDFC	39.8
TFC		TDFC + IFC	353.1
NFC	Engineering	12% of TPC	60.7
	Contingency	6% of TFC	70.6
	Other project costs	20% of TFC	21.2
TNFC		Sum of non-field costs	152.5
TPC		TFC + TNFC	505.6
Land cost		Average land cost	23.4
Total CAPEX			1,905.0

The plant's annual OPEX is estimated at US\$344M and is given in Figure 7.6. Notably, the OPEX is dominated by the cost of hydrogen which includes the cost of production at US\$2.0/kg (Department of Energy, 2023) and the cost of transportation at US\$0.18/kg (GOV.UK Department for Energy Security & Net Zero, 2023).

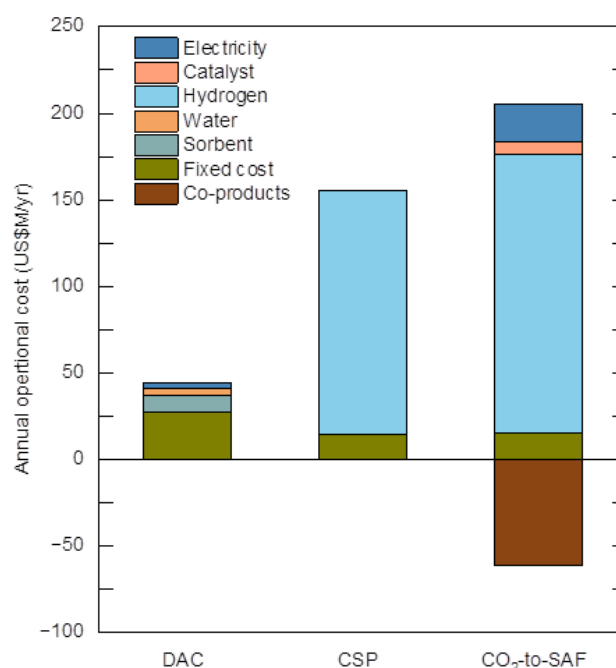


Figure 7.6 Annual operational cost of solar-driven DACCU in the base case disaggregated by process step

7.3.2 Comparison with DAC proposed by Carbon Engineering

The proposed solar-driven DAC (CSP-DAC) process demonstrates improvements in terms of electricity demand and overall efficiency compared to CE's natural gas combustion-based DAC (NG-DAC). The CSP-DAC process shows a 63.0% reduction in electricity demand (267 kWh/tco₂) compared to NG-DAC (see Figure 7.7a). This reduction is primarily due to the elimination of the ASU and lower CO₂ compression pressures. In the NG-DAC process,

CO₂ is compressed to 151 bar for transport and storage, whereas in the continuous utilization scenario, CO₂ is compressed only to 10 bar, which is also lower than the typical pressure for syngas production (30 bar).

Despite reduced electricity demand, DAC remains energy-intensive, with calcination being the primary energy consumer. The novel CSP-DAC plant can be self-sustaining, as the CSP provides the required heat, eliminating the need for onsite natural gas combustion. For CSP-DAC, the thermal energy requirement is 7.16 GJ/t_{CO2}, assuming a solar calciner thermal efficiency of 60%. This is higher than the 5.52 GJ/t_{CO2} required by CE's DAC, which operates with a natural gas combustion-based calciner at 89% thermal efficiency.

From the preliminary LCA, CSP-DAC produces 58.5% fewer CO₂ emissions (117 kg_{CO2}/t_{CO2}) compared to NG-DAC (see Figure 7.7b). This reduction aligns with previous LCA studies and is primarily due to the shift to low-carbon energy sources (Madhu et al., 2021). The reduction in life cycle CO₂ emissions is mainly attributed to a decrease of 62 kg_{CO2}/t_{CO2} from heat sources and an additional 56 kg_{CO2}/t_{CO2} from the use of solar electricity.

In terms of cost, although the CAPEX for the CSP-DAC plant (US\$1376M) is higher than that of CE's DAC plant (~US\$1200M) (IEAGHG, 2021, Keith et al., 2018), the net levelized cost of CSP-DAC (US\$265/t_{CO2}) is lower than NG-DAC (US\$274/t_{CO2}) (see Figure 7.7c). This cost advantage is due to the higher net carbon removal efficiency of CSP-DAC (91.7%) compared to NG-DAC (79.9%). As a result, the proposed CSP-DAC is not only more cost-effective but also better suited for the direct utilization of air-captured CO₂.

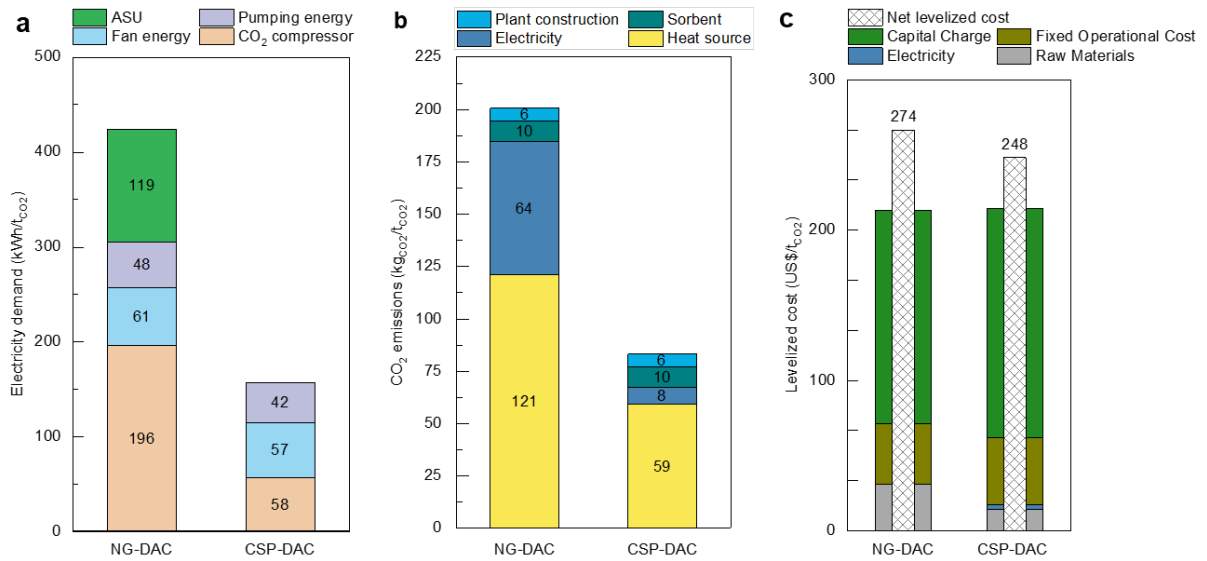


Figure 7.7 Comparison between natural gas combustion-based DAC (NG-DAC) and the proposed solar-driven DAC (CSP-DAC) for (a) electricity demand, (b) life cycle CO₂ emissions, and (c) levelized cost.

7.3.3 Comparison with previous DACCS

When CO₂ captured from air is intended for storage, the additional cost of transportation and storage increases the total expenses. A recent assessment by IEAGHG estimates the DACCS projects, which consider CO₂ capture, transport, and storage, will likely have levelized costs ranging from approximately US\$300 to 600 per ton of CO₂ stored, based on global average solar PV costs (IEAGHG, 2021). In contrast, the proposed solar-driven DACCU pathway achieves a lower levelized cost range (US\$98-413/t_{CO2}) as shown in Figure 7.8a, while also avoiding the technological and economic uncertainties associated with CO₂ transport and storage. The cost advantage is primarily due to the combination of CO₂ utilization to produce value-added SAF, which helps offset total costs. Moreover, there is potential for profitability if the revenue generated from the CO₂ utilization process exceeds the overall costs.

7.3.4 Comparison with previous DACCU

Previous synthetic fuel production through DAC and FTS pathways typically includes three stages: DAC, syngas production, and FTS. In contrast, the proposed process bypasses the syngas production stage entirely and eliminates the need for CO₂ purification and H₂ preparation since the mixed gas (CO₂ and H₂) produced from the solar calciner can be directly used for downstream processes. This streamlining makes the newly proposed process more cost-effective compared to previous stepwise DACCU processes. For example, Rojas-Michaga et al. (2023) reported the MSP of jet fuel at US\$6.55/kg_{jet} for a solid-based DAC with CO₂ utilization. Similarly, Marchese et al. accessed a CE-based DAC with CO₂ utilization for wax production, with MSP ranging from US\$5.6 to 10.0/kg_{wax} depending on plant configurations (Marchese et al., 2021). These costs are substantially higher than our proposed process in Figure 7.8b, where the MSP is only US\$4.42/kg_{SAF} at the base case and ranges from US\$3.30 to 5.54/kg_{SAF} under optimistic and pessimistic scenarios.

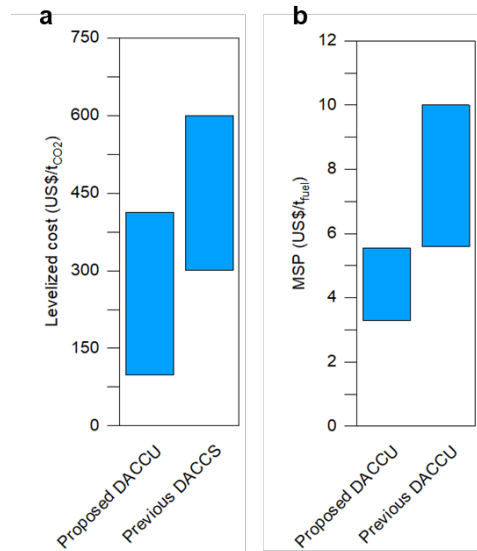


Figure 7.8 Comparison of proposed DACCU with previous DACCS and DACCU studies in terms of (a) levelized cost and (b) MSP.

7.4 Sensitivity analysis under optimistic and pessimistic scenarios

To further understand and investigate potential cost reductions in the solar-driven DACCU process, a single-variable sensitivity analysis was performed on key variables across each section and the entire process (see Table 7.1 for optimistic and pessimistic scenarios). In doing so, this work will enhance the in-depth understanding of process operations and highlight the most important factors to overcome to enable commercial success.

The CO₂ capture productivity of the DAC plant is influenced by operating and design variables, including CO₂ concentration in the air, air velocity (V_{air}), and air travel distance (ATD). Figure 7.9 maps CO₂ capture productivity at varying CO₂ concentrations (400 ppm to 450 ppm), V_{air} (1 to 2 m/s), and CO₂ capture rate at ~50%, ~75%, and ~90% (through ATD controlled at 3.5, 7, and 11.7 meters). Three coloured layers represent the CO₂ capture rate at around 50%, 75% and 90%. Under these conditions, the commercial-scale DAC plant can capture between 55.9 and 216.9 tonnes of CO₂ per hour, impacting energy and material consumption, and ultimately, the final costs.

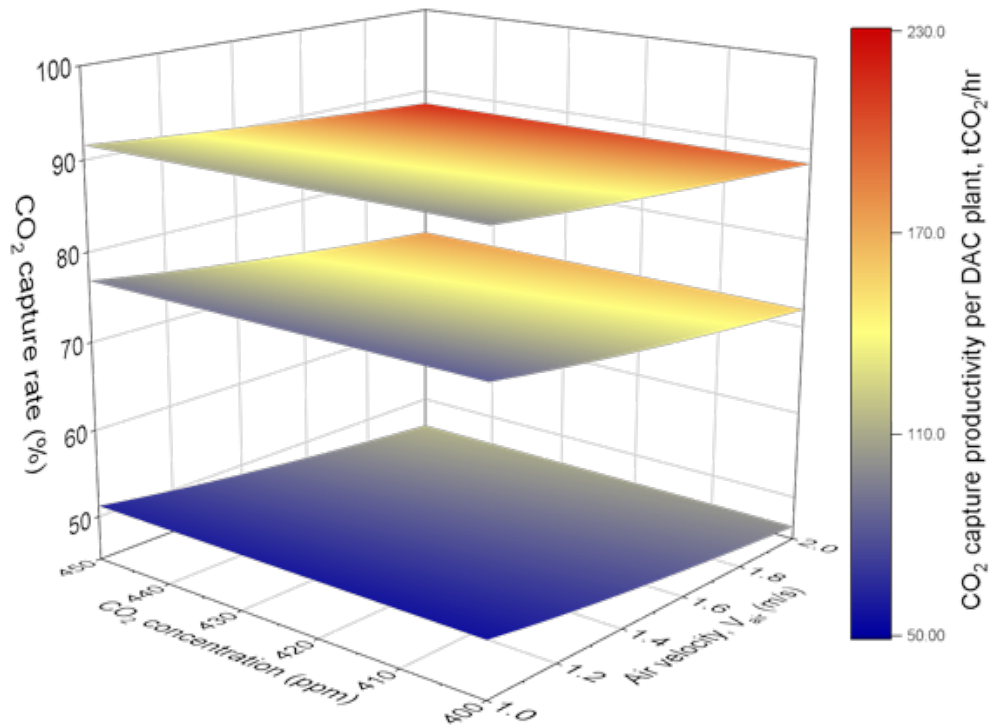


Figure 7.9 Map of DAC plant CO₂ capture productivity as a function of CO₂ concentration, V_{air} and ATD.

The total hydrogen flow rate varies with solar calciner size which impacts the fluidisation conditions (see Figure 7.10). Given the early design stage, the cost of the solar calcination process is inherently uncertain and refers to the economic evaluations from CSP plants. Sensitivity analysis examines the thermal efficiency of the solar calciner (η_{th}), solar multiple (SM), and the capital cost of the CSP plant. The base case assumes 60% thermal efficiency (Buck and Sment, 2023, Bellos, 2023), with sensitivity scenarios at 40% and 80%. The baseline SM is set at 3, with variations tested at 2.5 and 3.5. To address CSP CAPEX

uncertainty, this work varies the CSP CAPEX by $\pm 50\%$. These analyses provide critical insights into the cost dynamics and optimisation potential of the CSP-DAC system.

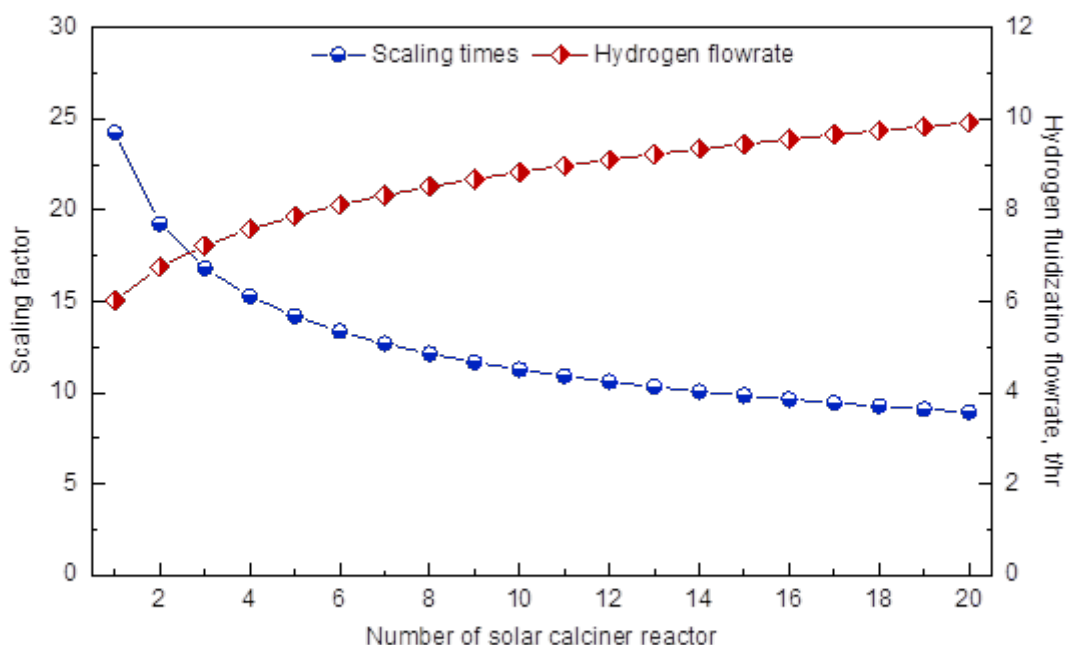


Figure 7.10 The impact of scaling factor on the number of solar calciners and total hydrogen flow rate

The CO₂-to-SAF process applied an ex-situ water removal approach associated with gas recycling to improve CO₂ conversion and SAF yield. Figure 7.11 projects the improvements in CO₂ conversion and SAF yield at different gas recovery ratios. Without gas recovery, potential SAF and co-products from unreacted H₂, CO₂, and CO are wasted resulting in an MSP of US\$10.35/kg and an LCOD of US\$431/tCO₂. Maximizing gas recovery significantly improves product revenue, underscoring its importance if technology permits.

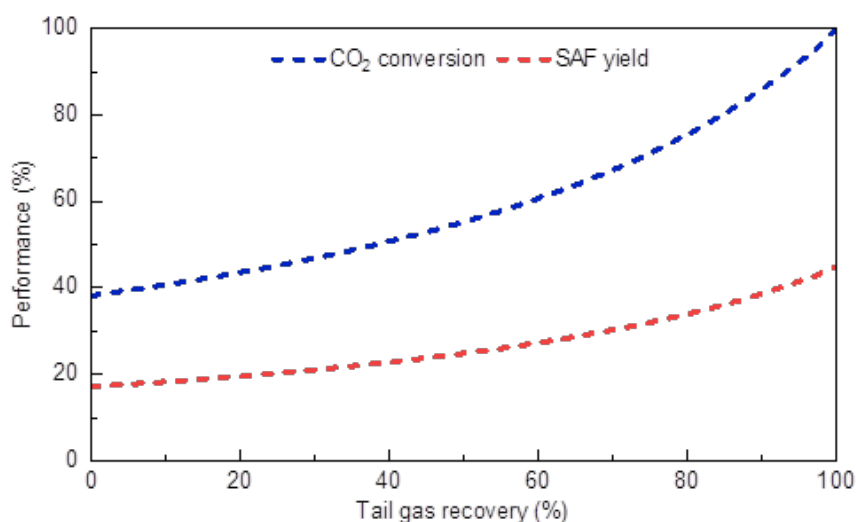


Figure 7.11 Process improvement on CO₂ conversion and SAF yield under gas recovery rate from 0-99%

Based on the process variables investigated, the summary of economic sensitivity analysis results of the MSP and LCOD are illustrated in Figure 7.12 and Figure 7.13. It was found that the H₂ production cost and weighted average cost of capital (WACC) are the primary cost drivers. Reducing the hydrogen production cost to US\$1/kg results in MSP decreasing to US\$3.3/kg (Figure 7.12) and LCOD dropping to US\$111/t_{CO2} (Figure 7.13), approaching the US\$100/t_{CO2} threshold. Notably, the market price of SAF is the dominant factor for LCOD due to its cost-compensation effect. Other key factors include the gas recycle ratio, land cost, CAPEX of CSP, PV electricity price and thermal efficiency of solar calciner which show considerable variability in their impact on the MSP and LCOD. Parameters such as plant lifetime, air velocity, gas recycle ratio, and solar multiple exhibit smaller impacts but remain integral to the overall cost structure.

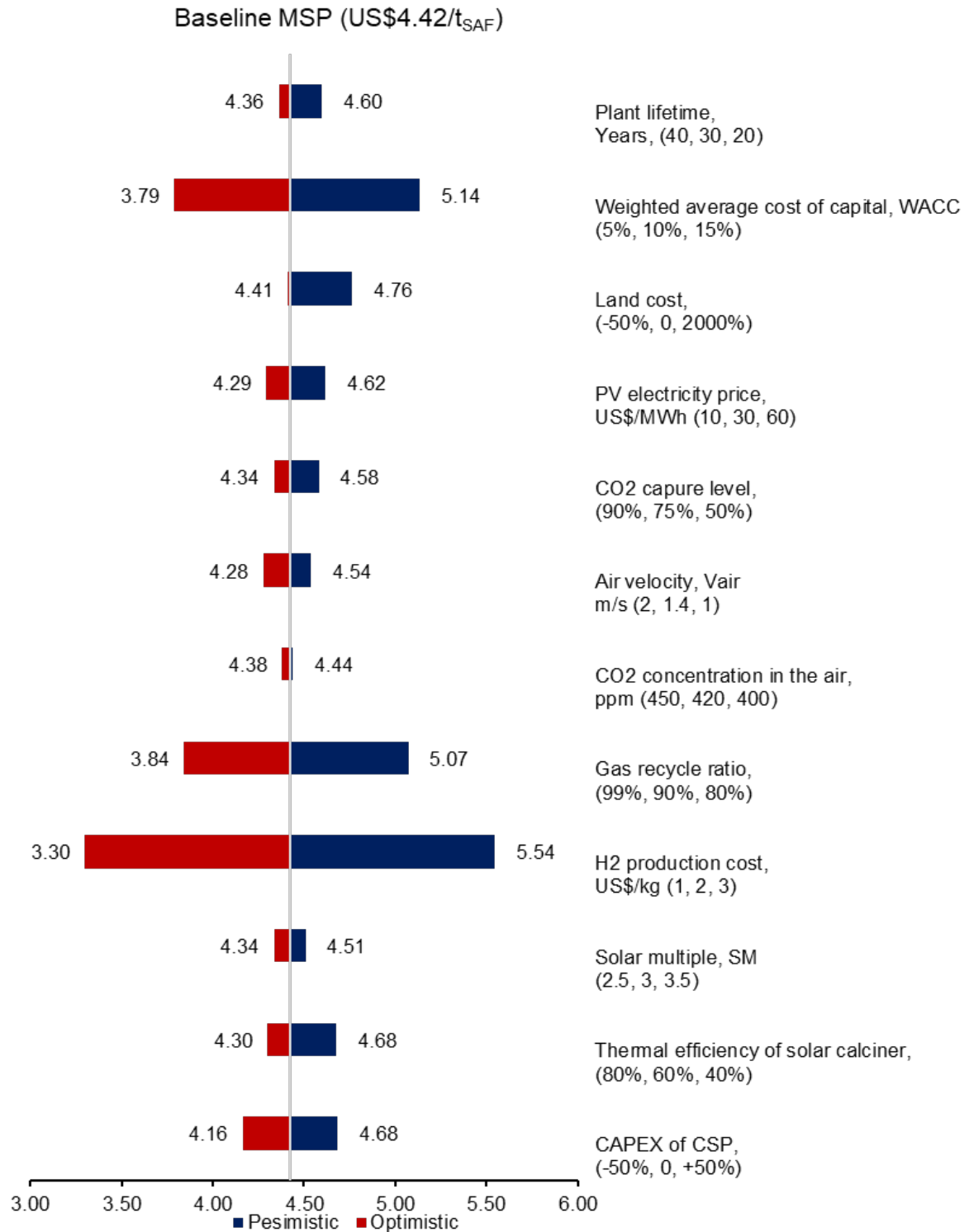


Figure 7.12 Single variable sensitivity analysis of baseline cost for MSP of SAF

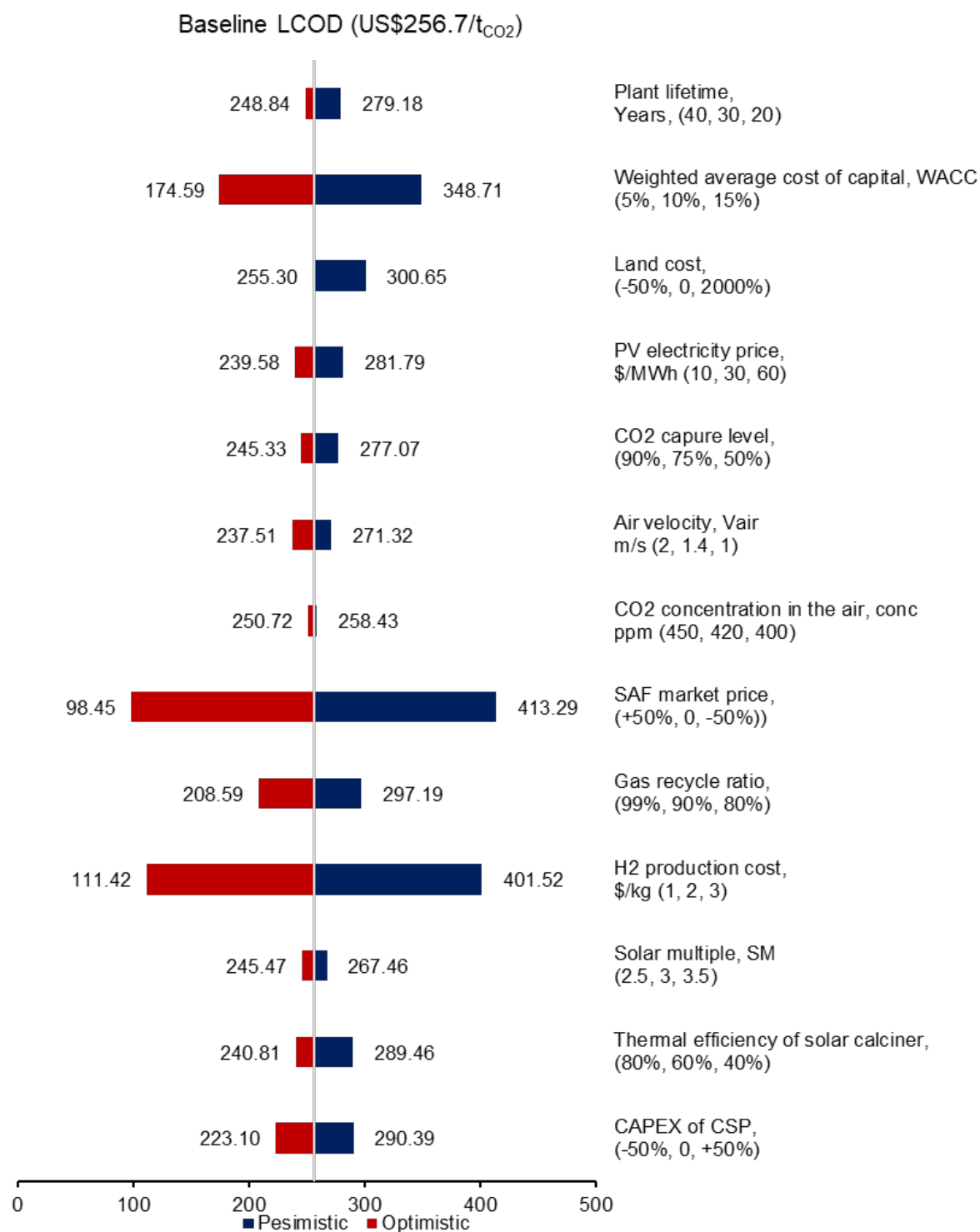


Figure 7.13 Single variable sensitivity analysis of baseline cost for LCOD

Table 7.5 Sensitivity analysis summary of MSP, related to Figure 7.12

Sensitivity parameter	Sensitivity parameter ranges				MSP (US\$/kg)		%MSP difference (from base case)		Justification and parameter range
	Unit	Optimistic case	Base case	Pessimistic case	Optimistic MSP	Pessimistic MSP	Optimistic %	Pessimistic %	
CO ₂ concentration in the air	ppm	450	420	400	4.38	4.44	-1.1	0.3	Ranges of CO ₂ concentration in the air (NASA, 2024). 450 ppm represents the global warming 2°C target.
Air velocity	m/s	2	1.4	1	4.28	4.54	-3.4	2.5	Carbon Engineering's pilot plant operation condition (Keith et al., 2018)
Air travel distance	m	11.7	7	3.5	4.34	4.58	-2.0	3.5	Based on the process model, controlling the air travel distance, the CO ₂ capture rate was modelled at around 50%, 75% and 90%
Thermal efficiency of solar calciner	%	80%	60%	40%	4.30	4.68	-2.8	5.7	Referring to CSP plant (Bellos, 2023, Zhao et al., 2024)
Solar multiple	NA	2.5	3	3.5	4.34	4.51	-2.0	1.9	Referring to the CSP plant (NREL, 2024b, NREL, 2024a)
CAPEX of CSP	US\$M	198.5	397	595.5	4.16	4.68	-5.9	5.9	±50% based on process model
Gas recovery ratio	%	99	90	80	3.84	5.07	-13.2	14.6	Based on the process model
Hydrogen production cost	US\$/kg	1	2	3	3.30	5.54	-25.4	25.3	Baseline is at US\$2/kg which is the short-term USA target (Department of Energy, 2023). US\$1/kg is the long-term target. Sensitivity analysis investigates ±50% of hydrogen production cost.
Plant lifetime	year	40	30	20	4.36	4.60	-1.4	3.9	Baseline is at 30 years, and sensitivity analysis investigates ±10 years of plant lifetime (Fasihi et al., 2019)

WACC	%	5	10	15	3.79	5.14	-14.4	16.1	Baseline is at 10% (IEAGHG, 2021), and sensitivity analysis investigates $\pm 50\%$ of WACC (Ameli et al., 2021).
PV electricity price	US\$/MWh	10	30	60	4.29	4.62	-3.0	4.4	PV cost based on ref (IEA, 2023b)
Land cost	US\$/m ²	1.37	2.74	54.82	4.41	4.76	-0.3	7.7	Baseline land cost is based on ref (Buck and Sment, 2023). The optimistic case uses -50% cost while the pessimistic cost is based on ref (landsearch, 2024).

Table 7.6 Sensitivity analysis summary of LCOD, related to Figure 7.13

Sensitivity parameter	Sensitivity parameter ranges				LCOD (US\$/tCO ₂)		%LCOD difference (from base case)		Justification and parameter range
	Unit	Optimistic case	Base case	Pessimistic case	Optimistic LCOD	Pessimistic LCOD	Optimistic %	Pessimistic %	
CO ₂ concentration in the air	ppm	450	420	400	250.7	258.4	-2.3	0.7	Ranges of CO ₂ concentration in the air (NASA, 2024). 450 ppm represents the global warming 2°C target.
Air velocity	m/s	2	1.4	1	237.5	271.3	-7.5	5.7	Carbon Engineering's pilot plant operation condition (Keith et al., 2018)
Air travel distance	m	11.7	7	3.5	245.3	277.1	-4.4	7.9	Based on the process model, controlling the air travel distance, the CO ₂ capture rate was modelled at around 50%, 75% and 90%

Thermal efficiency of solar calciner	%	80%	60%	40%	240.8	289.5	-6.2	12.7	Referring to CSP plant (Bellos, 2023, Zhao et al., 2024)
Solar multiple	NA	2.5	3	3.5	245.5	267.5	-4.4	4.2	Referring to the CSP plant (NREL, 2024b, NREL, 2024a)
CAPEX of CSP	US\$M	198.5	397	595.5	223.1	290.4	-13.1	13.1	±50% based on process model
Gas recovery ratio	%	99	90	80	208.6	297.2	-18.8	15.8	Based on the process model
SAF market price	US\$/kg	1.24	2.47	3.71	98.4	413.3	-61.7	61.0	Baseline SAF market price uses 2022 data (IATA, 2024). Sensitivity analysis investigates ±50% of SAF market price.
Hydrogen production cost	US\$/kg	1	2	3	111.4	401.5	-56.6	56.4	Baseline is at US\$2/kg which is the short-term USA target(Department of Energy, 2023). US\$1/kg is the long-term target. Sensitivity analysis investigates ±50% of hydrogen production cost.
Plant lifetime	Year	40	30	20	248.4	279.2	-3.1	8.7	Baseline is at 30 years, and sensitivity analysis investigates ±10 years of plant lifetime(Fasihi et al., 2019)
WACC	%	5	10	15	174.6	348.7	-32.0	35.8	Baseline is at 10%(IEAGHG, 2021), and sensitivity analysis investigates ±50% of WACC(Ameli et al., 2021).
PV electricity price	US\$/MWh	10	30	60	239.6	281.8	-6.7	9.8	PV cost based on ref(IEA, 2023b)
Land cost	US\$/m ²	1.37	2.74	54.82	255.3	300.7	-0.6	17.1	Baseline land cost is based on ref(Buck and Sment, 2023). The optimistic case uses -50% cost while the pessimistic cost is based on ref (landsearch, 2024).

7.5 Geographical analysis

The TEA further investigates the impact of geographic locations on key factors such as land occupation and hydrogen production costs. Figure 7.14 shows the land use of solar-driven DACCU plant in the selected locations which are coloured in the world map and illustrated with the land use in km². It is indicated that Chile, USA and China demonstrate lower land use, requiring 6.94 km², 7.64 km² and 8.51 km², respectively. The extensive uninhabited areas in these regions, such as deserts, make them suitable for the deployment of solar-driven DACCU plants.

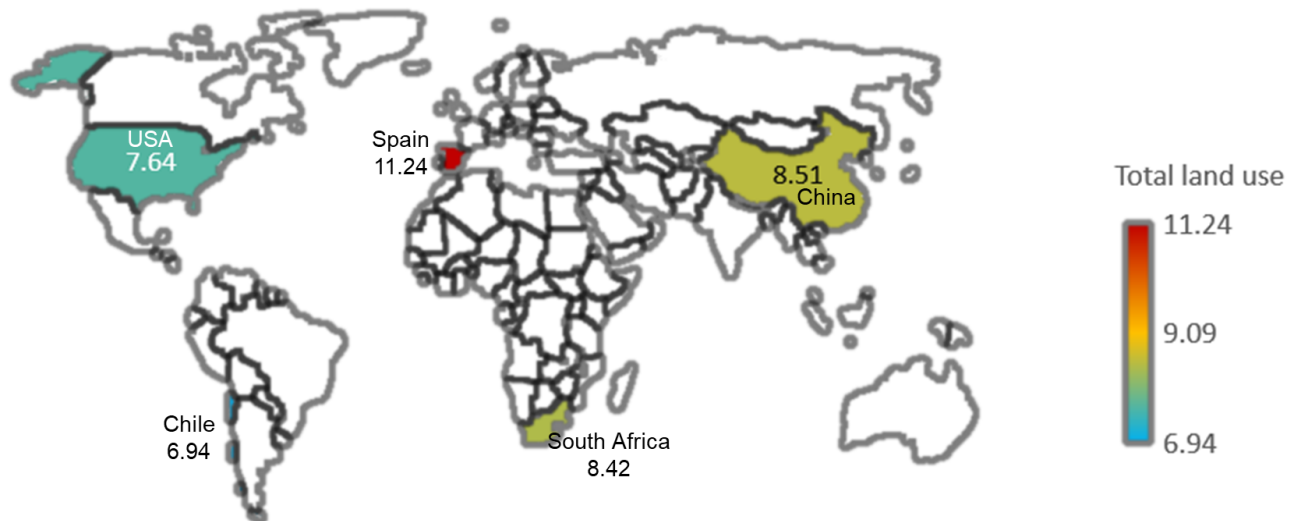


Figure 7.14 World map of land use for solar-driven DACCU plant

The cost of purchased hydrogen in this proposed DACCU plant emerges as a key factor as revealed by sensitivity analysis. This cost exhibits significant variability across different countries and hydrogen production technologies. To minimise environmental impact, this

analysis focuses on low-carbon hydrogen derived from several advanced technologies: alkaline electrolyser (AE), proton exchange membrane (PEM), solid oxide electrolysis cell (SOEC) and steam methane reforming (SMR) with carbon capture and storage (CCS). Table 7.5 gives the regional hydrogen cost from different hydrogen production technologies (IEA, 2023a, McKinsey & Company, 2024, Hydrogen Council, 2024), and PV electricity (IEA, 2023b) and WACC (Ameli et al., 2021) in different countries.

Table 7.7 Regional hydrogen cost, PV cost and WACC

Country	Hydrogen production technology and cost (US\$/kg)				PV electricity price (\$/MWh)	WACC (%)
	AE	PEM	SOEC	SMR with CCS		
USA	2.5 - 4.0	3.0 - 5.0	4.5 - 6.5	1.5 - 2.0	41	5.10
Chile	1.8 - 3.2	2.5 - 4.0	3.8 - 5.8	1.2 - 1.7	32	9.20
Spain	2.2 - 3.7	2.8 - 4.3	4.0 - 6.0	1.4 - 1.9	36	4.20
South Africa	2.3 - 3.8	2.9 - 4.4	4.2 - 6.2	1.3 - 1.8	42	11.80
China	2.0 - 3.5	2.7 - 4.2	3.9 - 5.9	1.1 - 1.6	23	6.60

The study shows marked regional differences in the LCOD and MSP, which are heavily influenced by local hydrogen production costs and WACC (Figure 7.15 and Figure 7.16). Under local WACC conditions (4.2%-11.8%) (Ameli et al., 2021), China demonstrates the lowest MSP when using hydrogen from AE (US\$3.9-5.6/kg) and SMR with CCS (US\$2.9-

3.5/kg). In contrast, Spain presents a cost advantage for PEM (US\$4.7-6.3/kg) and SOEC (US\$6.0-8.3/kg) technologies. When evaluating the plant cost under a global average WACC of 4.2%, previous low local WACC countries such as the USA and Spain lose their competitive edge. For hydrogen produced via SMR with CCS, the lowest MSP is attained in China (US\$2.7/kg) while South Africa's (US\$3.0/kg) surpasses both USA (US\$3.2/kg) and Spain (US\$3.1/kg). These findings underscore the substantial potential for cost reductions in solar-driven DACCU through the strategic selection of optimal deployment locations, particularly in regions with high solar irradiance, low land costs and favourable financial conditions.

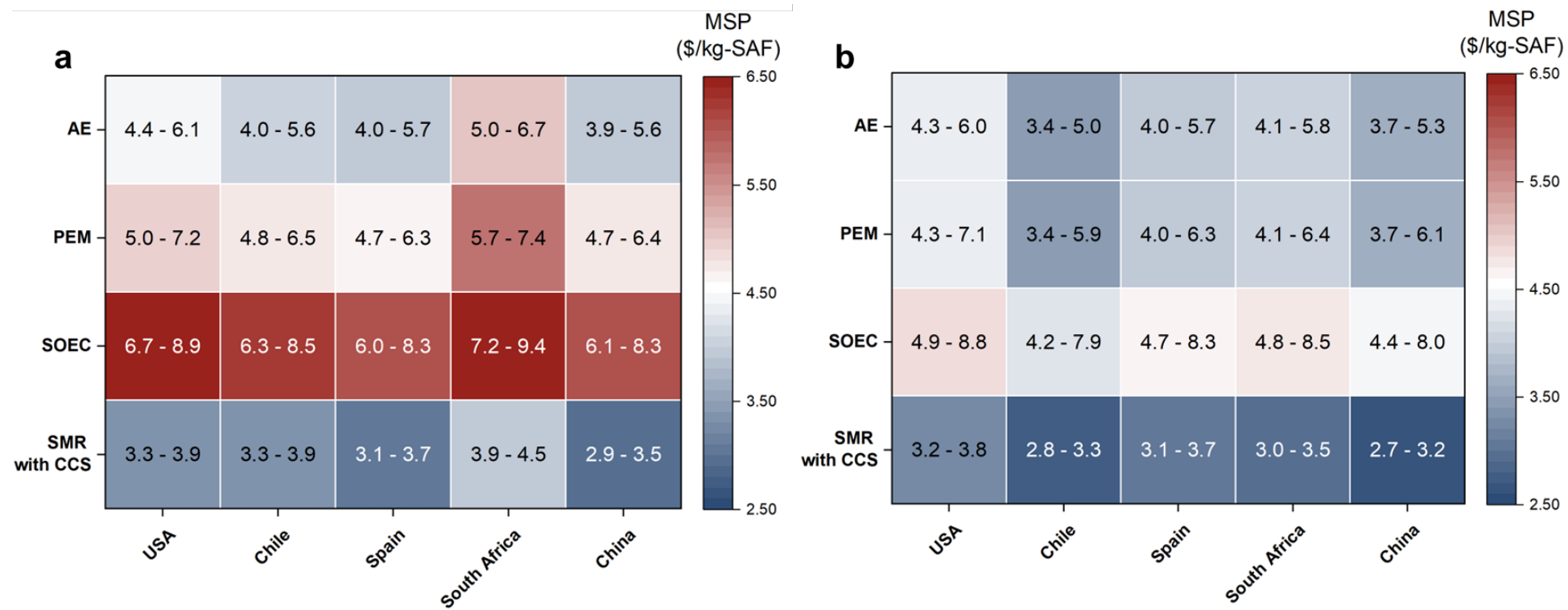


Figure 7.15 MSP of SAF with low-carbon hydrogen sourced at country-specific prices at (a) local WACC and (b) global averaged WACC of 4.2%.

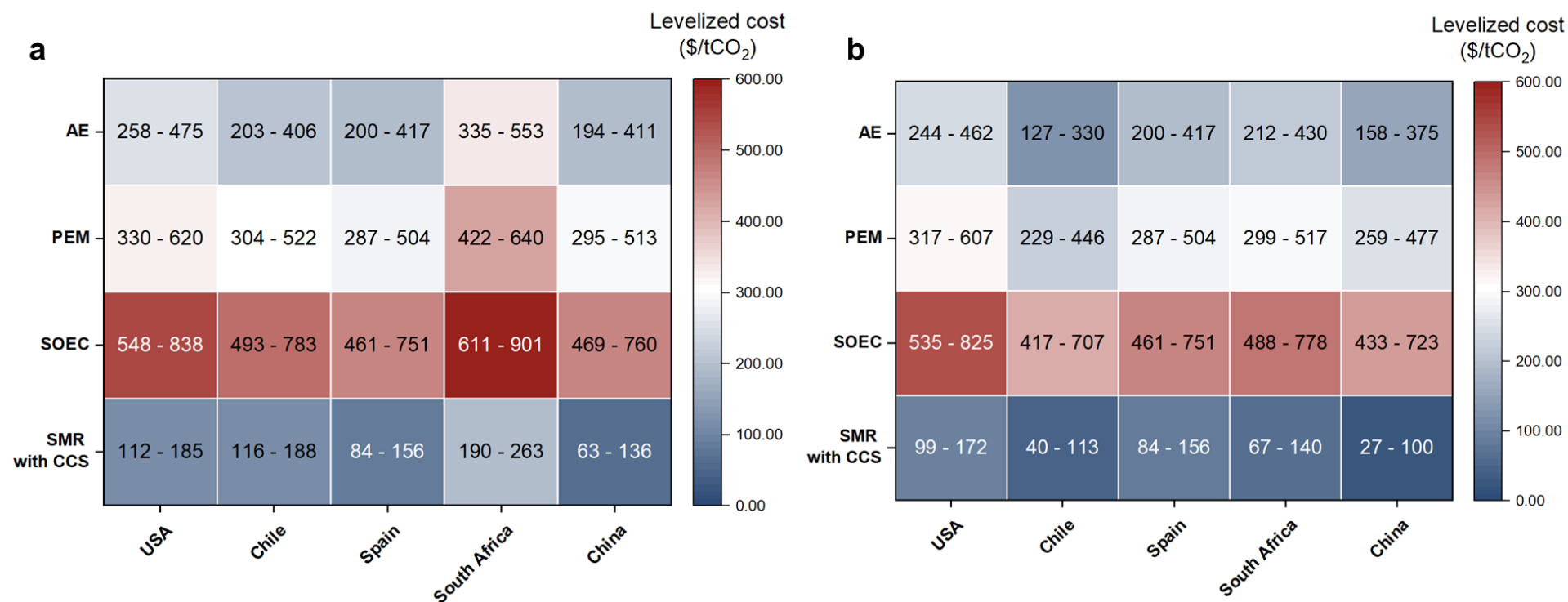


Figure 7.16 Levelized cost of DACCU with low-carbon hydrogen sourced at country-specific prices at (a) local WACC and (b) global averaged WACC of 4.2%.

7.6 Roadmap analysis

In this work, the base case represents the FOAK plants and is assumed to be deployed in the near term. However, the estimated costs are high with existing technology and market conditions. Here, this study presents a detailed roadmap for achieving a more competitive cost reduction for NOAK plants through a waterfall analysis, illustrating the cumulative repercussions of various process advancements. The MSP of SAF for the NOAK plant could be reduced to US\$2.01/kg, which is below the current market price of US\$2.4/kg (see Figure 7.17). The LCOD could decrease to -US\$62.82/t_{CO2}, indicating that the entire capture and utilization process is profitable (see Figure 7.18). As revealed from the single-variable sensitivity and geographical analyses, the cost-effective hydrogen production technology is prioritized as the initial step in the roadmap. Implementing these changes could eliminate more than 25% of the total cost for MSP of SAF and 56% for LCOD.

Subsequent technological advancements are essential to improve the efficiency of DAC, CSP, and CO₂-to-SAF processes thereby offsetting the total cost. Key factors include enhancing the gas recycle ratio in CO₂-FTS, increasing the thermal efficiency of the solar calciner in CSP, and optimising CO₂ capture efficiency in DAC. Besides, further studies on waste gas recycling and wax upgrading can boost total co-product credits (Zang et al., 2021a). Additionally, reducing the PV electricity price for the entire process shows potential for further cost reductions. Considering that hydrogen is produced offsite and purchased, its cost is not directly impacted by on-site electricity prices. However, the low price of renewable electricity significantly affects both the DACCU process and hydrogen production. Thus, securing low-cost renewable electricity is critical for overall economic viability.

Further cost reductions can be explored through government policies and incentives, such as carbon credits. The high carbon price can offset the costs and foster a robust carbon market, encouraging investment in DAC-based technologies. For instance, a higher carbon price above the levelized cost could make DAC or DACCU profitable. Programs like the 45Q project, which provides credits of US\$180 per ton of CO₂ permanently stored and US\$130 per ton for CO₂ used (IEA, 2023c), could significantly impact the economics of DAC projects. Lastly, promoting industry-academia collaborations and public-private partnerships will drive innovation and facilitate the sharing of best practices.

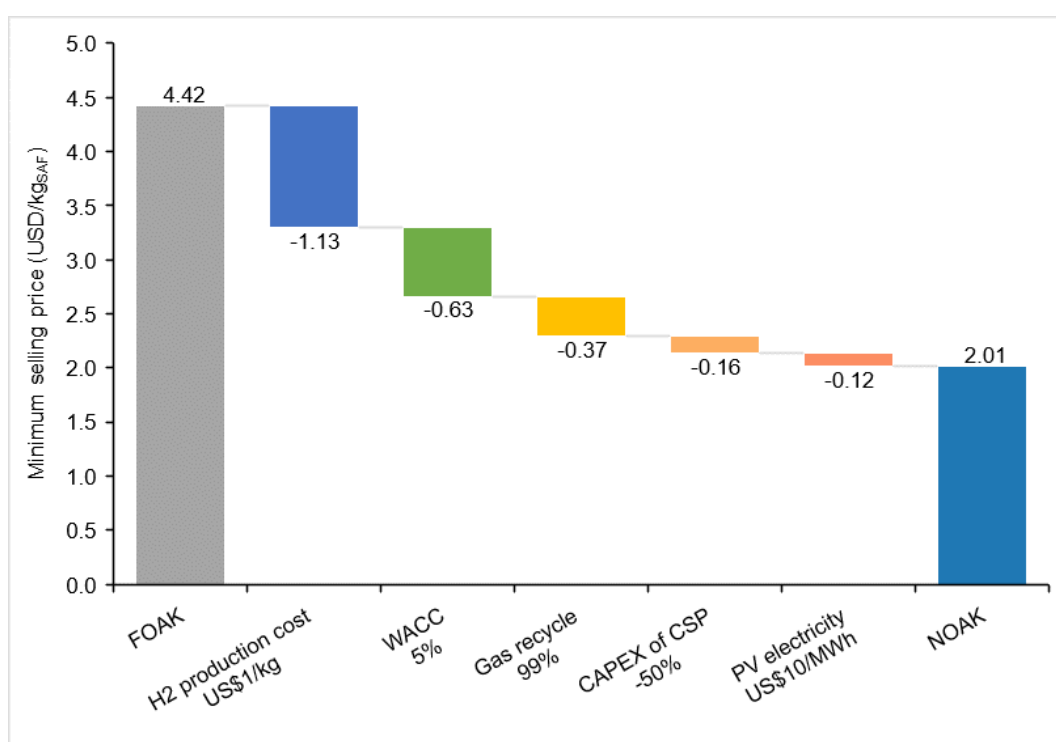


Figure 7.17 Roadmap to reducing base case cost of MSP by successive changes to cost-relevant parameters from FOAK to NOAK

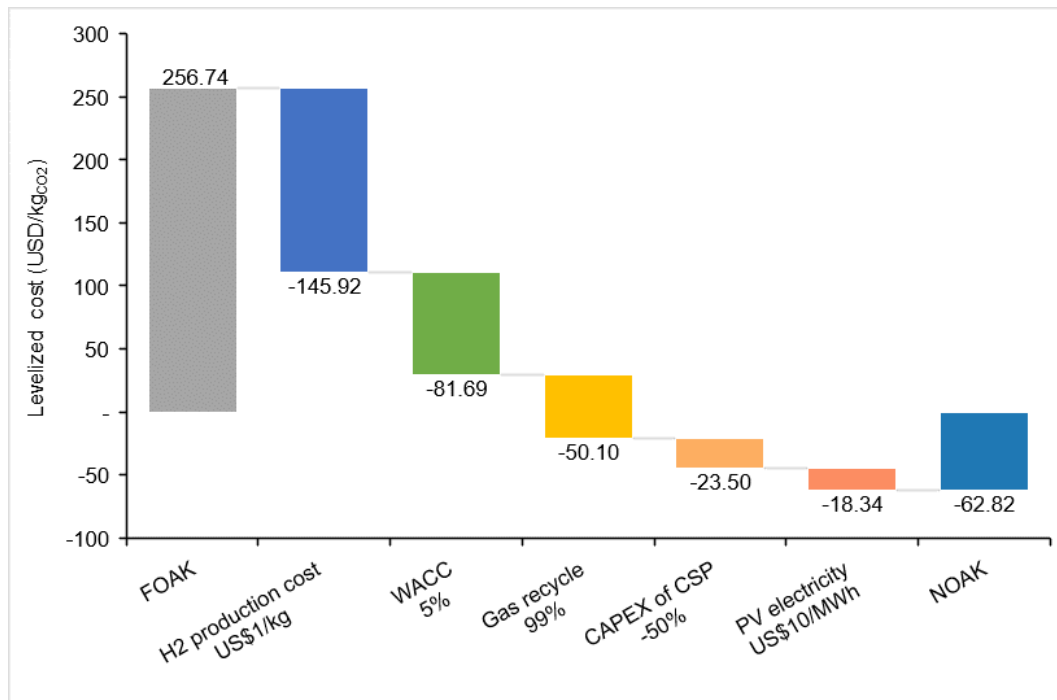


Figure 7.18 Roadmap to reducing base case cost of LCOD by successive changes to cost-relevant parameters from FOAK to NOAK

7.7 Conclusion

- (1) The TEA framework is provided to determine the technical and economic results from different parameters such as technology-dominated (e.g., ATD and reactor thermal efficiency) and region-dominated (e.g., DNI and WACC). The detailed research methods are given for calculating CAPEX, OPEX, LCOD, MSP, CO₂ emissions and land use, for sensitivity analysis and location screening.
- (2) In the base case scenario, the solar-driven DAC process shows a 63% reduction in electricity consumption (267 kWh/tCO₂) and a 59% decrease in process CO₂ emissions (117 kgCO₂/tCO₂) compared with conventional CE's DAC.

- (3) The proposed solar-driven DACCU process is cost-effective compared with the previous process: (i) the levelized cost of solar-driven DACCU (\$257/t_{CO2}) is cheaper than the DACCS (~\$300-\$600/t_{CO2}), (ii) the MSP of SAF (\$4.4/kg) is lower than the previous stepwise DACCU process (\$5.6–10.0/kg).
- (4) The sensitivity analysis indicates that the hydrogen production cost and WACC are two major cost drivers.
- (5) The geographical analysis addresses the regional impact on the global feasibility of such a solar-driven plant.
- (6) The roadmap analysis predicts the cost reduction potential for future plants. It shows that future plants have the potential to be more cost-competitive and even profitable if: (a) plants are deployed in locations with cost-effective hydrogen production technology and low WACC, (b) technological advancements are achieved across all sections, and (c) policy support such as carbon credits is introduced.

Chapter 8. Conclusions and recommendations

8.1 Conclusions of the thesis

Throughout the study presented herein a novel design has been proposed for an environmentally attractive and cost-effective large-scale (i.e., 1 MtCO₂/year) solar-driven L-DAC with CO₂ utilisation process to produce SAF. The proposed process has been developed at a 1 MtCO₂/year scale through modelling, simulation, validation and scale-up. The well-established process model is further evaluated through comprehensive process assessment including TEA, sensitivity analysis, geographic analysis and roadmap analysis. The following is concluded from the results of the study:

- (1) In Chapter 3, a steady-state commercial scale L-DAC model was developed in Aspen Plus® using a more advanced air contactor model compared with previous model-based studies (Sabatino et al., 2021, An et al., 2022). The process model was justified through comparison with the commercially available simulations from CE.
- (2) In Chapter 4, a steady-state pilot scale air-fluidised solar calciner (i.e., 1D four-stage horizontal fluidised bed) model was developed for the first time. The pilot model was implemented in Aspen Plus® and linked with ACM for enthalpy correlation and thermal efficiency calculation. The model was validated using two representative pilot experimental data (at high and low fluidisation flow rates) from the French PROMES laboratory.
- (3) Based on the pilot air-fluidised solar calciner, a specially designed hydrogen-fluidised solar calciner was proposed for the application in L-DAC process. The new design is inspired by the HDR in the steel industry and uses hydrogen as the fluidisation

medium rather than air. The hydrogen-fluidised solar calciner is initially developed at a pilot scale based on the fluidised bed scaling law and pilot air-fluidised solar calciner model. Subsequently, the hydrogen-fluidised solar calciner was scaled up from pilot scale to large scale based on scaling law (achieving hydrodynamic similarity and same reaction conversion at different scales).

- (4) In Chapter 5, a steady-state lab scale direct CO₂- FTS model (i.e., using Me-Fe-K catalyst for direct CO₂ conversion into jet fuel in a single reactor) was developed in Aspen Plus[®] linking with ACM based on the recent lab experiments at the University of Oxford. The model was validated using experimental ASF plot and reported hydrocarbon selectivity. Based on the assumptions, the model has been simulated at commercial scale and using an operating strategy (ex-situ water removal combined with gas recycling of unreacted CO₂, CO and H₂) for performance improvement.
- (5) In Chapter 6, a solar-driven DACCU process design (including two major sections: solar-driven DAC and CO₂-to-SAF) is proposed for the first time based on three current processes (i.e., L-DAC, solar calcination and CO₂-FTS). It uses a solar calciner for solar-driven L-DAC, which enables the next-generation fully renewable energy-driven L-DAC process. Since the specially designed solar calciner is fluidised by hydrogen (purchased from the hydrogen production plant), therefore the outlet mixed gas (CO₂ and H₂) from solar calciner can be regards as feedstock and directly utilised in the downstream CO₂-FTS process to produce SAF.
- (6) A steady-state solar-driven DACCU process model has been developed at commercial scale based on the separate model development, validation and scale-up in Chapters 3, 4 and 5. The process flow diagram, unit design and operation

parameters, and simulation results of commercial-scale solar-driven DACCU are given in detail.

- (7) In Chapter 7, the FOAK plant performance has been initially evaluated. The total CAPEX for a 1 MtCO₂/year solar-driven DACCU plant is projected to be US\$1905M. The CAPEX for the solar-driven DAC section is US\$1376M (72.3%) which is the major contributor while the CO₂-to-SAF section costs US\$506M (26.6%). Additionally, the plant requires US\$344M annual OPEX and it is noticeable that the cost of hydrogen (US\$2.18/kg) is the dominant OPEX contributor.
- (8) The TEA and preliminary LCA reveal the advantages of the solar-driven DAC process compared with conventional CE's DAC process. The new process has a 63% reduction in electricity consumption (267 kWh/tCO₂) and a 59% reduction in process CO₂ emissions (117 kgCO₂/tCO₂).
- (9) The proposed solar-driven DACCU process is cost-effective compared with previous processes because:
 - (a) The LCOD is US\$257/tCO₂, which is cheaper than the cost range of ~US\$300-600/tCO₂ reported for DACCS.
 - (b) The MSP of the proposed process is US\$4.4/kg, which is lower than the MSP obtained through the stepwise DACCU process (US\$5.6–10.0/kg).
- (10) A sensitivity analysis under optimistic and pessimistic scenarios indicates that the hydrogen production cost and WACC are two major cost drivers for the MSP of SAF. For the LCOD, the dominant cost driver is the market selling price of SAF because it is the avenue for the compensation of total cost.
- (11) Furthermore, the geographical analysis of the USA, Chile, Spain, South Africa and China addresses the regional impact on the global feasibility of such a solar-driven

plant. Under local WACC conditions, China shows the advantage of siting and demonstrates the lowest MSP when using hydrogen from AE (US\$3.9-5.6/kg) and SMR with CCS (US\$2.9-3.5/kg).

(12) Finally, the cost reduction potential is predicted for NOAK plants via a roadmap analysis to indicate the technology's potential for policymakers and industry investors. It is found that the SAF produced from solar-driven DACCU plants has the potential to be more cost-competitive and even profitable in the future if:

- (a) Plants are deployed in locations with low WACC.
- (b) The hydrogen used is purchased from the cost-effective hydrogen production technology.
- (c) Technological advancements are achieved across all sections (i.e., L-DAC, solar calcination and CO₂-FTS).
- (d) Policy support such as carbon credits is introduced.

8.2 Recommendations for future work

Based upon the results of this study, the following recommendations for future work are made:

- (1) The hydrogen-based solar calciner proposed here is used for solar-driven DACCU to produce SAF, whereas the insights presented here can be applied more broadly to high-temperature solar-aided particle processing processes such as the calcination process in the cement industry.
- (2) Considering the intermittent nature of solar energy, future research could focus on the 24-hour operation strategy for the solar calcination process such as (i) the heat

integration of solar calcination with thermal energy storage and (ii) the combination of solar calciner with electric calciner.

- (3) The newly proposed hydrogen-fluidised solar calciner is designed as a four-stage horizontal fluidised bed reactor in this work based on the pilot calciner design. Further studies could provide more efficient solar calciner designs (e.g. circulating fluidised solar calciner) and stable operation strategies (e.g. homogenous and steady particle temperature).
- (4) This work uses hydrogen as the fluidisation medium in the solar calciner and the major OPEX is from the cost of hydrogen. Therefore, finding an alternative fluidisation medium (e.g., syngas and CH_4) to replace hydrogen could potentially reduce the cost.
- (5) This work is based on the Fe-Mn-K catalyst for the CO_2 -FTS process, which directly converts air-captured CO_2 from DAC to SAF. Further studies could find other novel catalysts to achieve high CO_2 conversion and product yield. Also, the targeted main product depends on the selected catalyst, it would be possible to produce gasoline or wax according to different catalysts.
- (6) In this work, the hydrocracking process is not performed for simplicity at the preliminary design stage. Further research could carry out a more advanced syncrude upgrading process to increase the yield of SAF.
- (7) For geographical analysis, this work only considers the selected five locations for the proposed plant. Further studies could investigate the worldwide deployment potential and carry out a detailed analysis at a specific optimal siting (uninhabited areas such as deserts with high solar energy intensity and long daily sunlight hours).

- (8) Further research could investigate the implementation of effective heat recovery and water integration strategies for the entire solar-driven DACCU process, which could potentially reduce the overall energy consumption and operational costs (Holmes et al., 2024).
- (9) The LCA is only carried out for the L-DAC process in this work to show the environmental benefits of using solar energy. In the future, a comprehensive cradle-to-grave LCA is necessary for the entire solar-driven DACCU process to quantify environmental impacts and ensure compliance with stringent environmental standards.
- (10) Finally, the socio-political analysis is vital for understanding the implications of deploying large-scale DACCU plants, facilitating broader adoption through social acceptance, regulatory support, and policy incentives.

References

- IPOINTFIVE. 2024. *Carbon removal and sequestration* [Online]. Available: <https://www.1pointfive.com/> [Accessed 15 September 2024].
- AMELI, N., DESSENS, O., WINNING, M., CRONIN, J., CHENET, H., DRUMMOND, P., CALZADILLA, A., ANANDARAJAH, G. & GRUBB, M. 2021. Higher cost of finance exacerbates a climate investment trap in developing economies. *Nature Communications*, 12, 1-12.
- AN, K., FAROOQUI, A. & MCCOY, S. T. 2022. The impact of climate on solvent-based direct air capture systems. *Applied Energy*, 325, 119895.
- ASPENTECH. 2024a. *Aspen Custom Modeler: Quick and Easy* [Online]. Available: <https://www.aspentech.com/en/products/engineering/aspen-custom-modeler> [Accessed 20 August 2024].
- ASPENTECH. 2024b. *Aspen Plus: Leading Process Simulation Software* [Online]. Available: <https://www.aspentech.com/en/products/engineering/aspen-plus> [Accessed 20 August 2024].
- BACIOCCHI, R., STORTI, G. & MAZZOTTI, M. 2006. Process design and energy requirements for the capture of carbon dioxide from air. *Chemical Engineering and Processing: Process Intensification*, 45, 1047-1058.
- BELCHER, S. E. 2005. Mixing and transport in urban areas. *Philosophical Transactions of the Royal Society A: Mathematical, Physical and Engineering Sciences*, 363, 2947-2968.
- BELLOS, E. 2023. Progress in beam-down solar concentrating systems. *Progress in Energy and Combustion Science*, 97, 101085.
- BERGERO, C., GOSNELL, G., GIELEN, D., KANG, S., BAZILIAN, M. & DAVIS, S. J. 2023. Pathways to net-zero emissions from aviation. *Nature Sustainability*, 6, 404-414.
- BEUTTLE, C., CHARLES, L. & WURZBACHER, J. 2019. The role of direct air capture in mitigation of anthropogenic greenhouse gas emissions. *Frontiers in Climate*, 1, 10.

- BISOTTI, F., HOFF, K. A., MATHISEN, A. & HOVLAND, J. 2024. Direct Air capture (DAC) deployment: A review of the industrial deployment. *Chemical Engineering Science*, 283, 119416.
- BUCK, R. & SMENT, J. 2023. Techno-economic analysis of multi-tower solar particle power plants. *Solar Energy*, 254, 112-122.
- BUSHUYEV, O. S., DE LUNA, P., DINH, C. T., TAO, L., SAUR, G., VAN DE LAGEMAAT, J., KELLEY, S. O. & SARGENT, E. H. 2018. What should we make with CO₂ and how can we make it? *Joule*, 2, 825-832.
- CARBON ENGINEERING. 2021. *The Story Behind Carbon Engineering* [Online]. Carbon Engineering Available: <https://carbonengineering.com/our-story/> [Accessed 06 August 2021].
- CARBON ENGINEERING. 2023. *The story behind Carbon Engineering* [Online]. Available: <https://carbonengineering.com/our-story/> [Accessed 16 July 2023].
- CHEW, J. W., LAMARCHE, W. C. Q. & COCCO, R. A. 2022. 100 years of scaling up fluidised bed and circulating fluidised bed reactors. *Powder Technology*, 409, 117813.
- CHOI, Y. H., JANG, Y. J., PARK, H., KIM, W. Y., LEE, Y. H., CHOI, S. H. & LEE, J. S. 2017a. Carbon dioxide Fischer-Tropsch synthesis: A new path to carbon-neutral fuels. *Applied catalysis B: environmental*, 202, 605-610.
- CHOI, Y. H., RA, E. C., KIM, E. H., KIM, K. Y., JANG, Y. J., KANG, K. N., CHOI, S. H., JANG, J. H. & LEE, J. S. 2017b. Sodium - Containing Spinel Zinc Ferrite as a Catalyst Precursor for the Selective Synthesis of Liquid Hydrocarbon Fuels. *ChemSusChem*, 10, 4764-4770.
- COLELLI, L., SEGNERI, V., BASSANO, C. & VILARDI, G. 2023. E-fuels, technical and economic analysis of the production of synthetic kerosene precursor as sustainable aviation fuel. *Energy Conversion and Management*, 288, 117165.
- COOLINGTOWERDEPOT®. 2023. *The depot of all cooling towers* [Online]. Available: <http://www.coolingtowerdepot.com/content/cooling-towers> [Accessed 19 July 2023].

- CREDITS, C. 2023. *Blackrock places \$550m bet on Occidental's DAC Project stratos* [Online]. Available: <https://carboncredits.com/blackrock-places-550m-bet-on-occidentals-dac-project-stratos/> [Accessed 10 August 2024].
- CUI, Y., XU, Y. & ZHANG, X. 2024. Sustainable aviation fuel: Biomass fostered future aviation. *The Innovation Energy*, 1, 100007.
- DE JONGE, M. M., DAEMEN, J., LORIAUX, J. M., STEINMANN, Z. J. & HUIJBREGTS, M. A. 2019. Life cycle carbon efficiency of Direct Air Capture systems with strong hydroxide sorbents. *International Journal of Greenhouse Gas Control*, 80, 25-31.
- DEPARTMENT OF ENERGY 2023. U.S. National Clean Hydrogen Strategy and Roadmap.
- DESPOINT, L. & SELOSSE, S. 2022. An overview of CO₂ capture and utilization in energy models. *Resources, Conservation and Recycling*, 180, 106150.
- DONNELLY, T. J., YATES, I. C. & SATTERFIELD, C. N. 1988. Analysis and prediction of product distributions of the Fischer-Tropsch synthesis. *Energy & Fuels*, 2, 734-739.
- DUTTA, A., FAROOQ, S., KARIMI, I. A. & KHAN, S. A. 2017. Assessing the potential of CO₂ utilization with an integrated framework for producing power and chemicals. *Journal of CO₂ Utilization*, 19, 49-57.
- ENGINEERING, C. 2022. *New Partnership to deploy large-scale direct air capture in Norway* [Online]. Available: <https://carbonengineering.com/news-updates/partnership-dac-norway/> [Accessed 16 June 2024].
- ERANS, M., SANZ-PÉREZ, E. S., HANAK, D. P., CLULOW, Z., REINER, D. M. & MUTCH, G. A. 2022. Direct air capture: process technology, techno-economic and socio-political challenges. *Energy & Environmental Science*, 15, 1360-1405.
- ESENCE, T., BENOIT, H., PONCIN, D., TESSONNEAUD, M. & FLAMANT, G. 2020a. A shallow cross-flow fluidised-bed solar reactor for continuous calcination processes. *Solar Energy*, 196, 389-398.
- ESENCE, T., GUILLOT, E., TESSONNEAUD, M., SANS, J.-L. & FLAMANT, G. 2020b. Solar calcination at pilot scale in a continuous flow multistage horizontal fluidised bed. *Solar Energy*, 207, 367-378.

- FAIR, J. R., SEIBERT, A. F., BEHRENS, M., SARABER, P. & OLUJIC, Z. 2000. Structured packing performance experimental evaluation of two predictive models. *Industrial & Engineering Chemistry Research*, 39, 1788-1796.
- FASIHI, M., EFIMOVA, O. & BREYER, C. 2019. Techno-economic assessment of CO₂ direct air capture plants. *Journal of Cleaner Production*, 224, 957-980.
- FERNÁNDEZ-TORRES, M. J., DEDNAM, W. & CABALLERO, J. A. 2022. Economic and environmental assessment of directly converting CO₂ into a gasoline fuel. *Energy Conversion and Management*, 252, 115115.
- GLICKSMAN, L., HYRE, M. & WOLOSHUN, K. 1993. Simplified scaling relationships for fluidised beds. *Powder Technology*, 77, 177-199.
- GLICKSMAN, L. R. 1984. Scaling relationships for fluidised beds. *Chem. Eng. Sci.*; (United Kingdom), 39.
- GOV.UK. 2021. *Projects selected for Phase 1 of the Direct air capture and greenhouse gas removal programme* [Online]. Available: <https://www.gov.uk/government/publications/direct-air-capture-and-other-greenhouse-gas-removal-technologies-competition/projects-selected-for-phase-1-of-the-direct-air-capture-and-greenhouse-gas-removal-programme> [Accessed 06 August 2021].
- GOV.UK DEPARTMENT FOR ENERGY SECURITY & NET ZERO 2023. Hydrogen transport and storage cost.
- HEIDEL, K., KEITH, D., SINGH, A. & HOLMES, G. 2011. Process design and costing of an air-contactor for air-capture. *Energy Procedia*, 4, 2861-2868.
- HEIDEL, K. & ROSSI, R. 2017. United States Patent application: 0170327421. *High Temperature Hydrator (A1)*. Filed May, 10.
- HEPBURN, C., ADLEN, E., BEDDINGTON, J., CARTER, E. A., FUSS, S., MAC DOWELL, N., MINX, J. C., SMITH, P. & WILLIAMS, C. K. 2019. The technological and economic prospects for CO₂ utilization and removal. *Nature*, 575, 87-97.
- HILLESTAD, M. 2015. Modeling the Fischer–Tropsch product distribution and model implementation. *Chemical Product and Process Modeling*, 10, 147-159.

- HILSENATH, J. 1955. *Tables of thermal properties of gases: comprising tables of thermodynamic and transport properties of air, argon, carbon dioxide, carbon monoxide, hydrogen, nitrogen, oxygen, and steam*, US Department of Commerce, National Bureau of Standards.
- HODDENBAGH, J., WILFING, K., MILLER, K., HARDMAN, D., TRAN, H. & BAIR, C. 2001. Borate autocauticizing: a cost effective technology.
- HOLMES, G. & KEITH, D. W. 2012. An air–liquid contactor for large-scale capture of CO₂ from air. *Philosophical Transactions of the Royal Society A: Mathematical, Physical and Engineering Sciences*, 370, 4380-4403.
- HOLMES, G., NOLD, K., WALSH, T., HEIDEL, K., HENDERSON, M. A., RITCHIE, J., KLAVINS, P., SINGH, A. & KEITH, D. W. 2013. Outdoor prototype results for direct atmospheric capture of carbon dioxide. *Energy Procedia*, 37, 6079-6095.
- HOLMES, G. J. 2010. *A carbon dioxide absorpition performance evaluation for capture from ambient air*. University of Calgary.
- HOLMES, H. E., REALFF, M. J. & LIVELY, R. P. 2024. Water management and heat integration in direct air capture systems. *Nature Chemical Engineering*, 1, 208-215.
- HWANG, S.-M., HAN, S. J., PARK, H.-G., LEE, H., AN, K., JUN, K.-W. & KIM, S. K. 2021. Atomically alloyed Fe–Co catalyst derived from a N-coordinated Co single-atom structure for CO₂ hydrogenation. *ACS Catalysis*, 11, 2267-2278.
- HYDROGEN COUNCIL. 2024. *Hydrogen Insights 2023* [Online]. Available: <https://hydrogencouncil.com/en/hydrogen-insights-2023/> [Accessed 20 July 2024].
- IATA. 2024. *IATA Economics* [Online]. Available: <https://www.iata.org/en/publications/economics/> [Accessed 20 August 2024].
- IEA. 2019. *Putting CO₂ to Use* [Online]. IEA, Paris. Available: <https://www.iea.org/reports/putting-co2-to-use> [Accessed October 20, 2023].
- IEA. 2020a. *CCUS in Clean Energy Transitions – analysis* [Online]. Available: <https://www.iea.org/reports/ccus-in-clean-energy-transitions> [Accessed 09 September 2024].
- IEA 2020b. *Energy Technology Perspectives 2020*.

- IEA. 2022. *Aviation* [Online]. Available: <https://www.iea.org/energy-system/transport/aviation> [Accessed November 6, 2023].
- IEA 2023a. Global Hydrogen Review 2023 – Analysis.
- IEA 2023b. Global Hydrogen Review 2023: Assumptions Annex.
- IEA. 2023c. *Section 45Q Credit for Carbon Oxide Sequestration* [Online]. Available: <https://www.iea.org/policies/4986-section-45q-credit-for-carbon-oxide-sequestration?technology=CO2%20Storage> [Accessed 16 July 2023].
- IEA. 2024a. *CO₂ emissions in 2023* [Online]. Available: <https://www.iea.org/reports/co2-emissions-in-2023> [Accessed November 21 2024].
- IEA. 2024b. *Direct Air Capture* [Online]. IEA, Paris Available: <https://www.iea.org/energy-system/carbon-capture-utilisation-and-storage/direct-air-capture> [Accessed 2 August 2024].
- IEAGHG 2021. Global Assessment of Direct Air Capture Costs.
- IPCC 2023. Climate Change 2023: Synthesis Report. A Report of the Intergovernmental Panel on Climate Change. Contribution of Working Groups I, II and III to the Sixth Assessment Report of the Intergovernmental Panel on Climate Change IPCC, Geneva, Switzerland.
- ISHAQ, H. & CRAWFORD, C. 2023. CO₂-based alternative fuel production to support development of CO₂ capture, utilization and storage. *Fuel*, 331, 125684.
- KAMKENG, A. D. & WANG, M. 2023. Technical analysis of the modified Fischer-Tropsch synthesis process for direct CO₂ conversion into gasoline fuel: Performance improvement via ex-situ water removal. *Chemical Engineering Journal*, 462, 142048.
- KEITH, D. W., HA-DUONG, M. & STOLAROFF, J. K. 2006. Climate strategy with CO₂ capture from the air. *Climatic Change*, 74, 17-45.
- KEITH, D. W., HOLMES, G., ANGELO, D. S. & HEIDEL, K. 2018. A process for capturing CO₂ from the atmosphere. *Joule*, 2, 1573-1594.
- KELKAR, V. V. & NG, K. M. 2002. Development of fluidised catalytic reactors: Screening and scale - up. *AIChE journal*, 48, 1498-1518.

- KIANI, A., JIANG, K. & FERON, P. 2020. Techno-economic assessment for CO₂ capture from air using a conventional liquid-based absorption process. *Frontiers in Energy Research*, 8, 92.
- KINCAID, N., MUNGAS, G., KRAMER, N., WAGNER, M. & ZHU, G. 2018. An optical performance comparison of three concentrating solar power collector designs in linear Fresnel, parabolic trough, and central receiver. *Applied Energy*, 231, 1109-1121.
- KNOWLTON, T., KARRI, S. & ISSANGYA, A. 2005. Scale-up of fluidised-bed hydrodynamics. *Powder Technology*, 150, 72-77.
- KURUP, P., GLYNN, S. & AKAR, S. 2022. Manufacturing cost analysis of advanced parabolic trough collector. AIP Conference Proceedings, 2022. AIP Publishing LLC, 020006.
- LACKNER, K. S. 2009. Capture of carbon dioxide from ambient air. *The European Physical Journal Special Topics*, 176, 93-106.
- LANDSEARCH. 2024. *Price of Land per Acre by State - LandSearch* [Online]. Available: <https://www.landsearch.com/price> [Accessed 10 July 2024].
- LANGIE, K. M. G., TAK, K., KIM, C., LEE, H. W., PARK, K., KIM, D., JUNG, W., LEE, C. W., OH, H.-S. & LEE, D. K. 2022. Toward economical application of carbon capture and utilization technology with near-zero carbon emission. *Nature Communications*, 13, 7482.
- LEBLING, K., MCQUEEN, N., PISCIOTTA, M. & WILCOX, J. 2021. Direct air capture: resource considerations and costs for carbon removal. *World Resources Institute*, 6.
- LI, C., SHI, H., CAO, Y., KUANG, Y., ZHANG, Y., GAO, D. & SUN, L. 2015. Modeling and optimal operation of carbon capture from the air driven by intermittent and volatile wind power. *Energy*, 87, 201-211.
- LI, L., LIU, Q., HUANG, T. & PENG, W. 2022. Mineralization and utilization of CO₂ in construction and demolition wastes recycling for building materials: A systematic review of recycled concrete aggregate and recycled hardened cement powder. *Separation and Purification Technology*, 298, 121512.
- LIU, C. M., SANDHU, N. K., MCCOY, S. T. & BERGERSON, J. A. 2020. A life cycle assessment of greenhouse gas emissions from direct air capture and Fischer–Tropsch fuel production. *Sustainable Energy & Fuels*, 4, 3129-3142.

- LU, X., MCELROY, M. B. & KIVILUOMA, J. 2009. Global potential for wind-generated electricity. *Proceedings of the National Academy of Sciences*, 106, 10933-10938.
- MADHU, K., PAULIUK, S., DHATHRI, S. & CREUTZIG, F. 2021. Understanding environmental trade-offs and resource demand of direct air capture technologies through comparative life-cycle assessment. *Nature Energy*, 6, 1035-1044.
- MAHMOUDKHANI, M., HEIDEL, K., FERREIRA, J., KEITH, D. & CHERRY, R. S. 2009. Low energy packed tower and caustic recovery for direct capture of CO₂ from air. *Energy Procedia*, 1, 1535-1542.
- MARCHESE, M., BUFFO, G., SANTARELLI, M. & LANZINI, A. 2021. CO₂ from direct air capture as carbon feedstock for Fischer-Tropsch chemicals and fuels: Energy and economic analysis. *Journal of CO₂ Utilization*, 46, 101487.
- MCKINSEY & COMPANY. 2024. *Global Energy Perspective 2023: Hydrogen outlook* [Online]. Available: <https://www.mckinsey.com/industries/oil-and-gas/our-insights/global-energy-perspective-2023-hydrogen-outlook> [Accessed 20 July 2024].
- MEIRI, N., RADUS, R. & HERSKOWITZ, M. 2017. Simulation of novel process of CO₂ conversion to liquid fuels. *Journal of CO₂ Utilization*, 17, 284-289.
- MIDREX. 2022. *Midrex H₂ The Future of Ironmaking* [Online]. Available: <https://www.midrex.com/technology/midrex-process/midrex-h2/> [Accessed 12 July 2023].
- NASA. 2024. *Carbon dioxide concentration* [Online]. Available: <https://climate.nasa.gov/vital-signs/carbon-dioxide/?intent=121> [Accessed 12 August 2024].
- NASSAR, R., HILL, T. G., MCLINDEN, C. A., WUNCH, D., JONES, D. B. & CRISP, D. 2017. Quantifying CO₂ emissions from individual power plants from space. *Geophysical Research Letters*, 44, 10,045-10,053.
- NREL. 2024a. *NSRDB: National Solar Radiation Database* [Online]. Available: <https://nsrdb.nrel.gov/data-viewer> [Accessed 20 July 2024].
- NREL. 2024b. *Power Tower Projects* [Online]. Available: <https://solarpaces.nrel.gov/by-technology/power-tower> [Accessed 20 July 2024].

- NREL. 2024c. *System Advisor Model* [Online]. Available: <https://sam.nrel.gov/> [Accessed 20 August 2024].
- OTITOJU, O., OKO, E. & WANG, M. 2021. Technical and economic performance assessment of post-combustion carbon capture using piperazine for large scale natural gas combined cycle power plants through process simulation. *Applied Energy*, 292, 116893.
- PANZONE, C., PHILIPPE, R., CHAPPAZ, A., FONGARLAND, P. & BENGHAOUER, A. 2020. Power-to-Liquid catalytic CO₂ valorization into fuels and chemicals: focus on the Fischer-Tropsch route. *Journal of CO₂ Utilization*, 38, 314-347.
- PRATS-SALVADO, E., JAGTAP, N., MONNERIE, N. & SATTTLER, C. 2024. Solar-Powered Direct Air Capture: Techno-Economic and Environmental Assessment. *Environmental Science & Technology*, 58, 2282-2292.
- QUÉRÉ, C., ANDREW, R. M., FRIEDLINGSTEIN, P., SITCH, S., HAUCK, J., PONGRATZ, J., PICKERS, P. A., IVAR KORSBAKKEN, J., PETERS, G. P. & CANADELL, J. G. 2018. Global carbon budget 2018. *Earth System Science Data*.
- ROBIE, R. A. & HEMINGWAY, B. S. 1995. *Thermodynamic properties of minerals and related substances at 298.15 K and 1 bar (105 Pascals) pressure and at higher temperatures*, US Government Printing Office.
- ROJAS-MICHAGA, M. F., MICHAÏLOS, S., CARDOZO, E., AKRAM, M., HUGHES, K. J., INGHAM, D. & POURKASHANIAN, M. 2023. Sustainable aviation fuel (SAF) production through power-to-liquid (PtL): A combined techno-economic and life cycle assessment. *Energy Conversion and Management*, 292, 117427.
- RÜDISÜLI, M., SCHILDHAUER, T. J., BIOLLAZ, S. M. & VAN OMMEN, J. R. 2012. Scale-up of bubbling fluidised bed reactors—A review. *Powder Technology*, 217, 21-38.
- SABATINO, F., GRIMM, A., GALLUCCI, F., VAN SINT ANNALAND, M., KRAMER, G. J. & GAZZANI, M. 2021. A comparative energy and costs assessment and optimisation for direct air capture technologies. *Joule*, 5, 2047-2076.
- SACCHI, R., BECATTINI, V., GABRIELLI, P., COX, B., DIRNAICHNER, A., BAUER, C. & MAZZOTTI, M. 2023. How to make climate-neutral aviation fly. *Nature Communications*, 14, 3989.

- SANZ-PÉREZ, E. S., MURDOCK, C. R., DIDAS, S. A. & JONES, C. W. 2016. Direct capture of CO₂ from ambient air. *Chemical reviews*, 116, 11840-11876.
- SEGAL, A. & EPSTEIN, M. 2001. The optics of the solar tower reflector. *Solar Energy*, 69, 229-241.
- SIEVERT, K., SCHMIDT, T. S. & STEFFEN, B. 2024. Considering technology characteristics to project future costs of direct air capture. *Joule*, 8, 979-999.
- SIMON, A., KAAHAAINA, N. B., FRIEDMANN, S. J. & AINES, R. D. 2011. Systems analysis and cost estimates for large scale capture of carbon dioxide from air. *Energy Procedia*, 4, 2893-2900.
- SOCOLOW, R., DESMOND, M., AINES, R., BLACKSTOCK, J., BOLLAND, O., KAARSBERG, T., LEWIS, N., MAZZOTTI, M., PFEFFER, A. & SAWYER, K. 2011. Direct air capture of CO₂ with chemicals: a technology assessment for the APS Panel on Public Affairs. American Physical Society.
- STOLAROFF, J. K., KEITH, D. W. & LOWRY, G. V. 2008. Carbon dioxide capture from atmospheric air using sodium hydroxide spray. *Environmental science & technology*, 42, 2728-2735.
- TODIC, B., BHATELIA, T., FROMENT, G. F., MA, W., JACOBS, G., DAVIS, B. H. & BUKUR, D. B. 2013. Kinetic model of Fischer–Tropsch synthesis in a slurry reactor on Co–Re/Al₂O₃ catalyst. *Industrial & Engineering Chemistry Research*, 52, 669-679.
- TREGAMBI, C., TROIANO, M., MONTAGNARO, F., SOLIMENE, R. & SALATINO, P. 2021. Fluidised beds for concentrated solar thermal technologies—A review. *Frontiers in Energy Research*, 9, 618421.
- VAN DER GIESEN, C., KLEIJN, R. & KRAMER, G. J. 2014. Energy and climate impacts of producing synthetic hydrocarbon fuels from CO₂. *Environmental science & technology*, 48, 7111-7121.
- VARDON, D. R., SHERBACOW, B. J., GUAN, K., HEYNE, J. S. & ABDULLAH, Z. 2022. Realizing “net-zero-carbon” sustainable aviation fuel. *Joule*, 6, 16-21.

- WANG, R., ZHAO, Y., BABICH, A., SENK, D. & FAN, X. 2021. Hydrogen direct reduction (H-DR) in steel industry—An overview of challenges and opportunities. *Journal of Cleaner Production*, 329, 129797.
- YAO, B., XIAO, T., MAKGAE, O. A., JIE, X., GONZALEZ-CORTES, S., GUAN, S., KIRKLAND, A. I., DILWORTH, J. R., AL-MEGREN, H. A. & ALSHIHRI, S. M. 2020. Transforming carbon dioxide into jet fuel using an organic combustion-synthesized Fe-Mn-K catalyst. *Nature Communications*, 11, 6395.
- YE, R.-P., DING, J., GONG, W., ARGYLE, M. D., ZHONG, Q., WANG, Y., RUSSELL, C. K., XU, Z., RUSSELL, A. G. & LI, Q. 2019. CO₂ hydrogenation to high-value products via heterogeneous catalysis. *Nature communications*, 10, 5698.
- YOUNG, J., MCQUEEN, N., CHARALAMBOUS, C., FOTEINIS, S., HAWROT, O., OJEDA, M., PILOGÉ, H., ANDRESEN, J., PSARRAS, P. & RENFORTH, P. 2023. The cost of direct air capture and storage can be reduced via strategic deployment but is unlikely to fall below stated cost targets. *One Earth*, 6, 899-917.
- YUSUF, Z. & CAMERON, J. 2004. Decarbonization reactions between sodium metaborate and sodium carbonate. *Industrial & engineering chemistry research*, 43, 8148-8154.
- ZANG, G., SUN, P., ELGOWAINY, A. A., BAFANA, A. & WANG, M. 2021a. Performance and cost analysis of liquid fuel production from H₂ and CO₂ based on the Fischer-Tropsch process. *Journal of CO₂ Utilization*, 46, 101459.
- ZANG, G., SUN, P., YOO, E., ELGOWAINY, A., BAFANA, A., LEE, U., WANG, M. & SUPEKAR, S. 2021b. Synthetic methanol/Fischer–Tropsch fuel production capacity, cost, and carbon intensity utilizing CO₂ from industrial and power plants in the United States. *Environmental Science & Technology*, 55, 7595-7604.
- ZAYED, M. E., ZHAO, J., ELSHEIKH, A. H., LI, W., SADEK, S. & ABOELMAAREF, M. M. 2021. A comprehensive review on Dish/Stirling concentrated solar power systems: Design, optical and geometrical analyses, thermal performance assessment, and applications. *Journal of Cleaner Production*, 283, 124664.
- ZEMAN, F. 2014. Reducing the cost of Ca-based direct air capture of CO₂. *Environmental science & technology*, 48, 11730-11735.

- ZHANG, L., DANG, Y., ZHOU, X., GAO, P., VAN BAVEL, A. P., WANG, H., LI, S., SHI, L., YANG, Y. & VOVK, E. I. 2021. Direct conversion of CO₂ to a jet fuel over CoFe alloy catalysts. *The Innovation*, 2, 100170.
- ZHAO, J., KORBA, D., MISHRA, A., KLAUSNER, J., RANDHIR, K., AUYEUNG, N. & LI, L. 2024. Particle-based high-temperature thermochemical energy storage reactors. *Progress in Energy and Combustion Science*, 102, 101143.
- ZHOU, Z., SUN, Z. & DUAN, L. 2022. Chemical looping: A flexible platform technology for CH₄ conversion coupled with CO₂ utilization. *Current Opinion in Green and Sustainable Chemistry*, 100721.